

5-22-2023

Gpr75 Deficiency Attenuates High Fat Diet-Driven Obesity and Glucose Intolerance

Sakib Hossain
NYMC

Follow this and additional works at: https://touro scholar.touro.edu/nymc_students_theses



Part of the [Animal Studies Commons](#), [Endocrinology Commons](#), [Medicine and Health Sciences Commons](#), and the [Pharmacology Commons](#)

Recommended Citation

Hossain, Sakib, "Gpr75 Deficiency Attenuates High Fat Diet-Driven Obesity and Glucose Intolerance" (2023). *NYMC Student Theses and Dissertations*. 55.
https://touro scholar.touro.edu/nymc_students_theses/55

This Doctoral Dissertation - Open Access is brought to you for free and open access by the Students at Touro Scholar. It has been accepted for inclusion in NYMC Student Theses and Dissertations by an authorized administrator of Touro Scholar. For more information, please contact touro.scholar@touro.edu.

Gpr75 Deficiency Attenuates High Fat Diet-Driven Obesity and Glucose Intolerance

Sakib Hossain

**A Doctoral Dissertation in the Program in Pharmacology
Submitted to the Faculty of the Graduate School of Biomedical Sciences
in Partial Fulfillment of the Requirements
for the Degree of Doctor of Philosophy
at New York medical College**

2023

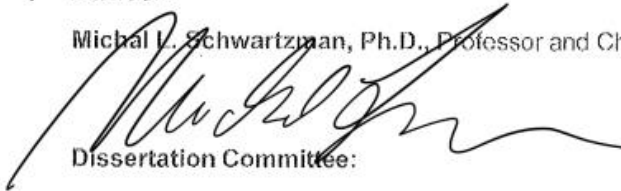
Signature page

Gpr75 Deficiency Attenuates High Fat Diet-Driven Obesity and Glucose Intolerance

Sakib Hossain

Advisor:

Michal L. Schwartzman, Ph.D., Professor and Chair of Pharmacology

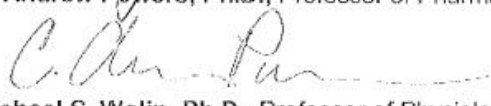


Dissertation Committee:

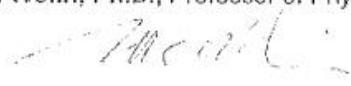
Jerry L. Nadler, MD, MACP, FAHA, FACE, Professor of Pharmacology



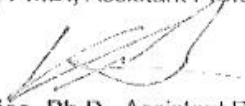
C. Andrew Powers, Ph.D., Professor of Pharmacology



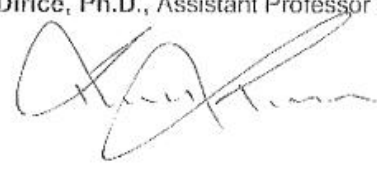
Michael S. Wolin, Ph.D., Professor of Physiology



Victor Garcia, Ph.D., Assistant Professor of Pharmacology



Ercument Dirice, Ph.D., Assistant Professor of Pharmacology



Acknowledgements

I would like to express the utmost gratitude to my mentor Dr. Michal Schwartzman, who helped me realize that becoming a successful scientist requires determination and passion, rather than intelligence alone. Without Dr. Schwartzman's guidance and full support, I would not be the critical thinker I am today. To my committee members, Dr. Jerry Nadler, Dr. Andrew Powers, Dr. Michael Wolin, Dr. Victor Garcia, and Dr. Ercument Dirice, thank you for your assistance and guidance throughout the entirety of my project. Your feedback, suggestions, and knowledge pushed me beyond my limits every day. I would also like to sincerely thank the members of the Schwartzman and Garcia labs, Ankit Gilani, Kevin Agostinucci, Jon Pascale, Danielle Diegisser, Elizabeth Villegas, and Ghezal Froogh. We spent so much time together that we became a family. Thank you for all the help with experiments – particularly troubleshooting and experimental design – but even more importantly, thank you for all the precious memories and good times that we shared. I will never forget this chapter of my life and the people who made it memorable. Finally, I would like to thank my family for all their support and words of encouragement over the years. Thank you!

Table of Contents

Title	...i
Signature Page	...ii
Acknowledgments	...iii
Table of Contents	...iv
List of Figures	...vi
List of Abbreviations	...x
Abstract	...xiv
Introduction and Background	
Obesity	...1
Clinical manifestation of Obesity	...2
Obesity – Driven Diabetes Mellitus	...3
Obesity-Driven Adipose Tissue Dysfunction & Inflammation	...4
Obesity-Driven Mitochondrial Dysfunction	...7
20-HETE	...9
The 20-HETE Receptor – GPR75	...12
Genetic Component of Obesity	...13
Central Hypothesis	...15
Specific Aims	...16
Materials and Methods	...20

Results	
Aim 1:	...28
To determine whether deficiencies in <i>Gpr75</i> genomic expression impact high fat diet-driven obesity and glucose handling	
Aim 2:	...52
To evaluate if protection from obesity is linked to caloric intake or caloric expenditure	
Aim 3:	...64
To explore the potential cellular mechanisms underlying the protection from obesity and glucose intolerance	
Discussion	...83
Significance	...92
Limitations and Future Directions	...93
Bibliography	...94

List of Figures

Figure 1: Obesity related consequences	...1
Figure 2: Adipose phenotypes	...6
Figure 3: Uncoupling protein localization and physiological effect	...8
Figure 4: Biological effects of 20-HETE	...11
Figure 5: Experimental scheme	...27
Figure 6: Male mice with <i>Gpr75</i> deficiency show no differences in weight gain after 14 weeks of control diet (CD) feeding	...29
Figure 7: Female mice with <i>Gpr75</i> deficiency show no differences in weight gain after 14 weeks of control diet (CD) feeding	...30
Figure 8: Male mice with <i>Gpr75</i> deficiency have attenuated weight gain after HFD-feeding	...31
Figure 9: Female mice with <i>Gpr75</i> deficiency have attenuated weight gain after HFD-feeding	...32
Figure 10: Male mice with <i>Gpr75</i> deficiency have attenuated fat mass accumulation over 14-weeks of HFD	...34
Figure 11: Female mice with <i>Gpr75</i> deficiency have attenuated fat mass accumulation over 14-weeks of HFD	...35
Figure 12: <i>Gpr75</i> deficient mice show no differences in fat free mass at baseline or after 14-weeks of HFD compared to WT	...36
Figure 13: VAT, SAT, and BAT sections of male <i>Gpr75</i> deficient mice have smaller adipocytes compared to WT mice after HFD-feeding	...38

Figure 14: VAT, SAT, and BAT sections of female <i>Gpr75</i> deficient mice have smaller adipocytes compared to WT mice after HFD-feeding	...39
Figure 15: <i>Gpr75</i> deficiency prevents HFD-induced adipose tissue dysfunction	...42
Figure 16: <i>Gpr75</i> deficiency prevents HFD-induced adipose tissue dysfunction cont.	
Figure 17: <i>Gpr75</i> deficiency attenuates HFD-induced increases in fasting blood sugar (FBS)	...45
Figure 18: <i>Gpr75</i> deficiency attenuates HFD-induced impairment of glucose clearance after glucose challenge in males	...47
Figure 19: <i>Gpr75</i> deficiency attenuates HFD-induced impairment of glucose clearance after glucose challenge in females	...49
Figure 20: <i>Gpr75</i> deficiency attenuates HFD-induced impairment of glucose clearance after insulin challenge	...51
Figure 21: <i>Gpr75</i> deficiency prevents HFD-induced insulin resistance	...53
Figure 22: Male mice with <i>Gpr75</i> deficiency display no differences in energy intake compared to WT mice throughout 14 weeks of control diet (CD) feeding	...55
Figure 23: Female mice with <i>Gpr75</i> deficiency display no differences in energy intake compared to WT mice throughout 14 weeks of control diet (CD) feeding	...56
Figure 24: Male <i>Gpr75</i> deficient mice show no differences in energy intake compared to WT mice during HFD-feeding	...57
Figure 25: Female <i>Gpr75</i> deficient mice show no differences in energy intake compared to WT mice during HFD-feeding	...58
Figure 26: Male and female mice with <i>Gpr75</i> deficiency show no differences in energy expenditure compared to WT mice throughout 14 weeks of CD feeding	...60

Figure 27: Male and female <i>Gpr75</i> deficient mice display attenuated HFD-driven decreases in energy expenditure	...61
Figure 28: Baseline total energy expenditure (TEE) analyzed by ANCOVA with total body mass (TBM) or lean body mass (LBM) as covariates for males	...63
Figure 29: Male total energy expenditure (TEE) analyzed by ANCOVA with total body mass (TBM) or lean body mass (LBM) as covariates after HFD-feeding	...64
Figure 30: Baseline total energy expenditure (TEE) analyzed by ANCOVA with total body mass (TBM) or lean body mass (LBM) as covariates for females	...65
Figure 31: Female total energy expenditure (TEE) analyzed by ANCOVA with total body mass (TBM) or lean body mass (LBM) as covariates after HFD-feeding	...66
Figure 32: <i>Gpr75</i> deficient male mice display higher expression of <i>Pgc1α</i> in BAT and SAT after 14 weeks of HFD feeding	...68
Figure 33: <i>Gpr75</i> deficient female mice display higher expression of <i>Pgc1α</i> in BAT and SAT after 14 weeks of HFD feeding	...69
Figure 34: <i>Gpr75</i> deficient male mice display higher expression of <i>Ucp1</i> in BAT and SAT after 14 weeks of HFD feeding	...70
Figure 35: <i>Gpr75</i> deficient female mice display higher expression of <i>Ucp1</i> in BAT and SAT after 14 weeks of HFD feeding	...71
Figure 36: <i>Gpr75</i> deficient male mice display higher expression of <i>Ucp1</i> in BAT and SAT at baseline	...72
Figure 37: <i>Gpr75</i> deficient female mice display higher expression of <i>Ucp1</i> in BAT and SAT at baseline	...73

Figure 38: <i>Gpr75</i> deficient mice display higher UCP1 protein levels compared to WT after HFD feeding	...75
Figure 39: Mitochondria respiration in BAT from HFD-fed WT and KO mice	...76
Figure 40: <i>Gpr75</i> deficient male mice display higher expression of <i>Ucp3</i> and <i>mfn1</i> in skeletal muscle after HFD feeding	...77
Figure 41: Male WT and <i>Gpr75</i> deficient mice show similar levels of tumor necrosis factor-alpha (<i>Tnfα</i>) at baseline	...79
Figure 42: Female WT and <i>Gpr75</i> deficient mice show similar levels of tumor necrosis factor-alpha (<i>Tnfα</i>) at baseline	...80
Figure 43: Male <i>Gpr75</i> deficient mice show protection from HFD-induced increases in tumor necrosis factor-alpha (<i>Tnfα</i>)	...81
Figure 44: Female <i>Gpr75</i> deficient mice show protection from HFD-induced increases in tumor necrosis factor-alpha (<i>Tnfα</i>)	...82
Figure 45: <i>Gpr75</i> deficient mice show protection from HFD-induced increases in tumor necrosis factor-alpha (<i>Tnfα</i>) in skeletal muscle	...83
Figure 46: <i>Gpr75</i> deficiency prevents HFD-induced impairment of insulin receptor phosphorylation	...84
Figure 47: <i>Gpr75</i> deficiency prevents HFD-induced impairment of protein kinase B (Akt) phosphorylation	...85

List of Abbreviations

20-HETE	20-hydroxy-5,8,11,14-eicosatetraenoic acid
ADP	Adenine diphosphate
ALK	Anaplastic lymphoma kinase
ATP	Adenine triphosphate
AUC	Area under curve
BAC	Bacterial artificial chromosome
BAT	Brown adipose tissue
BK _{Ca}	Calcium-activated K ⁺ channel
BMI	Body mass index
cAMP	Cyclic adenosine monophosphate
CCR	C-C chemokine receptor
CCL5	CC motif chemokine ligand 5
CDC	Centers for Disease Control and Prevention
CD	Chow diet
CVD	Cardiovascular disease
CYP	Cytochrome P450
DHA	Omega-3 docosahexaenoic acid
DIO	Diet induced obesity
eNOS	Endothelial nitric oxide synthase
ETC	Mitochondrial electron transport chain
FADH ₂	Flavin adenine dinucleotide
FFA	Free fatty acid

FFAR	Free fatty acid receptor
GLUT4	Insulin regulated glucose transporter
GPCR	G-protein coupled receptor
GPR75	G-protein coupled receptor -75
GTT	Glucose tolerance test
H&E	Hematoxylin and eosin
HET	Heterozygous
HFD	High fat diet
ICAM-1	Intercellular adhesion molecule-1
IL	Interleukin
IP ₃	Inositol triphosphate
IR	Insulin receptor
IRS-1	Insulin receptor substrate-1
ITT	Insulin tolerance test
JNK	c-Jun N-terminal kinases
KO	Knockout
LBM	Lean body mass
MAS	Mitochondrial assay buffer
MAPK	Mitogen activated protein kinase
Mfn-1	Mitofusin-1
MicroCT	Microcomputed tomography
MMP	Metalloproteinase
MLC	Myosin light chain

NADH	Nicotinamide adenine dinucleotide - hydrogen
NE	Neutrophil elastase
NF- κ B	Nuclear factor kappa B
NIH	National Institutes of Health
Nrf2	Nuclear factor E2-related factor 2
HOMA-IR	Homeostatic model assessment of insulin resistance
PGC1 α	Peroxisome proliferator-activated receptor gamma coactivator 1 α
PPAR γ	Peroxisome proliferator-activated receptor gamma
PI3K/Akt	Phosphoinositide 3-kinase/protein kinase B
PKA	Protein kinase A
PKC	Protein kinase C
PLC	Phospholipase C
PTEN	Phosphatase and tensin homologue deleted on chromosome 10
ROS	Reactive oxygen species
SAT	Subcutaneous adipose tissue
SM	Skeletal muscle
STAT	Signal transducer and activator of transcription factor
T1DM	Type 1 diabetes mellitus
T2DM	Type 2 diabetes mellitus
Tnf α	Tumor necrosis factor alpha
TBM	Total body mass
TEE	Total energy expenditure

TRPV	Vanilloid receptor
UCP	Uncoupling protein
VAT	Visceral adipose tissue
VO ₂	Volume of oxygen consumption
VCO ₂	Volume of carbon dioxide production
VSMC	Vascular smooth muscle cells
WAT	White adipose tissue
WHR	Waist-to-hip ratio
WHO	World Health Organization
WT	Wildtype

Abstract

With the Centers for Disease Control and Prevention (CDC) estimating that over 43% of Americans are obese in 2022, obesity is clearly an American health crisis. In fact, obesity has been linked to several prevalent medical conditions – hypertension, heart disease, liver disease, and type 2 diabetes mellitus (T2DM) – amounting to over 200 billion dollars of burden on the healthcare system in 2022 (as cited in Hossain *et al.*, 2023). The etiology of obesity involves complex interactions between genes regulating caloric intake and energy expenditure with environmental and behavioral factors. In fact, it is estimated that up to 40% of variation in body mass index (BMI) can be explained by genetic factors. Recently, a collaboration between Regeneron Pharmaceuticals and the Schwartzman-Garcia labs at New York Medical College published an exome sequencing study of individuals across the United Kingdom, United States, and Mexico which concluded that individuals possessing non-functioning, truncated mutations to the orphan G protein coupled receptor (GPCR), GPR75, had lower BMI and 54% reduced likelihood of obesity. The present study was undertaken to fully characterize the metabolic phenotype of *Gpr75* deficient mice when fed a high fat diet (HFD) and explore potential mechanisms by which GPR75 activation links to increased adiposity and decreased glucose tolerance. Mice with genomic *Gpr75* deficiency were subjected to HFD feeding (60% kilocalories from fat) for a period of 14 weeks. At baseline (8-10 weeks of age) *Gpr75* deficient mice have similar weight when compared to wild-type littermates. Body composition analysis using microcomputed tomography (microCT) also showed no differences in fat mass or fat-free mass (i.e., muscle mass) between the

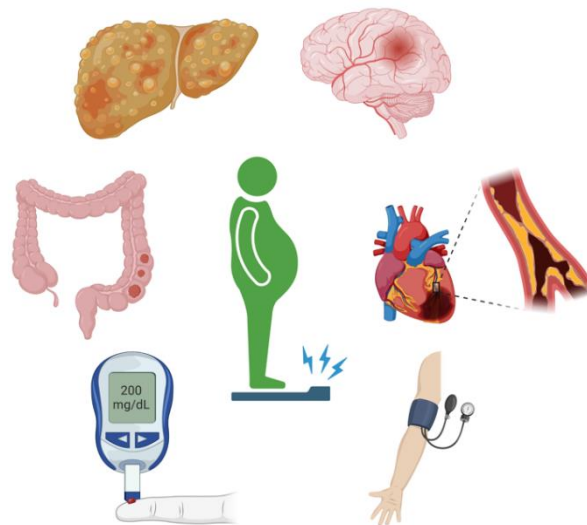
transgenic and wild-type animals. Intraperitoneal glucose and insulin administration further indicated no differences in glucose handling between transgenic and wild-type mice at baseline. After 14 weeks of HFD-feeding we observed significant differences in weight gain, with male and female wild-type mice gaining double the amount of weight as the transgenic mice. This corresponded with impairment in glucose clearance in response to insulin administration in wild-type mice indicating insulin resistance, a hallmark of T2DM, which was significantly attenuated in the transgenic mice. Surprisingly, mice with *Gpr75* deficiency show no differences in caloric intake compared to wild-type animals throughout the feeding period. In contrast, whole-body energy expenditure calculated from volume of oxygen consumption (VO_2) and carbon dioxide (VCO_2) production decreased in response to HFD-feeding for wild-type animals, while remaining unchanged compared to baseline for transgenic animals. This correlated with increased expression of mitochondrial uncoupling proteins (UCPs) in different adipose tissue depots, whose role in diet-induced obesity prevention has been published. With these results, we provide strong evidence that GPR75 contributes to diet-induced obesity and glucose intolerance, possibly by impairing the mitochondria-energy expenditure axis. Thus, the development of GPR75 blockers may provide a novel therapeutic approach for the fight against obesity and related complications (Hossain *et al.*, 2023).

Introduction and Background

Obesity

Obesity is one of the world's largest health problems. While once considered a problem for the rich in westernized countries, it now spans all income levels. The World Health Organization (WHO) estimates that over 2 billion people will be considered obese by 2030, with the highest concentration of people in the United States – an estimated 42.4% of the population (as cited in Hossain *et al.*, 2023). The *Global Burden of Disease*, published in *The Lancet*, indicates that cardiovascular disease (CVD), cancer, hypertension, and stroke, are associated with increased morbidity and mortality rates (as cited in Hossain *et al.*, 2023). While obesity does not directly cause any of these conditions, it is a major risk factor and significantly increases the likelihood of occurring (**Figure 1**) (Kopelman, 2000; Mayoral *et al.*, 2020; Shukla *et al.*, 2014). Indeed, many of the leading causes of mortality have benefitted from modern research and advent of pharmacotherapy. Unfortunately, there is very little – aside from lifestyle modifications – to combat obesity (Goossens, 2017).

Figure 1: Obesity related consequences



Clinical Manifestation of Obesity

Obesity is generally defined as an excessive accumulation of fat, and since there is no simple method to assess fat mass accumulation clinically, medical personnel typically diagnose obesity by calculating BMI. (Blundell *et al.*, 2014; di Angelantonio *et al.*, 2016). Epidemiological studies from the WHO indicate that BMI values between 18.5–25.0 kg/m² tend to be associated with low mortality rates, while values above 30 kg/m² are associated with increased morbidity. However, it is worth noting that today medical personnel are encouraged to measure waist-to-hip ratio (WHR) rather than BMI to assess fat accumulation/distribution, as BMI only offers suggestive information about body mass composition (Blundell *et al.*, 2014; di Angelantonio *et al.*, 2016; Stenholm *et al.*, 2008). Take for example top athletes, like tennis star Serena Williams or basketball legend LeBron James, who have BMI values approaching 30 kg/m² due to increased muscle rather than fat mass (Pilis *et al.*, 2019; Reale *et al.*, 2020).

Even still, absolute fat mass is not unambiguously related to metabolic health. For example, insulin sensitizing agents are widely used to treat T2DM and improve cardiovascular health despite documented adipogenic properties – which is particularly true for peroxisome proliferator-activated receptor gamma (*PPAR-γ*) agonists (Fonseca, 2003; Reasner, 2002; Yasmin & Jayaprakash, 2017). Furthermore, lipodystrophy, characterized by a deficiency in adipose tissue, has been linked to poor cardiovascular health and insulin resistance (Ganda, 2000; Gavrilova *et al.*, 2000; Kim *et al.*, 2000). In fact, surgical grafting of healthy adipose into lipodystrophic mice has been shown to alleviate insulin resistance (Gavrilova *et al.*,

2000). Numerous studies have highlighted the importance of body fat distribution as a major determinant of metabolic health. For example, it has been well established that intra-abdominal adipose tissue accumulation is closely related to cardiometabolic risk factors, while the expansion of lower body (gluteofemoral) adipose tends to be associated with lower total- and low-density lipoprotein-cholesterol, lower aortic calcification, and reduced arterial stiffness (Malis *et al.*, 2005; Snijder *et al.*, 2004; Yusuf *et al.*, 2005). The exact mechanisms underlying the benefits of gluteofemoral fat are unclear, though it may be linked to anti-inflammatory effects of long-chain polyunsaturated fatty acids, particularly omega-3 docosahexaenoic acid (DHA) (Ibrahim, 2010; Patel & Abate, 2013).

Obesity-Driven Diabetes Mellitus

Diabetes mellitus is typically characterized by chronic hyperglycemia. Type 1 diabetes (T1DM) occurs as a result of autoimmune destruction of pancreatic beta cells and the absolute loss of insulin, while T2DM generally occurs as a result of impaired insulin signaling (Toi *et al.*, 2020). While both forms of diabetes can be lethal when uncontrolled, the prevalence of T2DM is far higher than T1DM, accounting for more than 90% of all diabetes cases (Beckman *et al.*, 2013; Sumamo Schellenberg *et al.*, 2013; Toi *et al.*, 2020). The National Institutes of Health (NIH) estimates that more than 425 million people globally were diagnosed with T2DM in 2017; however, that number is projected to be over 630 million by 2045 (as cited in Toi *et al.*, 2020). This is of major concern as life expectancy decreases significantly with uncontrolled diabetes. Cross-sectional epidemiological studies indicate that after age 50, life

expectancy is 6 years shorter for people with T2DM than for people without it (Beckman *et al.*, 2013; Sumamo Schellenberg *et al.*, 2013).

Under normal conditions uptake and metabolism of glucose by beta cells of the islets of Langerhans stimulates insulin secretion via calcium induced vesicular fusion (Posner, 2017). Insulin receptor activation on target cells tends to initiate a complex signal transduction cascade involving the recruitment and phosphorylation of homologous insulin receptor substrates (IRS -1, -2, -3) and activation of the phosphoinositide 3-kinase/protein kinase B (PI3K/Akt) pathway (Haeusler *et al.*, 2018; Manning & Toker, 2017; Samuel & Shulman, 2012). Downstream effects are largely tissue specific, such as glucose disposal in myocytes, lipolysis in adipocytes, as well as lipogenesis and gluconeogenesis in hepatocytes (Haeusler *et al.*, 2018). Indeed, approximately 90% of insulin-stimulated glucose disposal occurs in skeletal muscle. Insulin resistance occurs when insulin-sensitive target tissues lose insulin response. This tends to cause hyperglycemia and dyslipidemia, due to the effects on skeletal muscle and liver/adipose respectively (Manning & Toker, 2017; Samuel & Shulman, 2012). While the cause of insulin resistance is multifactorial, adipose tissue dysfunction, inflammation, and mitochondrial dysfunction seem to play important roles in development.

Obesity-Driven Adipose Tissue Dysfunction & Inflammation

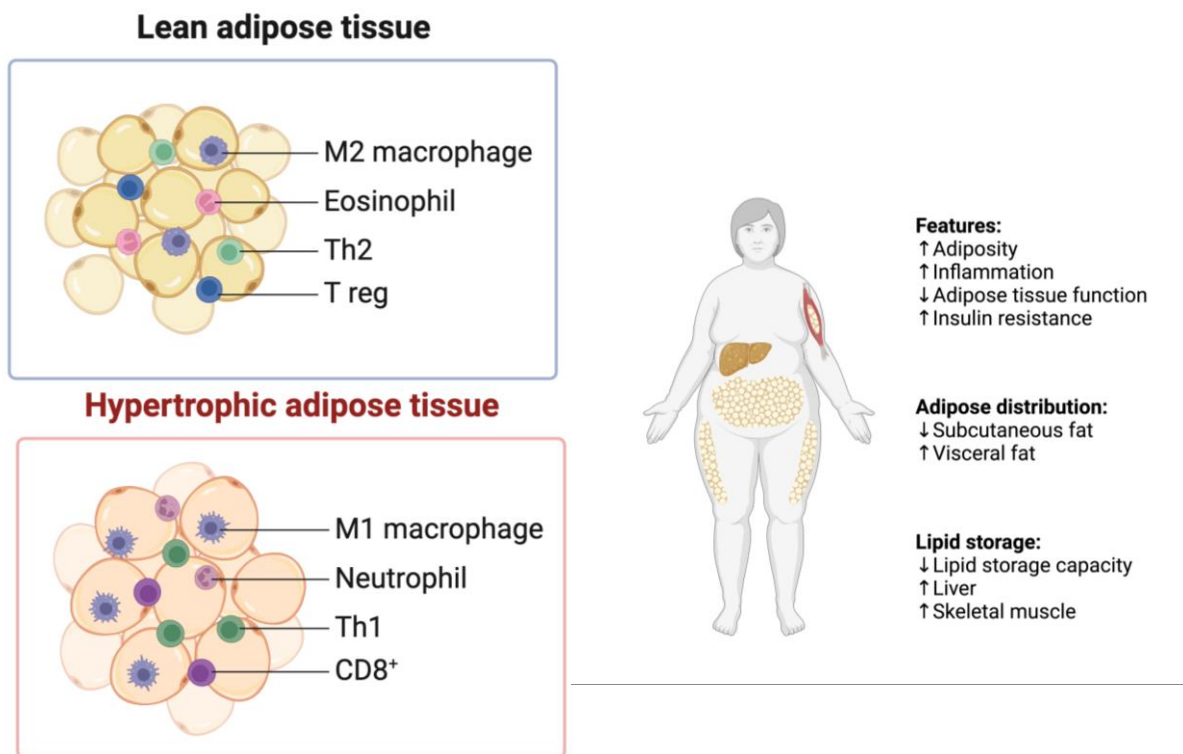
Adipose tissue plays a pivotal role in maintaining energy homeostasis. In times of overnutrition (i.e., caloric excess) adipocytes store lipids and become hypertrophic (Frayn, 2001; Hardy *et al.*, 2011; Stinkens *et al.*, 2015; Wernstedt Asterholm *et al.*, 2014). The opposite occurs during caloric deficiency, when lipid

stores (i.e., triglycerides) are broken down via lipolysis and released as free fatty acids (FFAs) to be used as an energy source (Stinkens *et al.*, 2015). Chronic overnutrition alters adipocyte phenotype and tends to stimulate an inflammatory cascade. Under normal conditions adipose tissue is enriched with anti-inflammatory immune cells – particularly M2 macrophages – which tend to secrete anti-inflammatory cytokines including interleukin -4, -5, -13 (Curat *et al.*, 2004; Weisberg *et al.*, 2003; Zeyda *et al.*, 2007) (**Figure 2**). Caloric excess, particularly with HFD, promotes lipid overloading, hypertrophy, and changes in adipocyte morphology whereby expression of C-C chemokine receptor type 2 (CCR2) predominates (Curat *et al.*, 2006). Neutrophils are now considered the first immune cells to be recruited to obese adipose tissue, where they bind to adipocytes via intercellular adhesion molecule 1 (ICAM-1) and stimulate production of interleukin-1 β (IL-1 β) and tumor necrosis factor α (TNF α) (Hardy *et al.*, 2011; McDonnell *et al.*, 2012; Rausch *et al.*, 2008). Neutrophils also secrete neutrophil elastase (NE) which tends to stimulate macrophage recruitment. In fact, genetic deletion of NE in rodents has been shown to reduce macrophage infiltration in HFD-fed rodent studies (Watanabe *et al.*, 2019). M1 macrophage recruitment to adipose tissue further stimulates the secretion of pro-inflammatory cytokines TNF α , IL-6 and IL-18 (Curat *et al.*, 2006; Weisberg *et al.*, 2003; Zeyda *et al.*, 2007) (**Figure 2**). In fact, histological analysis of adipose from human and mouse models of obesity show that M1 macrophages make up nearly 40% of inflamed adipose tissue (Stefanovic-Racic *et al.*, 2012).

Pro-inflammatory cytokines, particularly TNF α , directly inhibit normal insulin signaling (**Figure 2**) through activation of JNK or IKK β /NF- κ B signaling pathways

(Hotamisligil *et al.*, 1994; Li *et al.*, 2022; Tang *et al.*, 2002; Xu *et al.*, 2003). JNK activation and phosphorylation of the insulin receptor substrate-1 (IRS-1) at serine-302 or serine-307 inhibits PI3K/Akt pathway activation required for GLUT4 translocation (Rondinone & Smith, 1996; Rui *et al.*, 2001). In fact, studies show that siRNA silencing of TNF α improves insulin sensitivity and glucose tolerance in obese mice (Aouadi *et al.*, 2013). Importantly, FFAs have been shown to directly induce activation JNK and IKK β /NF- κ B signaling and promote insulin resistance in the absence of cytokines (Puri *et al.*, 2019; Sobczak *et al.*, 2019). This was supported by studies linking lipotoxicity and skeletal muscle insulin resistance in animal models with muscle-specific overexpression of lipoprotein lipase in (Puri *et al.*, 2019).

Figure 2: Adipose phenotypes



Obesity-Driven Mitochondrial Dysfunction

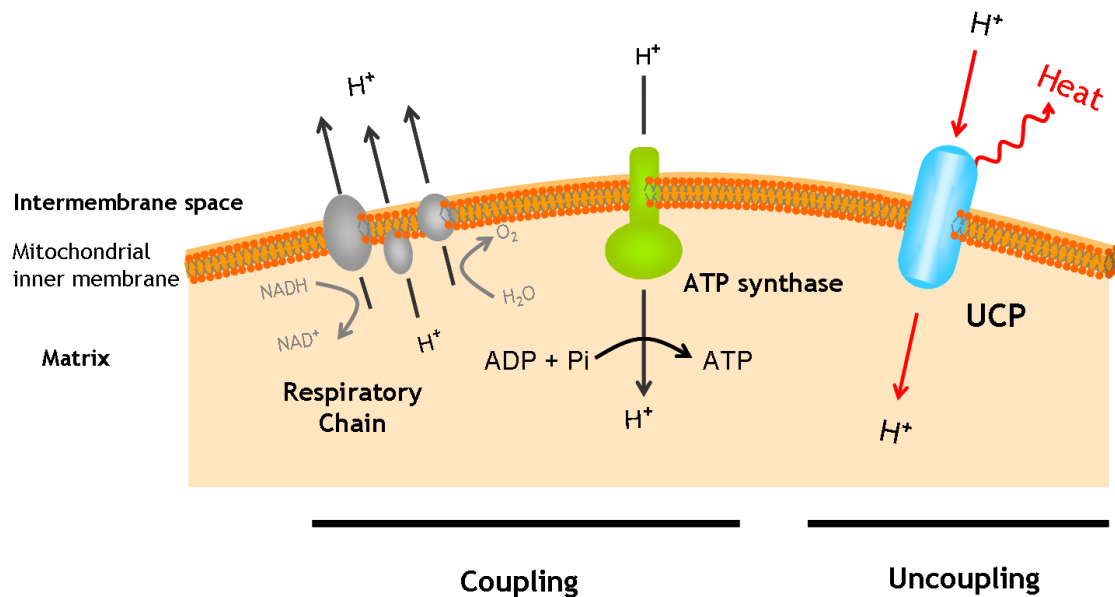
All eukaryotic cells require energy to survive and replicate, and this energy is typically supplied by mitochondria. In fact, mitochondria synthesize more than 95% of adenosine triphosphate (ATP) cells need to survive (Chouchani *et al.*, 2016). The cascade of events required for ATP generation can be simplified into (1) generation of an electrical potential between the mitochondrial matrix and inner membrane space via the pumping of protons, and (2) conversion of electrical energy into chemical energy as protons pass back into the matrix through the ATP synthase (Chouchani *et al.*, 2016; Wu *et al.*, 2012; Yoneshiro *et al.*, 2013). Importantly, mitochondrial oxidative phosphorylation requires molecular oxygen. In fact the generation of superoxide and hydrogen peroxide from the breakdown of molecular oxygen in the electron transport chain have been implicated in DNA damage (Boveris & Chance, 1973; Starkov & Fiskum, 2003).

With excessive nutrition, adipose tissue expansion is followed by ectopic lipid deposition throughout the body – skeletal muscle and liver in particular (Frayn, 2001; Goossens, 2017; Liesa & Shirihai, 2013; Shukla *et al.*, 2014). Oxidation of these lipids provides an increased supply of reduced cofactors (NADH and FADH₂) to the mitochondrial electron transport chain (ETC), thus enhancing ROS production (Liesa & Shirihai, 2013; Mishra & Chan, 2016). ROS are generally recognized as harmful particles as they damage intracellular proteins, lipids, and nucleic acids. In fact, ROS have been shown to play a major, albeit confusing, role in the development of insulin resistance. Studies show that acute diffusion of hydrogen peroxide into 3T3L1 adipocytes resulted in oxidation/inactivation of phosphatase and tensin homologue

deleted on chromosome 10 (PTEN), which tended to enhance glucose uptake via Akt and GLUT4; however, chronic ROS treatment led to Akt inactivation and insulin resistance (Ma *et al.*, 2018; Manna *et al.*, 2017). A study by Tang *et al.* showed that stimulation of the nuclear factor E2-related factor 2 (Nrf2) antioxidant pathway by sodium butyrate (NaB) enhances Glut4 and Irs-1 expression in gastrocnemius muscle to attenuate HFD-induced insulin resistance in rats (Tang *et al.*, 2022)

Importantly, oxidative phosphorylation is not perfectly coupled to ATP generation. Mitochondrial uncoupling proteins (UCPs) located on the inner membrane tend to act as channels for proton flux back to the matrix (**Figure 3**). However, the proton flux is coupled to heat generation instead of energy production (Fedorenko *et al.*, 2012; Ukropec *et al.*, 2006; Wu *et al.*, 2012).

Figure 3: Uncoupling protein localization and physiological effect



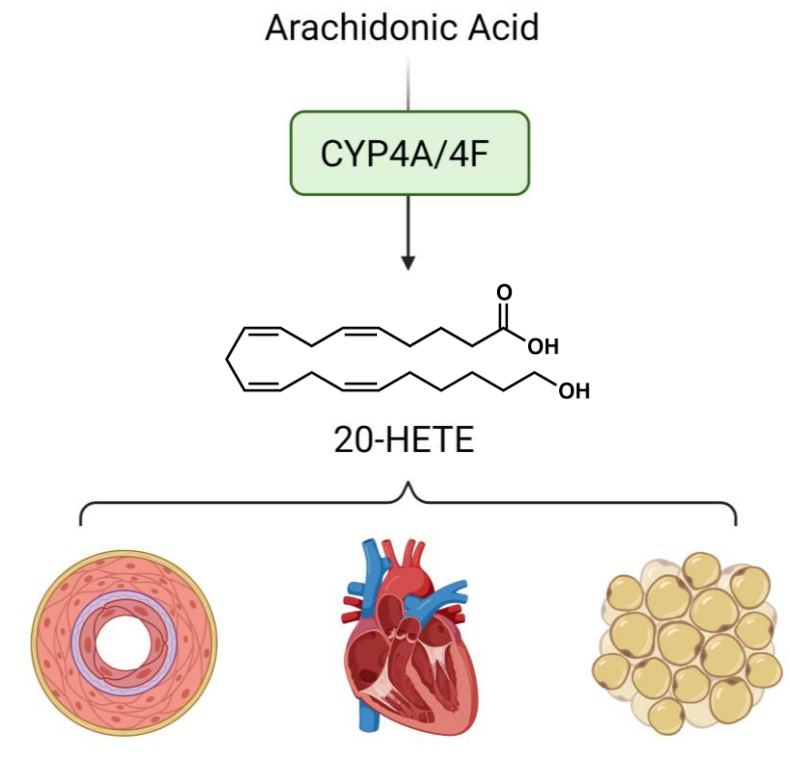
The generation of heat, known as thermogenesis, in brown adipose tissue (BAT) plays an important role in maintenance of body heat. Importantly, since oxidative phosphorylation is uncoupled, production of ROS is reduced, while still providing a sink for energy dissipation. Thus, thermogenesis is a novel target for counteracting the development of metabolic disorders such as obesity and T2DM. Studies indicate that transgenic mice with ectopic *Ucp1* expression in white adipose tissue (WAT) are resistant to HFD-induced obesity compared to wild-type controls (Ukropec *et al.*, 2006). Furthermore, numerous studies indicate that exogenous stimulation of UCP1 attenuates diet-induced obesity and insulin resistance in well-established models of obesity. This was shown by Chen *et al.* using the phytochemical hyperforin and Wang *et al.* using interleukin-27 (Chen *et al.*, 2021; Wang *et al.*, 2021).

20-HETE

20-hydroxyeicosatetraenoic acid (20-HETE) is the omega-hydroxylation metabolite of arachidonic acid whereby Cytochrome P450 (CYP) 4A and 4F isozymes insert a hydroxyl group at the terminal sp^3 carbon, thus making it biologically active (**Figure 4**). In humans the major 20-HETE synthases are CYP4A11 and CYP4F2. CYP4A10, CYP4A12, and CYP4A14 convert arachidonic acid to 20-HETE in mice; however, CYP4A12 is the major 20-HETE synthase (Froogh 2022; Kroetz & Xu 2005). 20-HETE production has been well documented in the heart, lung, kidney, vasculature, fat, as well as other organ beds (Escalante *et al.*, 1990). This is due to the widespread expression of Cytochrome P450 enzymes throughout the body.

The role of 20-HETE in vasculature function has been well documented. Vascular smooth muscle cells (VSMC) are a major site of action for 20-HETE. In fact, 20-HETE is a strong constrictor of microcirculatory vessels through these actions. 20-HETE promotes VSMC constriction by inhibiting the calcium-activated K⁺ channel (BK_{Ca}) (Toth *et al.*, 2013). This may involve a variety of mechanisms, including but not limited to, activation of protein kinase C (PKC), mitogen activated protein kinase (MAPK), and Src-type tyrosine kinases (Muthalif *et al.*, 2001; Stec *et al.*, 2007). Rho kinase, which phosphorylates myosin light chain (MLC) and increases the sensitivity of the contractile apparatus to Ca²⁺, is also a target of 20-HETE (Randriamboavonjy *et al.*, 2003). Importantly, 20-HETE also activates the transient receptor potential and vanilloid receptor (TRPV) family of calcium permeable channels (Toth *et al.*, 2013). These ion channels play a major role in regulating vascular tone. Furthermore, 20-HETE has been shown to stimulate superoxide production and inflammatory cytokine production in pulmonary artery vascular smooth muscle cells (Lakhkar *et al.*, 2016). Vascular endothelium is another critical target for 20-HETE. Within the endothelium 20-HETE has been shown to uncouple the endothelial nitric oxide synthase (eNOS), thus reducing nitric oxide production while increasing superoxide (Cheng *et al.*, 2010). The resulting activation of nuclear factor kappa light chain enhancer of activated B cells (NF-κB)-mediated pro-inflammatory program increases secretion of Il-6, Il-8, and Tnfα (Cheng *et al.*, 2010). In fact, inhibition of 20-HETE signaling has been shown to inhibit NF-κB activation and attenuate vascular inflammation (Cheng *et al.*, 2010; Toth *et al.*, 2013). **(Figure 4)**

Figure 4: Biological effects of 20-HETE



The role of 20-HETE in the pathogenesis of obesity is relatively unclear; however, some studies indicate that 20-HETE levels in blood or urine correlate with BMI in humans (Barden *et al.*, 2007; Peterson *et al.*, 2016; Tsai *et al.*, 2009). Furthermore, high-fat diets have been shown to induce 20-HETE synthases – CYP4A/F enzymes. In fact, transgenic mice with overexpression of the 20-HETE synthase (CYP4A12) show further increases in CYP4A12 expression and plasma 20-HETE levels as a result of high-fat diet feeding (Gilani *et al.*, 2018). Indeed, exogenous administration of 20-HETE to mesenchymal stem cells undergoing adipogenesis results in adipocyte hypertrophy and inflammation, which is mediated by the cyclooxygenase-2 (COX-2) derived 20-HETE metabolite 20-hydroxy

prostaglandin E2 (20-OH-PGE2) (Kim *et al.*, 2013). 20-HETE seems to play an important role in glucose metabolism and insulin signaling as well. Cultured endothelial cells (HUVEC) treated with 20-HETE display impaired insulin-stimulated phosphorylation of IRS-1 at Tyr632, thus leading to impaired insulin signaling (Boucher *et al.*, 2014; Gilani *et al.*, 2021; Li *et al.*, 2014). Other studies have found that 20-HETE stimulates glucose-stimulated insulin secretion mouse islets by binding to the free fatty acid receptor 1 (FFAR1) (Liu *et al.*, 2013; Tunaru *et al.*, 2018).

The 20-HETE Receptor – GPR75

GPR75 is currently classified as a class A orphan receptor. Initially, expression was thought to be limited to cells surrounding retinal arterioles as well as areas of the brain; however, GPR75 expression is now considered to be quite widespread including the luminal side of the proximal tubule in the kidney as well as beta cells in pancreatic islets (Garcia *et al.*, 2017; Pascale *et al.*, 2021). Studies show that CC motif chemokine ligand 5 (CCL5) increases IP3 and intracellular calcium in HEK cells overexpressing Gpr75 via a Gq protein-coupled PLC-mediated signal transduction pathway (Dedoni *et al.*, 2018). Furthermore, studies show that exogenous administration of CCL5 increased intracellular calcium in beta cells via GPR75 and stimulated insulin secretion from mouse and human islets in vitro (Liu *et al.*, 2013). However, there are no documented binding studies of CCL5 to GPR75 and CCL5 pairing to GPR75 could not be repeated in a β -arrestin assay (Dedoni *et al.*, 2018; Pascale *et al.*, 2021;). Other studies indicate that the vasoactive eicosanoid 20-HETE tends to bind to and activate GPR75. For example, Garcia *et al.* showed high affinity

binding of 20-HETE to GPR75 and the activation of Gq signaling mediated by intracellular Ca^{2+} accumulation and β -arrestin recruitment (Garcia *et al.*, 2017). Indeed, these were negated by 20-HETE receptor blockers (Pascale *et al.*, 2021). Furthermore, 20-HETE increased epithelial-mesenchymal transition, release of metalloproteinase-2 (MMP-2), cell migration and invasion in prostate cancer cells (PC-3). Which was impaired by GPR75 antagonism/silencing (as cited in Pascale *et al.*, 2021)

Genetic Component of Obesity

Decades of research have identified abnormalities in many genes play a causative role in obesity. For example, *ob/ob* (*LEP deficient*) and *db/db* (*LEPR deficient*) mouse models tend to show a similar pattern of obesity development. However, *ob/ob* mice are documented to show only mild insulin resistance, while *db/db* mice develop severe diabetes (Pelletier *et al.*, 2020). Unfortunately, mechanistic details underlying leptin signaling and development of obesity and diabetes remain poorly investigated. Conversely recent studies have identified gene abnormalities that may play a causative role in leanness. For example, genetic deletion of Anaplastic lymphoma kinase (ALK), a receptor tyrosine kinase, in mice resulted in thin animals with marked resistance to diet- and leptin-mutation-induced obesity (de Munck *et al.*, 2021). This occurs through enhanced energy expenditure via sympathetic control of adipose tissue lipolysis (de Munck *et al.*, 2021; Pelletier *et al.*, 2020).

The exome sequencing of 645,626 individuals from the United Kingdom, United States, and Mexico indicated that truncated variants of GPR75 were associated with

1.8 kilograms per square meter lower BMI and 54% lower odds of obesity in the heterozygous state (Akbari *et al.*, 2021). Studies in transgenic mice with *Gpr75* deletion indicate that mice are thin at weaning and tend to be hypophagic (Powell *et al.*, 2022). Further studies indicate that deletion of *Gpr75* in mice resulted in resistance to weight gain in a high-fat diet model (Hossain *et al.* 2023). Based on this information GPR75 may be an exciting target for obesity treatment and the underlying mechanisms attenuating HFD-induced weight gain need to be explored.

Central Hypothesis

Gpr75 deficiency attenuates high fat diet-driven obesity and glucose intolerance

Specific Aims

Aim 1: To determine whether deficiencies in *Gpr75* genomic expression impact high fat diet-driven obesity and glucose handling.

Transgenic mice with *Gpr75* deficiency, *Gpr75*^{-/-} (KO) and *Gpr75*^{+/-} (HET), were generated by Regeneron Pharmaceuticals using their proprietary *VelociMouse* technology whereby bacterial artificial chromosome vectors (BAC), with the *Gpr75* genomic sequence replaced with *LacZ*, were introduced into embryonic stem cells for homologous recombination. 8–10-week-old mice will be fed high fat diet (60% kilocalories from fat) for a period of 14 weeks. Development and progression of obesity will be analyzed through multiple methods. Body weight will be measured weekly to identify differences in weight gain between genotypes. Furthermore, microCT will be used to directly measure differences in visceral adipose (VAT) and subcutaneous adipose (SAT) accumulation between genotypes throughout the feeding period. After 14 weeks of HFD feeding sections of VAT, SAT, and BAT will be analyzed by hematoxylin and eosin (H&E) staining to visualize morphological differences, such as adipocyte size and lipid accumulation. Since obesity tends to be associated with adipose dysfunction, plasma adipokines will be measured through multiplex immunoassay – with particular emphasis on leptin and adiponectin. Obesity-induced impairments in glucose handling will be determined through measurement of fasting blood sugar, fasting plasma insulin, glucose tolerance, and insulin tolerance. It should be noted that additional KO, HET, and WT mice will be fed chow/control diet (13% kilocalories from fat) for 14 weeks and similar parameters will be measured as a control. By comparing changes in these parameters, we will

determine whether *Gpr75* expression correlates to HFD-induced obesity and diabetes.

Aim 2: To evaluate if protection from obesity is linked to caloric intake or caloric expenditure

The complex interplay of mechanisms involved in maintaining healthy body composition can be simplified as: energy intake = energy expenditure. In this paradigm changes in body weight occur as a result of either feeding or energy expenditure modification. Energy expenditure can be divided into obligatory energy expenditure – caloric breakdown/energy expenditure by mitochondria for cellular and organ function – and physical energy expenditure. An emerging division of energy expenditure is adaptive thermogenesis – caloric breakdown and resulting release of heat. While physical energy expenditure is a well-documented inducer of caloric breakdown and weight loss, numerous publications indicate that stimulation of adaptive thermogenesis also prevents against obesity. The goal of this aim is to determine whether changes in HFD-driven weight gain between *Gpr75* deficient and WT mice are due to reduced energy intake or enhanced energy expenditure. To address this issue weekly food consumption will be measured for all animals and used to calculate energy intake in kilocalories. Furthermore, animals will be subjected to indirect calorimetry at baseline and after 14 weeks of HFD-feeding to identify any differences in oxygen consumption – an indirect measurement of whole-body energy expenditure.

Aim 3: To explore the potential cellular mechanisms underlying the protection from obesity and glucose intolerance.

The molecular mechanisms regulating whole-body energy expenditure are relatively well documented. The role of peroxisome proliferator activated receptor - gamma coactivator alpha 1 (PGC- 1 alpha) in energy homeostasis is critical. Activation of the beta-3 adrenergic receptor tends to stimulate cyclic adenosine monophosphate (cAMP) mediated protein kinase A (PKA) activation. The resulting interaction of PGC -1 alpha with PPAR-gamma induces transcription of the uncoupling proteins (UCPs). Since UCPs play a critical role in adaptive thermogenesis we will measure gene and protein expression of PGC- 1 alpha and UCP1 in different adipose depots (VAT, SAT, and BAT). Since mice tend to have significant BAT depots compared to humans, we will also measure the expression of UCP3 isoform predominately found in skeletal muscle.

The link between inflammation and insulin resistance is well documented. We will measure the level of inflammatory markers, such as TNF- α , within different adipose beds and skeletal muscle via RT-PCR. Since 90% of glucose disposal occurs in skeletal muscle through insulin signaling, we will analyze activity of key markers of insulin signaling, including the phosphorylation of the insulin receptor and Akt activation, via western blot.

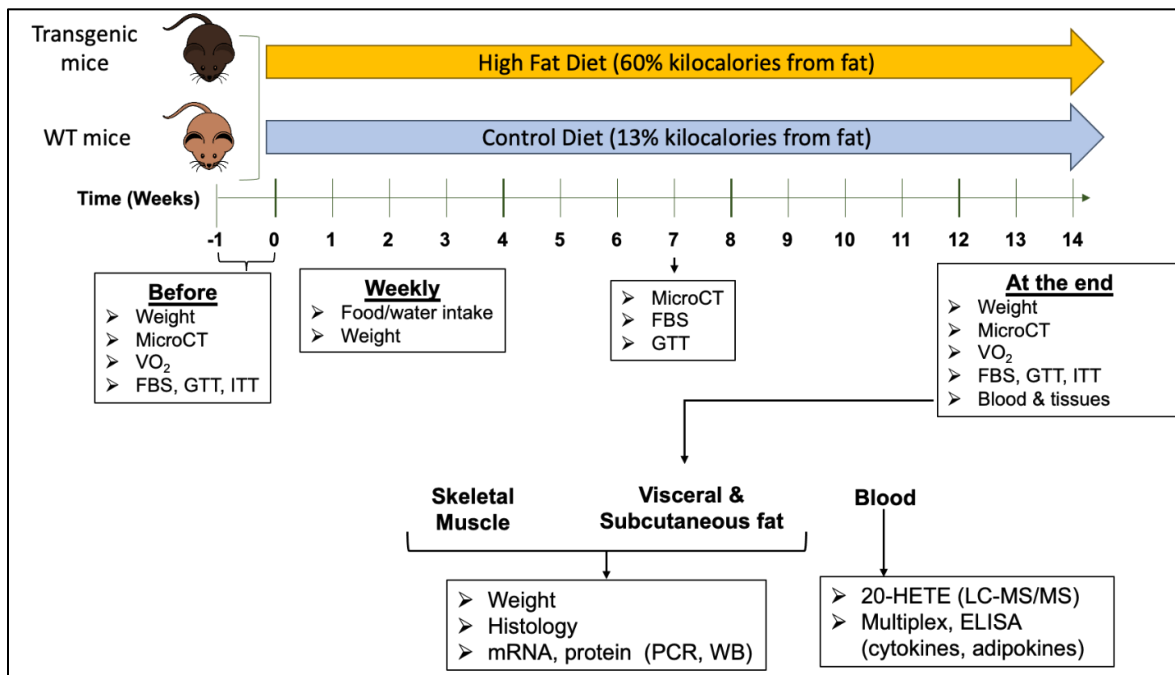
Materials and Methods

Experimental animals

“All experimental protocols were approved by the Institutional Animal Care and Use Committee (IACUC #) in accordance with the National Institutes of Health Guidelines for the Care and Use of Laboratory Animals. Mice null for *Gpr75* (*Gpr75*^{-/-}; KO) were generated by Regeneron Pharmaceuticals using the VelociMouse technology and are all on C57BL/6 background. Mice heterozygous (*Gpr75*^{+/-}; HET) for the *Gpr75* were bred to generate age-matched wild type (*Gpr75*^{+/+}; WT), HET and KO littermates that were used for experimentation. Male and female mice (10-12-week-old, 20.24±0.9g; n=45) were housed in static polycarbonate caging units (29.2 x 19.1 x 12.7 cm shoebox style) with stainless-steel wire bar lids, and 7-cm-deep isolator cage filter tops in a pathogen free facility. Three to four animals were placed in a cage with Alpha-dri paper pulp cellulose animal bedding, free access to food (LabDiet 5001) and acidified water, 14-h/10-h light/dark cycle, and a temperature between 20-23°C with 40-60% humidity. Welfare of all animals was monitored daily by licensed veterinary technicians employed by New York Medical College. Male and female mice of all genotypes were randomly distributed (n = 8-12 per group based off 95% confidence level calculation) into two experimental groups of diet feeding for 14 weeks (**Figure 5**): 1) regular chow/control diet (CD; Rodent Laboratory Chow 5001; Purina, St. Louis, MO); and 2) HFD (cat. no. 03584; Envigo, Huntingdon, UK). The composition of diets in percent kilocalories (kcal) 1) CD: fat, 13.4%; carbohydrate, 58.0%; protein, 28.7%; 2) HFD: fat, 58.4%; carbohydrate, 26.6%; protein, 15.0%. All animals were monitored for changes in body weight on a weekly basis. Body

composition (microCT), fasting blood glucose, and glucose and insulin tolerance tests were measured before and at weeks 7 and 14. At the end of the experiment, mice were anesthetized with ketamine/xylazine intra-peritoneal dose at 100 mg/kg ketamine + 10 mg/kg xylazine. Blood was withdrawn and fat tissues including visceral (VAT), subcutaneous (SAT) and brown (BAT) adipose tissues were harvested for various assays. All monitoring tests and post feeding analyses are described below and were done in blinded fashion. The number of animals used in this study is indicated in the section on statistical” (Hossain *et al.*, 2023).

Figure 5: Scheme of experiment



Assessment of Energy Intake

“Mice were housed in groups of 2-4. HFD and chow diets were provided as pellets only once a week (150 grams per cage). Energy intake was calculated by subtracting the amount of food leftover on any given week from the amount of food given the previous week. This value was divided by the number of animals per cage to obtain the averaged amount of food consumed by a single animal in any given week. The amount of food (in grams) was then multiplied by the kcal/gram obtained from the manufacturer (5.4 and 4.07 Kcal/gram, for HFD and chow diet respectively). The results were presented as Kcal consumed. Results depicted as weekly and cumulative energy intake showed no statistical differences between the genotypes” (Hossain *et al.*, 2023).

Assessment of Energy Expenditure

“Whole body energy expenditure was determined using indirect calorimetry. Mice were placed in a gas analyzer (Oxylet; Panlab-Bioseb, Vitrolles, France) for 1 hour to obtain measurements of oxygen consumption ($\dot{V}O_2$) and carbon dioxide production (VCO_2). For each individual mouse, hourly measurements were performed twice. There were 2 animals studied per hour that were housed in two different chambers. Total energy expenditure (TEE) was calculated using the Lusk equation, $[(1.232 \cdot RQ) + 3.815] \cdot VO_2$, where RQ is the ratio VCO_2/VO_2 . TEE data were then analyzed using the National Mouse Metabolic Phenotyping Center website provided by the NIH. ANCOVA analysis was conducted with grouping variable set to genotype and CoVariate variable set to total (TBM) or lean (LBM)

body mass to identify whether TBM or LBM had an effect on the differences in energy expenditure between genotypes after HFD-feeding” (Hossain *et al.*, 2023).

Micro-Computed Tomography (microCT) scanning and analysis

“Whole body microCT scans were obtained from mice anesthetized with isoflurane (4% for induction and 2% during scan acquisition) using the Quantum GX2 microCT imaging system (PerkinElmer Inc). Settings were optimized for body composition including a voltage of 70 kV, field of view of 72 mm, and X-ray filter of Aluminum 1.0 mm. CT scans were acquired for 6 minutes and analyzed using Analyze 14.0 software (AnalyzeDirect). Fat was isolated for analysis by density threshold. Separation of visceral and subcutaneous fat was done by sequential manual tracing of coronal slices in 2D every 7 slices. Regions of similar density to fat were excluded using the same method to remove air within the lungs and equipment artifacts. The 3D sections are then reconstructed and processed to quantify volume. Fat free volume was calculated by subtracting total fat volume from total body volume (total body volume – (visceral fat volume + subcutaneous fat volume)” (Hossain *et al.*, 2023).

Fasting blood glucose, GTT and ITT, and assessment of insulin sensitivity

“Intra-peritoneal glucose and insulin tolerance tests were performed prior to HFD feeding, after 7 weeks of HFD feeding, and at the end of the experiment (14 weeks of HFD feeding). All experiments were conducted promptly at 10:00 am. Intra-peritoneal injection was chosen for route of administration to avoid administration error that may occur with oral route of administration. For GTT, after a 12-hour overnight fasting period in clean cages containing Alpha-dri paper pulp cellulose animal

bedding, 20% (vol/vol) dextrose was given through an intra-peritoneal injection in a 2 g/kg body weight proportion. Blood glucose levels were measured by tail pinch immediately before and at 15, 30, 60, 90, and 120 minutes after injection using a Bayer Contour blood glucose monitoring system (7097c). For ITT, after a 4-hour daytime fasting period in clean cages containing Alpha-dri paper pulp cellulose animal bedding, 0.75 U/kg body weight insulin (Humalog insulin lispro 100 units/mL) was administered by i.p. injection. Blood glucose was measured at 0, 15, 30, 60, 90, and 120 min in the same manner as stated for GTT. Afterwards blood was collected and centrifuged at 2,000 rpm for 15 min to separate the plasma. Ultra-Sensitive Mouse Insulin ELISA kit (cat. no. 90080, Crystal Chem.) was used to quantify plasma insulin levels as per manufacturer's instructions. Homeostatic model assessment of insulin resistance (HOMA-IR) was calculated as follows: fasting blood glucose (mmol/L) x fasting blood insulin (pmol/L)/ 22.5. Adiponectin was measured using Bio-Plex Pro Mouse Diabetes Adiponectin Assay (BIO-RAD #171F7002M). Levels of adiponectin were used to calculate leptin to adiponectin ratio, an index of insulin sensitivity" (Hossain *et al.*, 2023).

Multiplex immunoassays

"Bio-Plex Pro mouse diabetes immunoassay kit (BIO-RAD) was used to measure multiple markers of mouse diabetes and obesity as per the manufacturers protocol. Briefly, on a black 96-well microplate, magnetic capture antibody coupled beads were washed and incubated with diluted standards, blanks, and samples. This was followed by sequential addition of detection antibodies and Streptavidin-PE

for measurement. Data from the reactions was acquired using Bio-Plex 200 system and analyzed using Bio-Plex Manager 4.1 software” (Hossain *et al.*, 2023).

Seahorse

“Mitochondrial isolation and seahorse assay protocols were optimized in our laboratory and developed from previously published protocols from Agilent Technologies. In short, frozen BAT samples were homogenized in 1X mitochondrial assay buffer (MAS) (mannitol, sucrose, KH_2PO_4 , MgCl_2 , HEPES, EGTA, BSA). Samples were centrifuged at 10,000 xg for 10 min at 4°C. Supernatant was discarded and pellet was resuspended in 1X MAS and centrifuged again at 15,000 xg for 10 min at 4°C. Supernatant was again discarded, and crude mitochondrial extracts were resuspended in 1X MAS and quantified using the Pierce BCA protein assay kit (ThermoFisher, MA, USA). After quantification 20 micrograms of crude mitochondria was loaded into XFe 24 cell micro plate and centrifuged at 2,000xg for 20 minutes at 4°C. During centrifugation drugs were prepared as follows in 1X MAS: ADP (50 mmol/L); oligomycin (50 $\mu\text{mol/L}$); FCCP (50 $\mu\text{mol/L}$); antimycin A/rotenone (100 $\mu\text{mol/L}$ /20 $\mu\text{mol/L}$). For detailed cartridge loading volumes and Seahorse XFe24 assay protocol (equilibration, mix, wait, and measure times) please refer to Sakamuri *et al* (2018). Data is presented in our paper as fold-change from baseline respiration” (Hossain *et al.*, 2023).

qRT-PCR

“Total RNA was extracted from tissue using the miRNeasy Kit (Qiagen, 1038703) according to the manufacturer’s protocol. Complementary DNA (cDNA) was then synthesized from total RNA using the QuantiTect Reverse Transcription Kit

(Qiagen, 205311). Quantitative real time PCR analysis of cDNA was performed in the QuantStudio 5 Real-time PCR System using TaqMan Gene Expression Assays (*Gpr75*: Mm00558537_s1, *Tnf*: Mm00443258_m1, *Cyp4a12*: Mm00514494_m1, *Prdm16*: Mm00712556_m1, *Ppargc1*: Mm01208835_m1, *Ccl5*: Mm01302427_m1, *Mfn1*: Mm00612599_m1, *Ucp1*: Mm01244861_m1, *Actb*: Mm02619580_g1, *Ilf6*: Mm00446190_m1, *Ucp3*: Mm00494074_m1) with the following cycling conditions: 50 °C for 2 min, 95 °C for 10 min, followed by 40 cycles of 95 °C for 15 s and 60 °C for 1 min. Target gene expression was normalized to that of *Actin* and quantitative analyses were conducted using the $\Delta\Delta$ cycle threshold method” (Hossain *et al.*, 2023).

Western blot analysis

“After 14 weeks of diet, tissues were isolated from mice. To extract protein, tissues were homogenized in RIPA lysis buffer and centrifuged at 10,000 RPM for 15 minutes at 4°C. Protein extracts were run in a 4–20% Mini-PROTEAN TGX precast gel (Bio-Rad, Hercules, CA) at 120V for 1 hour, and then transferred onto a PVDF membrane using a Trans Blot Turbo transfer machine (Bio-Rad). Anti-phospho-IR-Tyr-972 (I1783) was purchased from Sigma, while anti-UCP1 (14670S), anti-phospho-Akt-Ser-473 (9271S), anti-Akt (9272S), and β -actin (3700S) were purchased from Cell Signaling Technology. Primary antibodies were diluted in 5% BSA and incubated with membrane overnight, while Li-Cor-specific secondary antibodies were diluted in 5% BSA and incubated with membrane for 2 hours at room temperature. Bands were quantified using Odyssey Application Software version 3.0.21” (Hossain *et al.*, 2023).

Histology

“H&E staining was performed using published protocols. High resolution whole-slides of H&E stained adipose were viewed under 20x magnification using an Echo Revolve microscope (Echo, San Diego, CA) in the bright-field setting. 1000 um x 1000 um pictures were taken of homogeneous areas and analyzed in ImageJ Software. Free-hand drawing tool was used to manually trace all cells and the Adipocyte Tools plugin was used to determine area of each traced object. Scale bar length was manually input into the software to ensure area of traced objects were to scale” (Hossain *et al.*, 2023).

Statistical Analysis

“The study was performed on 92 mice as follows: There were 52 mice that were placed on HFD: males, N= 8 WT, 9 HET, and 11 KO; females, N = 8 per group (WT, HET, KO). There were 40 mice that were placed on CD: males, N= 8 WT, 7 HET, and 7 KO; females N = 6 per group (WT, HET, KO). Statistical comparisons were performed using ANOVA and *post-hoc* Tukey’s test using Graph Pad Prism version 9.2.0 software. Energy expenditure data were also processed to analyze group and body size effects using ANCOVA. Primarily, figures are presented as dot plots indicating individual values with the mean and standard error of the mean (SEM). We (a) randomly distributed WT and *Gpr75*-genetically modified mice in different experimental groups; (b) performed all the studies in a blinded fashion; and (c) conducted each *in vitro* assay in duplicate with appropriate n-values” (Hossain *et al.*, 2023).

Results

Aim 1: To determine whether deficiencies in *Gpr75* genomic expression impact high fat diet-driven obesity and glucose handling

Mice with genomic *Gpr75* deletion generated by Regeneron Pharmaceuticals are on a C57Bl/6NTacXSW background and morphologically similar to wild-type animals at 8-10 weeks of age (age at start of experiment). The initial body weights of all genotypes were comparable averaging 20.71 ± 1.27 and 18.45 ± 1.68 grams for males and females, respectively. Regular chow diet feeding for 14 weeks showed that all three genotypes gained similar amounts of weight averaging 5.74 ± 0.12 and 5.16 ± 0.13 grams for males and females respectively (**Figure 6A-B, 7A-B**). However, 14 weeks of HFD feeding caused a divergence in weight between genotypes in an allele dependent manner, with male and female mice showing similar trends. Male WT mice more than doubled their weight (2.46-fold, change in body weight from baseline 29.32 ± 1.65 grams), while corresponding HET and KO mice added about 85% and 65% to their weights (change in body weight from baseline 19.42 ± 1.67 and 12.71 ± 1.15 grams for HET and KO respectively) (**Figure 8A-B**). This pattern of weight gain was similar in female mice albeit the difference between the genotypes was more pronounced; female WT mice doubled their weight, while HET and KO mice added 50% and 14% to their weight, respectively (change in body weight from baseline 16.70 ± 0.83 , 8.57 ± 1.37 , 5.87 ± 0.28 grams for WT, HET, and KO respectively) (**Figure 9A-B**) (Hossain *et al.*, 2023).

Figure 6

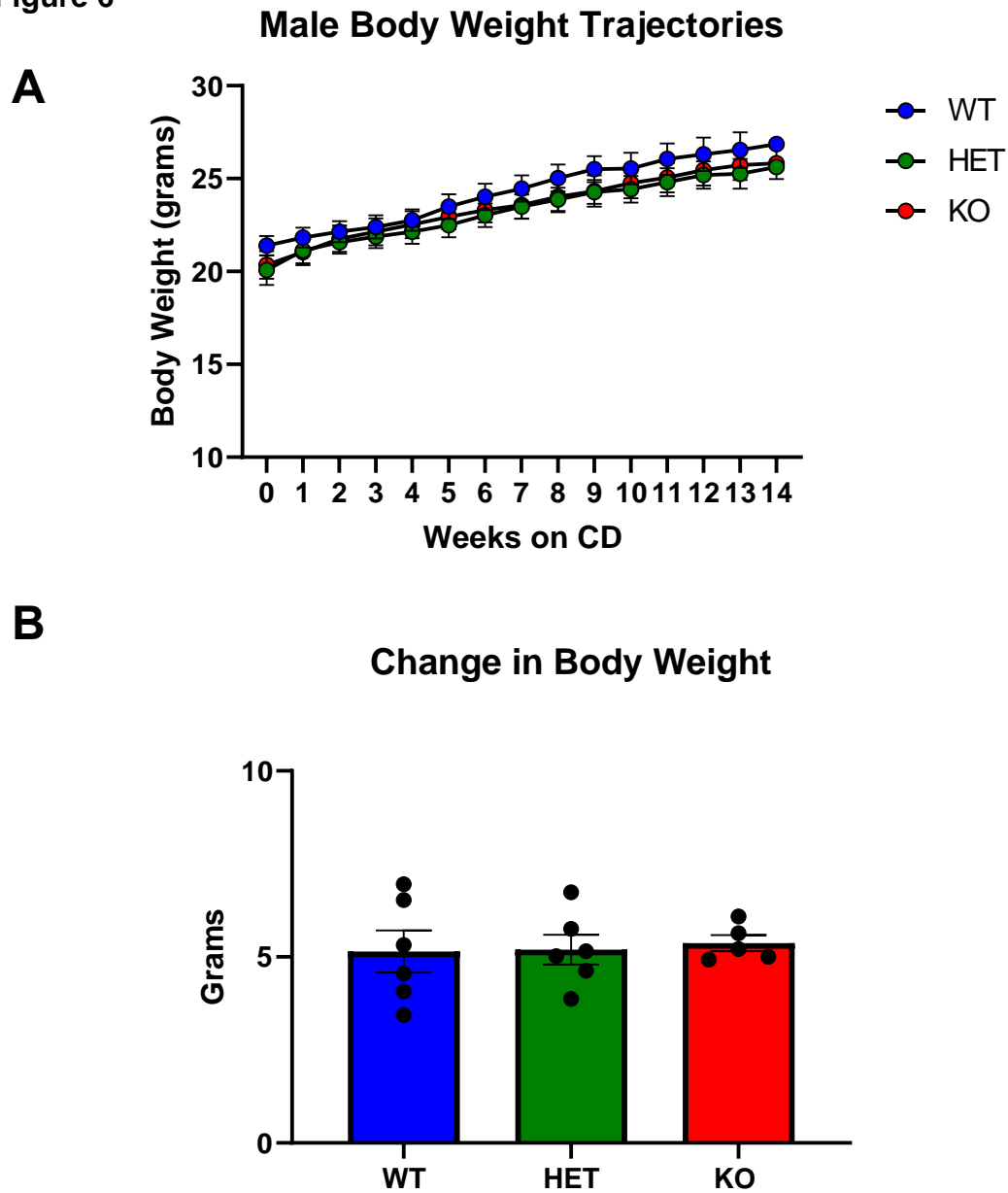
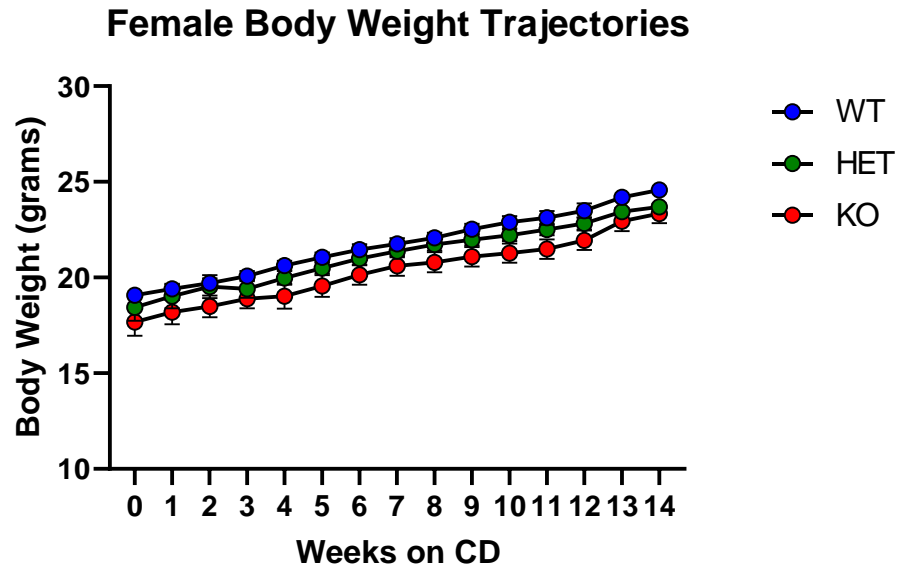


Figure 6: Male mice with *Gpr75* deficiency show no differences in weight gain after 14 weeks of control diet (CD) feeding (Hossain *et al.*, 2023).

(A) Body weight trajectories for male (n=5-6) WT, HET, and KO mice over the course of 14 weeks of CD-feeding **(B)** Overall change in body weight. Results are mean \pm SE, ns, not significant by two-way ANOVA with Tukey's multiple comparison test (Hossain *et al.*, 2023).

Figure 7

A



B

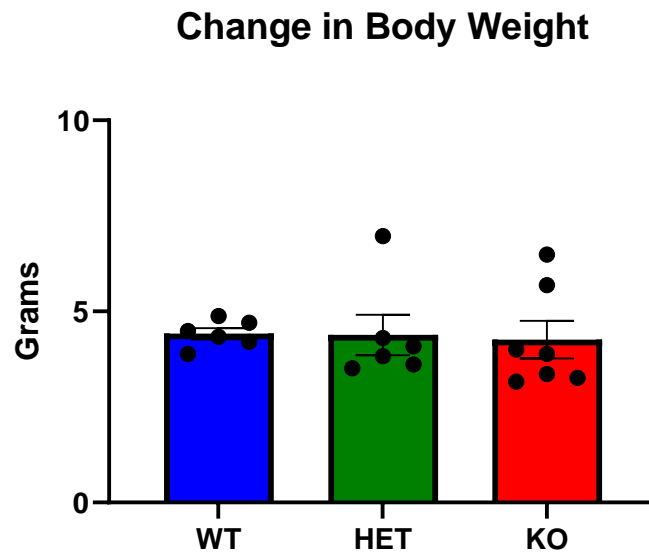


Figure 7: Female mice with *Gpr75* deficiency show no differences in weight gain after 14 weeks of control diet (CD) feeding (Hossain et al., 2023).

(A) Body weight trajectories for female (n=6-7) WT, HET, and KO mice over the course of 14 weeks of CD-feeding **(B)** Overall change in body weight. Results are mean \pm SE, ns, not significant by two-way ANOVA with Tukey's multiple comparison test (Hossain et al., 2023).

Figure 8

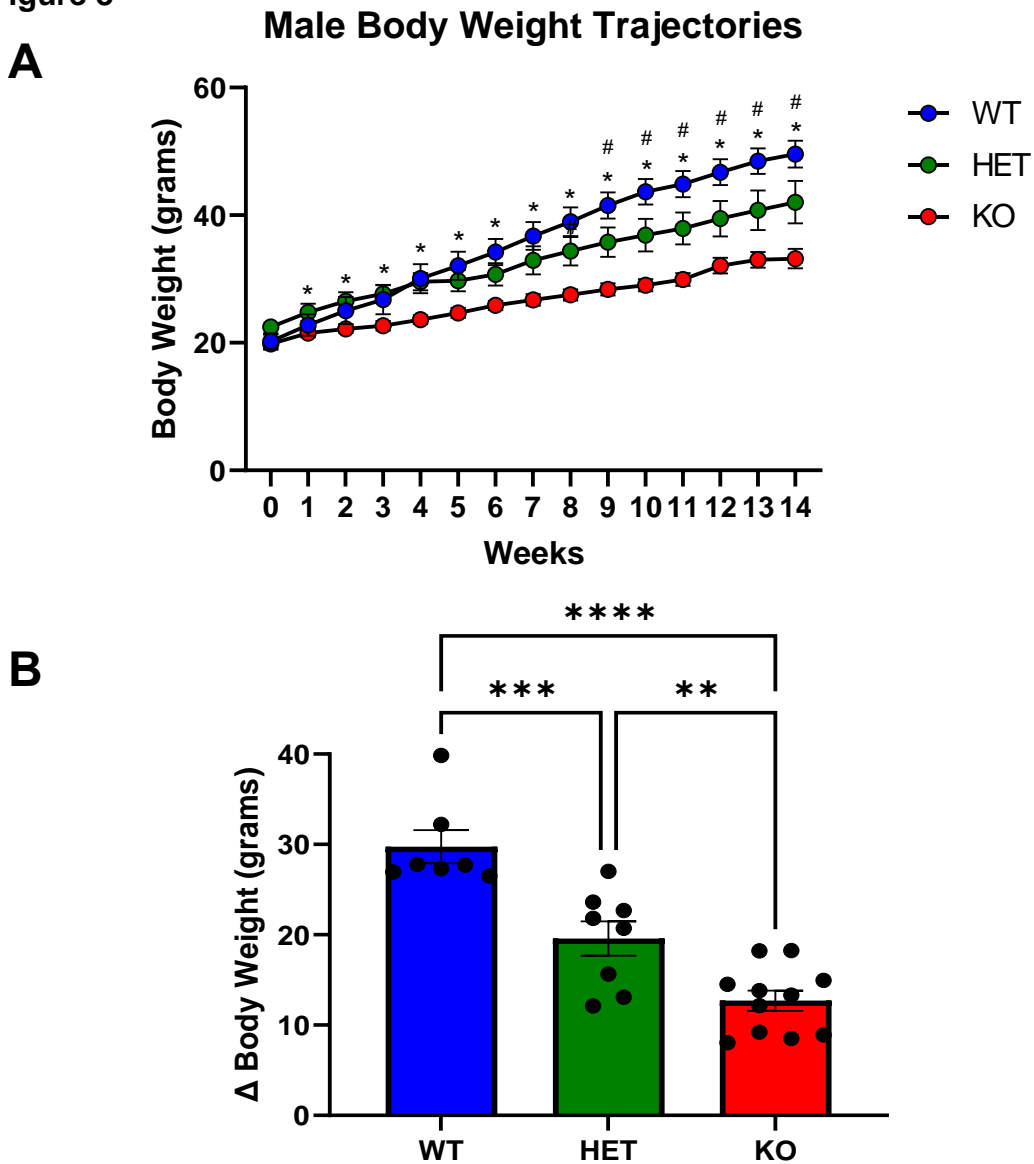
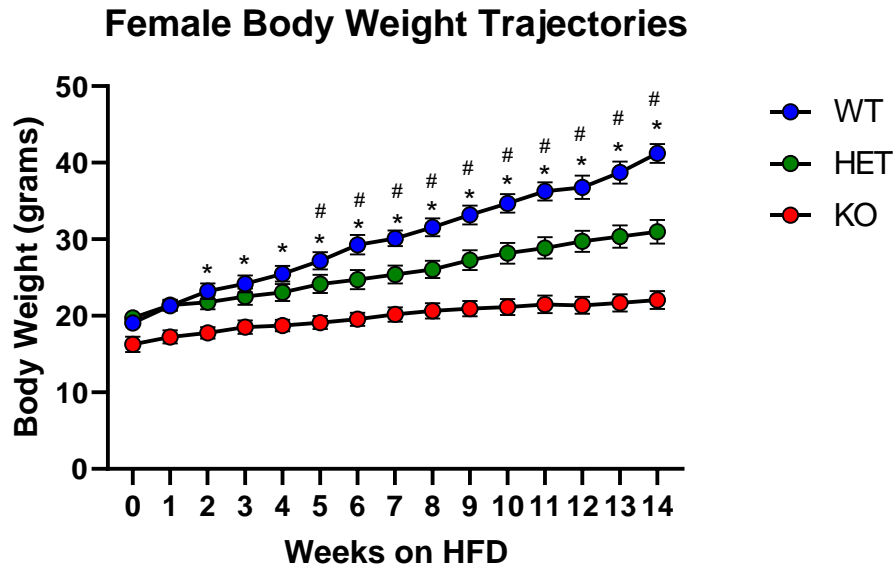


Figure 8: Male mice with *Gpr75* deficiency have attenuated weight gain after HFD-feeding (Hossain et al., 2023).

(A) Body weight trajectories for WT, HET, and KO mice (n=7-8) over the course of 14 weeks of HFD-feeding. **(B)** Total change in body weight from baseline after 14 weeks of HFD-feeding. Results are mean±SE, ns, not significant; **p<0.01, *** P<0.001 and ****p<0.0001 by two-way ANOVA with Tukey's multiple comparison test (Hossain et al., 2023).

Figure 9

A



B

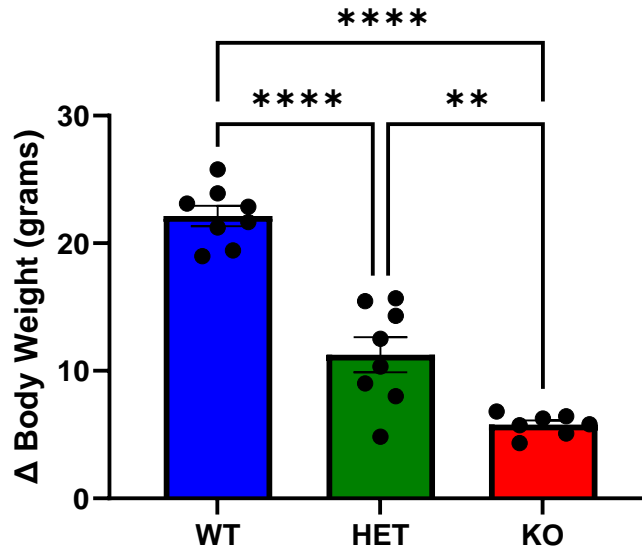


Figure 9: Female mice with *Gpr75* deficiency have attenuated weight gain after HFD-feeding (Hossain et al., 2023).

(A) Body weight trajectories for WT, HET, and KO mice (n=8) over the course of 14 weeks of HFD-feeding. **(B)** Total change in body weight from baseline after 14 weeks of HFD-feeding. Results are mean±SE, ns, not significant; **p<0.01, ***P<0.001 and ****p<0.0001 by two-way ANOVA with Tukey's multiple comparison test (Hossain et al., 2023).

Body composition analysis by microCT allowed us to quantitatively measure differences in visceral (VAT) and subcutaneous adipose tissue (SAT) volumes at baseline and throughout the HFD feeding period, which revealed striking differences between genotypes. At baseline there were no significant differences in VAT volume between genotypes regardless of sex, 698.75 ± 27.82 , 743.22 ± 43.33 , and 646.92 ± 76.95 mm³ for WT, HET, and KO males; 377.75 ± 14.91 , 352.96 ± 36.28 , and 287.67 ± 29.20 mm³ for WT, HET, and KO females. HFD feeding increased VAT volume by 9-fold for male WT mice whereas the volume increases in HET and especially in KO were largely attenuated, 8420.51 ± 293.87 , 6536.42 ± 290.49 , and 4065.35 ± 279.96 mm³ for WT, HET, and KO respectively (**Figure 10A-B**). Similarly, VAT volume increased significantly (10-fold) in HFD fed female WT mice to 7634.08 ± 298.40 mm³. In contrast, female HET mice displayed attenuated increases amounting to 50% of that seen in WT, whereas female KO mice VAT volume was largely unchanged, 3824.29 ± 234.65 and 1075.18 ± 91.07 mm³ respectively (**Figure 11A-B**). A similar trend was seen in SAT, where HFD feeding increased SAT volume in WT by 12- and 18-folds for males and females respectively (**Figure 10C and 11C**). This was compared to 4- and 2-fold increases for male and female KO mice (**Figure 10C and 11C**). Surprisingly, when we calculated fat-free volume by subtracting fat volume from total body volume we saw no differences between WT and KO at baseline and after HFD-feeding (**Figure 12A-B**). This suggests that the increase in body weight seen in WT mice was primarily due to increased fat volume (Hossain et al., 2023).

Figure 10

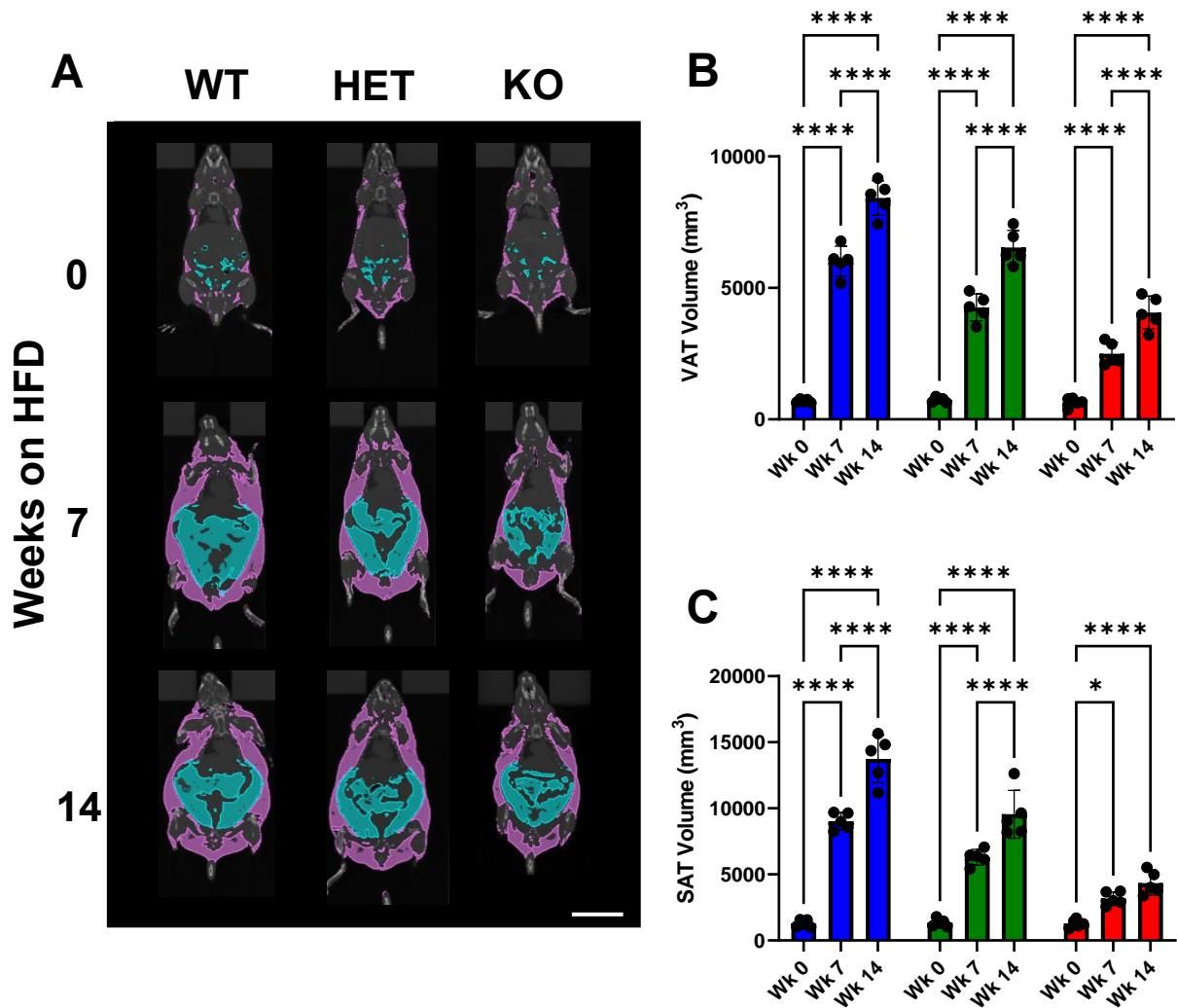


Figure 10: Male mice with *Gpr75* deficiency have attenuated fat mass accumulation over 14-weeks of HFD (Hossain et al., 2023).

(A) Representative microCT images of male WT, HET, and KO mice at weeks 0, 7 and 14 of HFD feeding (blue, visceral fat (VAT); purple, subcutaneous fat (SAT); scale bar = 20 mm). **(B-C)** VAT and SAT volumes at baseline, week 7, and week 14 mice. Results are mean±SE, ns, not significant; **p<0.01, *** P<0.001 and ****p<0.0001 by two-way ANOVA with Tukey’s multiple comparison test (Hossain et al., 2023).

Figure 11

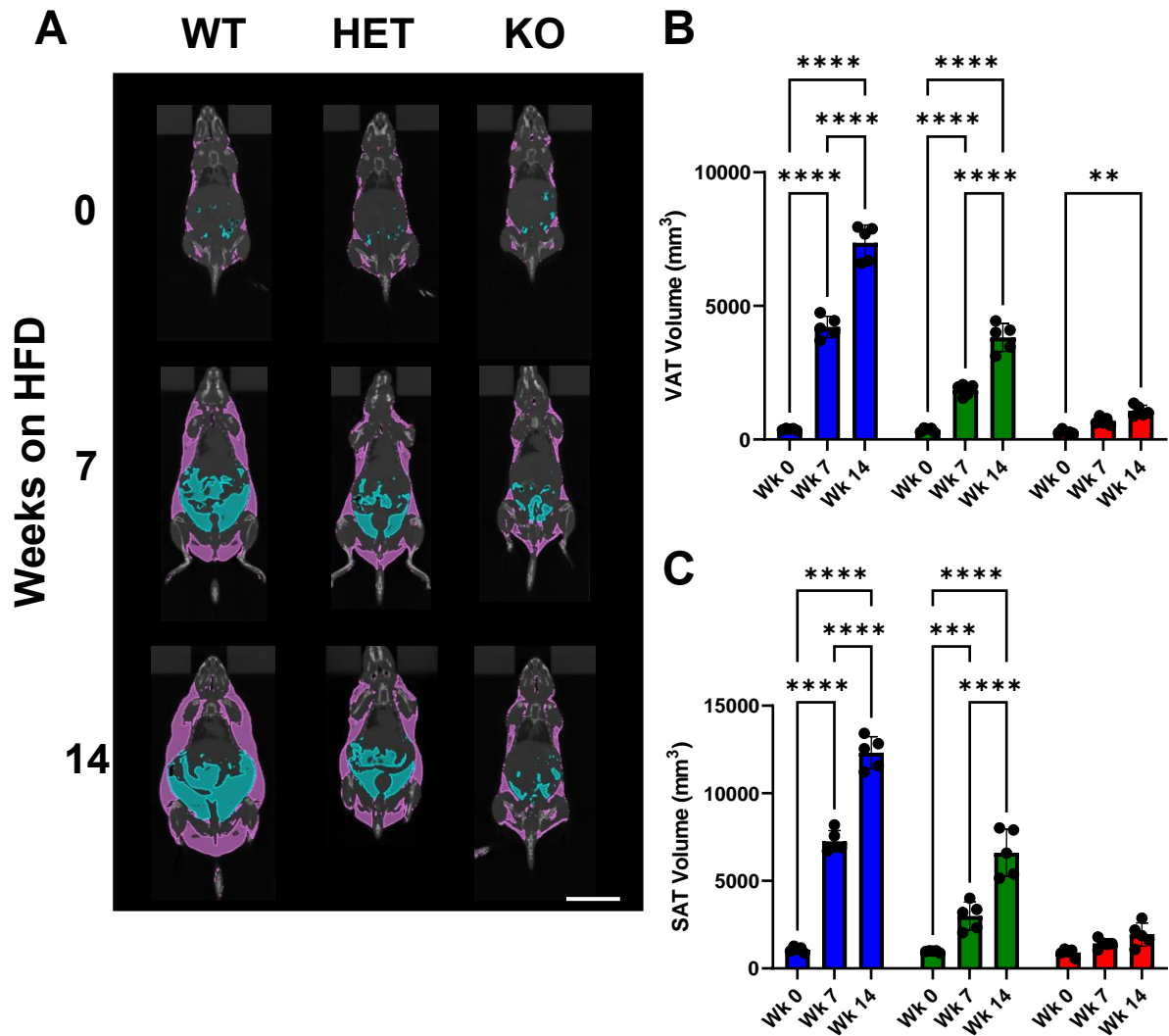


Figure 11: Female mice with *Gpr75* deficiency have attenuated fat mass accumulation over 14-weeks of HFD (Hossain et al., 2023).

(A) Representative microCT images of female WT, HET, and KO mice at weeks 0, 7 and 14 of HFD feeding (blue, visceral fat (VAT); purple, subcutaneous fat (SAT); scale bar = 20 mm). (B-C) VAT and SAT volumes at baseline, week 7, and week 14 mice. Results are mean \pm SE, ns, not significant; ** p <0.01, *** P <0.001 and **** p <0.0001 by two-way ANOVA with Tukey's multiple comparison test (Hossain et al., 2023).

Figure 12

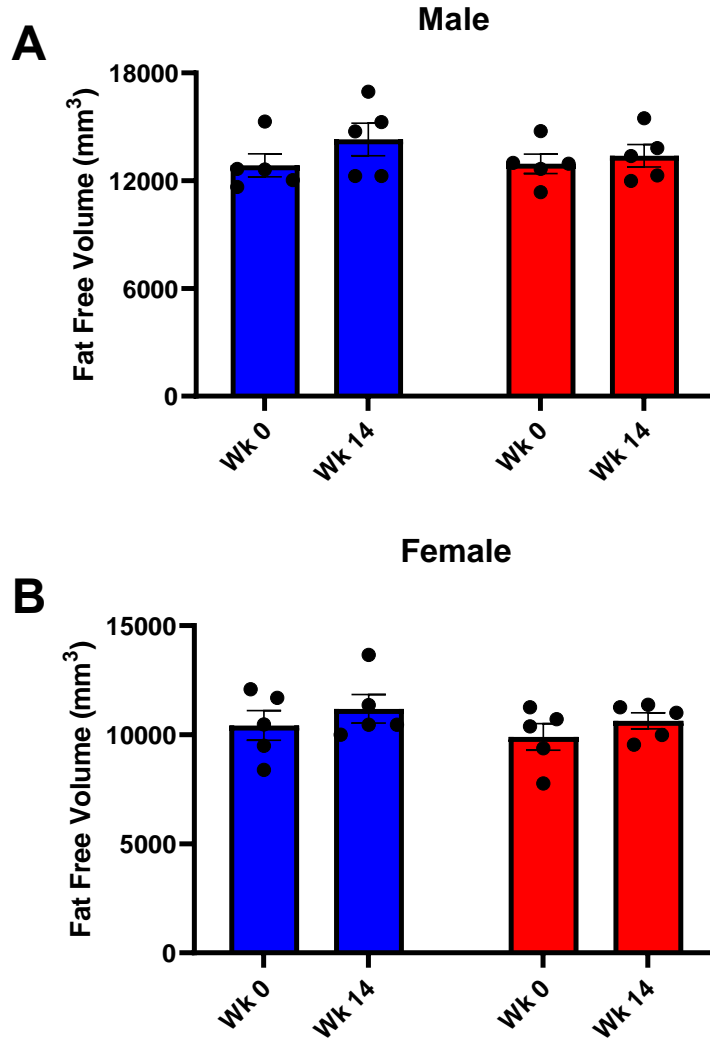


Figure 12: *Gpr75* deficient mice show no differences in fat free mass at baseline or after 14-weeks of HFD compared to WT (Hossain et al., 2023).

Fat free mass (volume) calculated from the microCT images as total body volume - fat volume (VAT+SAT) in male **(A)** and female **(B)** WT and KO mice at week 0 and week 14. Results are mean \pm SE; ns, not significant; ** $p < 0.01$, *** $P < 0.001$ and **** $p < 0.0001$ by two-way ANOVA with Tukey's multiple comparison test (Hossain et al., 2023).

H&E staining of VAT, SAT, and BAT sections showed no morphological differences between WT and KO mice at baseline regardless of sex, particularly there were no differences in adipocyte size. However, after 14 weeks of HFD feeding, adipocyte size from VAT and SAT sections of male WT mice markedly increased (3-fold) to 9396.124 ± 433.37 and $8642.198 \pm 240.65 \mu\text{m}^2$ respectively (**Figure 13A-C**). Male KO adipocytes were significantly smaller in size compared to WT, 4462.05 ± 460.49 and $4118.62 \pm 676.76 \mu\text{m}^2$ for VAT and SAT respectively (**Figure 13A-C**). A similar trend was seen in female mice, where VAT and SAT of WT mice increased significantly after HFD feeding to 5921.307 ± 551.219 and $5783.41 \pm 233.19 \mu\text{m}^2$ respectively (**Figure 14A-C**). Female KO adipocyte size was largely unchanged from baseline in both VAT and SAT, 2556.162 ± 175.20 and $2843.828 \pm 325.186 \mu\text{m}^2$ respectively (**Figure 14A-C**). H&E staining of BAT sections show that WT adipocytes obtain large lipid droplets after HFD feeding, which were much smaller and fewer in number in KO BAT sections regardless of sex (**Figure 13A and 14A**) (Hossain et al., 2023).

Figure 13

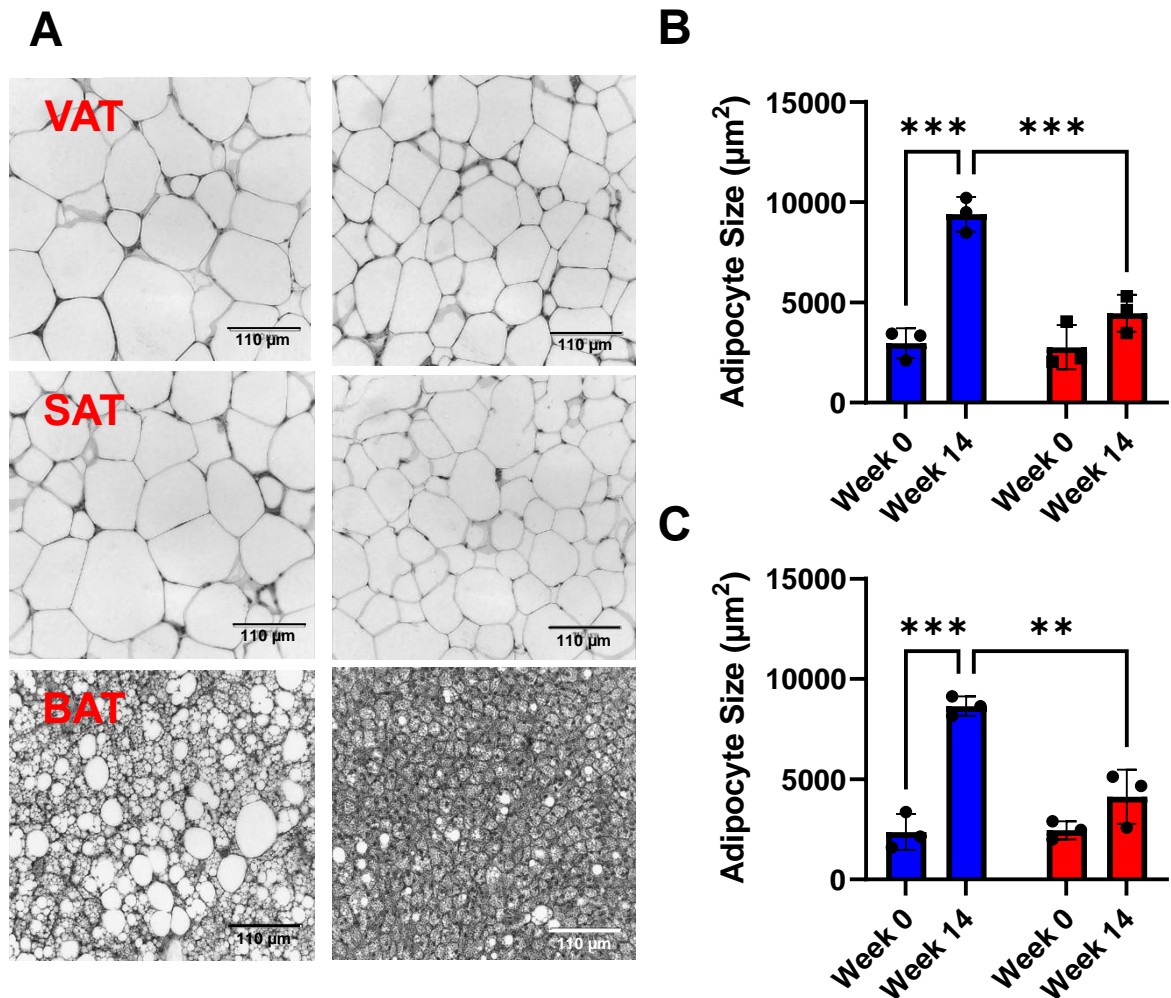


Figure 13: VAT, SAT, and BAT sections of male *Gpr75* deficient mice have smaller adipocytes compared to WT mice after HFD-feeding (Hossain et al., 2023).

(A) Representative H&E staining (B-C) Visceral and subcutaneous adipocyte size analysis at baseline and week 14 of HFD. Results are mean±SE (n=4); ns, not significant; **p<0.01, *** P<0.001 and ****p<0.0001 by two-way ANOVA with Tukey's multiple comparison test (Hossain et al., 2023).

Figure 14

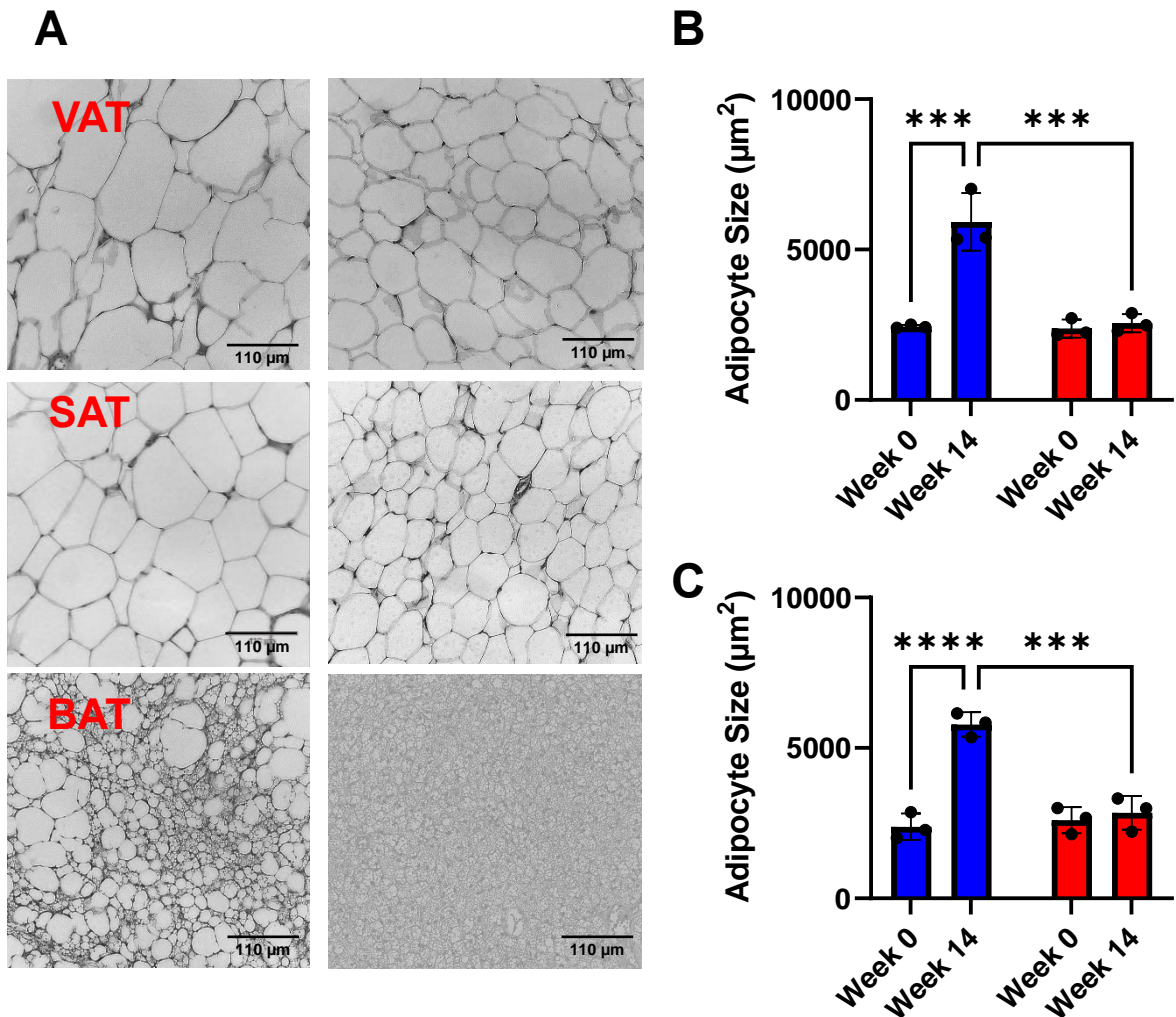


Figure 14: VAT, SAT, and BAT sections of female *Gpr75* deficient mice have smaller adipocytes compared to WT mice after HFD-feeding (Hossain et al., 2023).

(A) Representative H&E staining (B-C) Visceral and subcutaneous adipocyte size analysis at baseline and week 14 of HFD. Results are mean±SE (n=4); ns, not significant; **p<0.01, *** P<0.001 and ****p<0.0001 by two-way ANOVA with Tukey's multiple comparison test (Hossain et al., 2023).

Leptin is an adipokine that regulates many physiological processes from food intake and nonshivering thermogenesis to reproduction and angiogenesis. Its actions are mediated by the LepRb receptor in the hypothalamus. Leptin tends to have a paradoxical role in obesity – low levels of leptin are associated with high food intake and obesity development, while high levels of leptin are associated with leptin resistance and obesity as well. Our data shows that 14 weeks of chow diet feeding results in no differences in plasma leptin levels between genotypes, 1236.36 ± 114.035 , 1475.27 ± 139.47 , and 1253.041 ± 100.42 ng/mL for WT, HET, and KO respectively (**Figure 15A**). However, 14 weeks of HFD feeding caused a 31-fold increase in plasma leptin for WT mice (**Figure 15A**). HFD feeding caused significantly attenuated increases in plasma leptin for HET and KO, 14- and 6-fold respectively (**Figure 15A**).

Adiponectin is another adipokine that has been shown to have robust insulin sensitizing effects. In fact, doxycycline inducible deletion of adiponectin in mature adipocytes impairs glucose tolerance, while AdipoR1 agonists have been shown to ameliorate diabetes in obese rodent models. Our data shows that 14 weeks of chow diet feeding results in no significant differences in plasma adiponectin between genotypes. After HFD feeding plasma adiponectin levels were higher in both HET and KO mice, by 51 and 58% respectively, compared to corresponding mice on control diet and WT mice on HFD (**Figure 15B**). HFD fed WT mice had 7-fold higher values of leptin-to-adiponectin (**Figure 15C**) (Hossain et al., 2023).

Resistin is another adipokine linked to obesity. While its exact role in the development of insulin resistance is unknown, numerous studies have shown high serum levels of resistin in obese and diabetic patients. Our data showed no

differences in plasma resistin after CD feeding 97228.8 ± 16909.25 , 65670.04 ± 15409.62 , and 83660.09 ± 6034.9 pg/mL for WT, HET, and KO respectively (**Figure 16A**). 14 weeks of HFD feeding increased levels to 174314.2 ± 15409.62 , 138677.3 ± 10068.58 , and 132712.1 ± 11310.95 pg/mL for WT, HET, and KO respectively (**Figure 16A**). Likewise, plasma levels of plasminogen activator inhibitor-1 (PAI-1), which has been characterized as a functional biomarker of metabolic syndrome, showed no differences between genotypes after CD feeding. However, after 14 weeks of HFD feeding WT mice displayed a 2-fold increase, which was not seen in HET or KO mice, 1320.063 ± 181.39 , 530.56 ± 42.64 , and 443.23 ± 79.668 pg/mL for WT, HET, and KO respectively (**Figure 16B**) (Hossain et al., 2023).

Figure 15

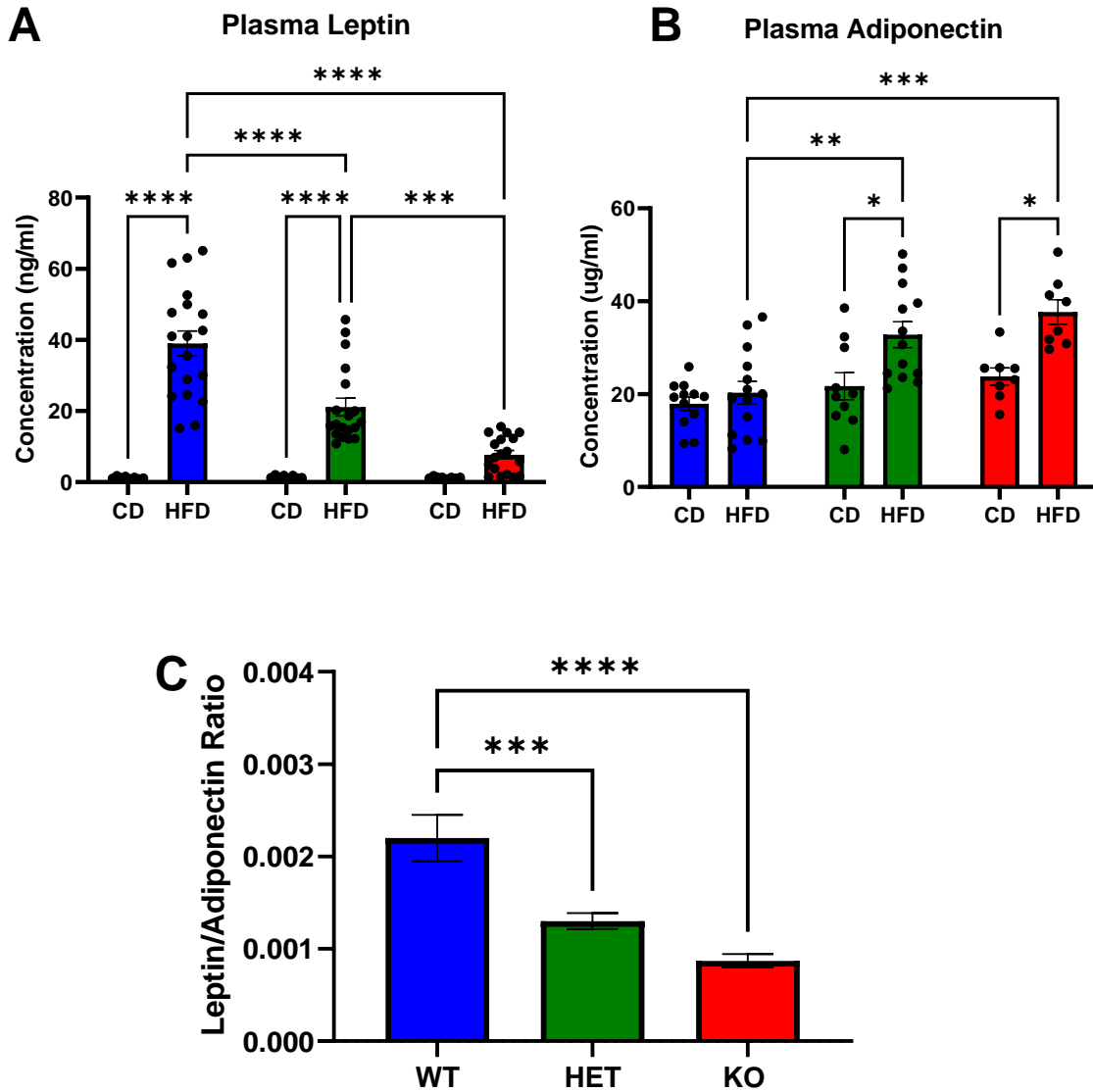


Figure 15: *Gpr75* deficiency prevents HFD-induced adipose tissue dysfunction (Hossain et al., 2023).

Plasma leptin **(A)** and **(B)** adiponectin after 14 weeks of chow (CD) or HFD feeding in WT, HET, and KO mice. **(C)** Leptin-adiponectin ratio after 14 weeks of HFD feeding. Results are mean \pm SE (n=10-20); ns, not significant; **p<0.01, *** P<0.001 and ****p<0.0001 by two-way ANOVA with Tukey's multiple comparison test (Hossain et al., 2023).

Figure 16

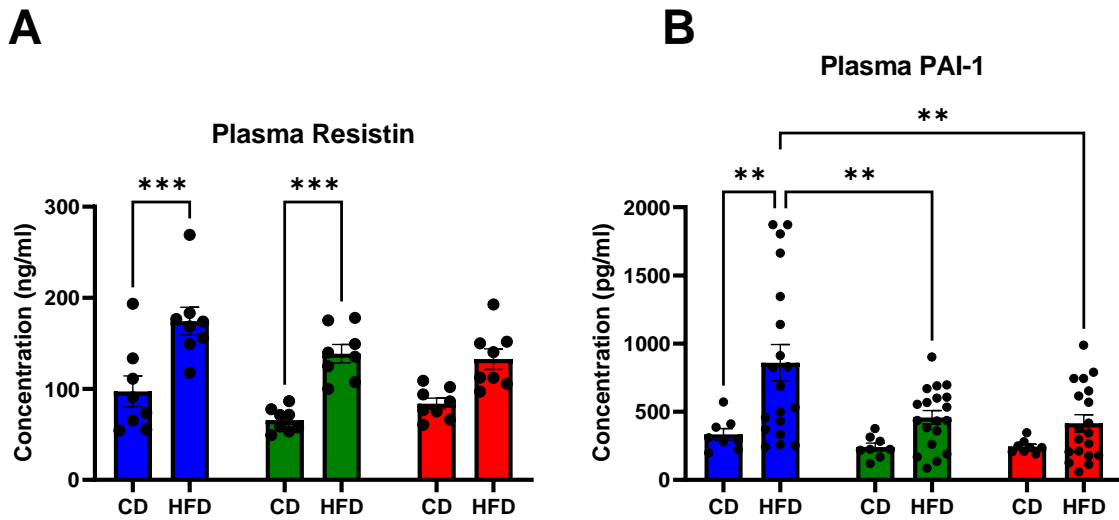


Figure 16: *Gpr75* deficiency prevents HFD-induced adipose tissue dysfunction cont. (Hossain et al., 2023).

Plasma resistin (A) and (B) PAI-1 after 14 weeks of chow (CD) or HFD feeding in WT, HET, and KO mice. Results are mean \pm SE (n=10-20); ns, not significant; **p<0.01, ***P<0.001 and ****p<0.0001 by two-way ANOVA with Tukey's multiple comparison test (Hossain et al., 2023).

All genotypes showed similar levels of fasting blood glucose (FBS) at baseline with male WT, HET, and KO mice at 119 ± 7 , 120 ± 7 and 125 ± 9 mg/dL, respectively, and female mice at 102 ± 3 , 99 ± 3 and 100 ± 3 mg/dL, respectively (**Figure 17A-B**). FBS significantly increased in all genotypes at weeks 7 and 14 of HFD feeding, although the increases were attenuated in HET and even more significantly so in KO mice regardless of sex. FBS levels after 14 weeks of HFD feeding were 232 ± 7 , 195 ± 7 and 172 ± 6 mg/dL for WT, HET, and KO males, respectively (**Figure 17A-B**). Surprisingly, female KO mice experienced no hyperglycemia in response to HFD feeding; 167 ± 4 , 129 ± 5 and 109 ± 2 mg/dL for WT, HET, and KO, respectively (**Figure 17A-B**) (Hossain et al., 2023).

Figure 17

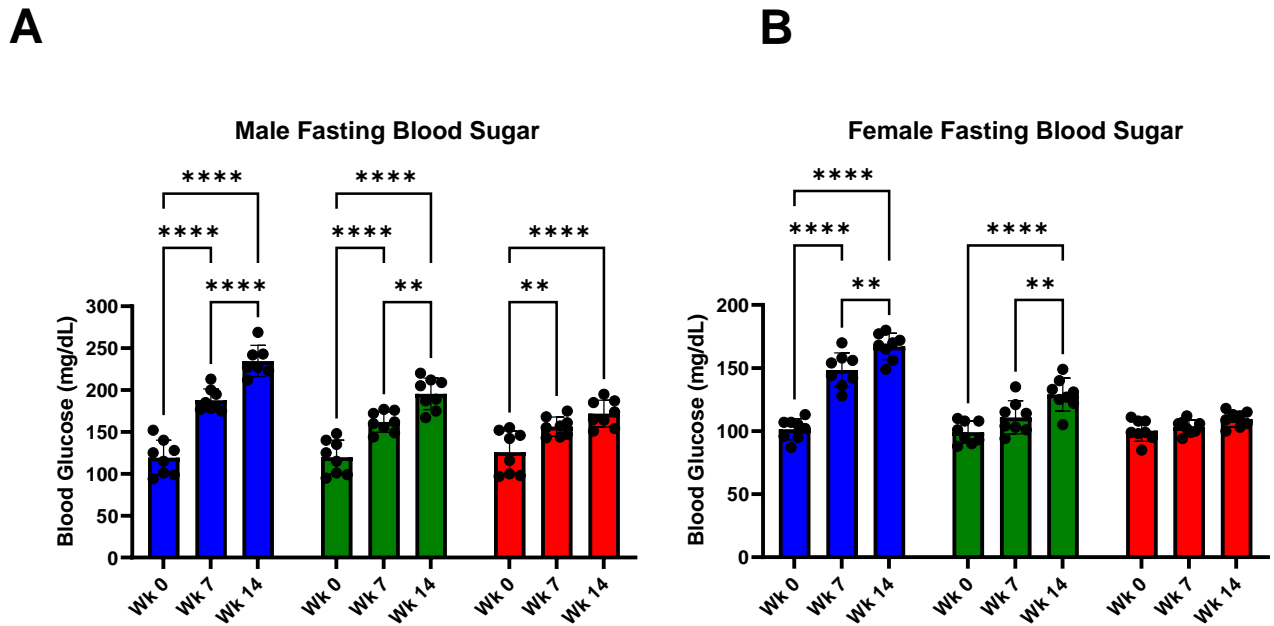


Figure 17: *Gpr75* deficiency attenuates HFD-induced increases in fasting blood sugar (FBS) (Hossain et al., 2023).

Twelve-hour fasting blood glucose of (A) males and (B) female WT, HET, and KO mice at weeks 0, 7 and 14 of HFD feeding. Results are mean \pm SE (n=8); ns, not significant; **p<0.01, *** P<0.001 and ****p<0.0001 by two-way ANOVA with Tukey's multiple comparison test (Hossain et al., 2023).

Since T2DM is characterized by an inability to clear glucose from the blood, an intraperitoneal glucose tolerance test was performed. **Figure 18A-C** shows measured blood glucose values for male WT, HET, and KO mice over a 120-minute interval post glucose challenge at weeks 0, 7, and 14 of HFD feeding. Area under the curve (AUC) analysis shows that male WT mice had a significant increase in AUC from week 0 to 14, 1225 ± 55.03 vs 2669 ± 65.69 . Male KO mice did not show significant increases in AUC from week 0 to 14, 1182 ± 63 vs 1988 ± 182 (**Figure 18D-F**). This indicates that *Gpr75*-deficiency attenuates HFD-induced impairment in glucose clearance seen in WT animals. Similar trends were observed in female mice, with WT mice showing significant increases in AUC from week 0 to 14, 1098 ± 63.14 vs 2366 ± 49 . While KO mice were largely protected, 1065 ± 39.66 vs 1307 ± 79 for week 0 and week 14 respectively (**Figure 19A-F**) (Hossain et al., 2023).

Figure 18

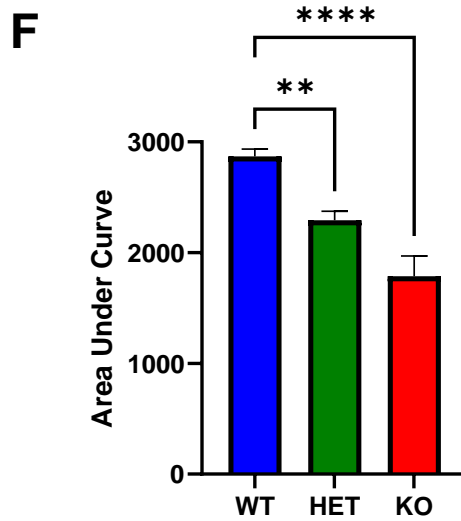
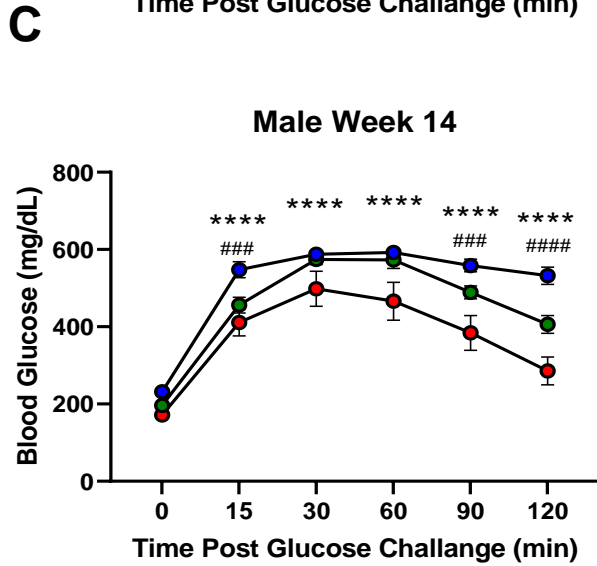
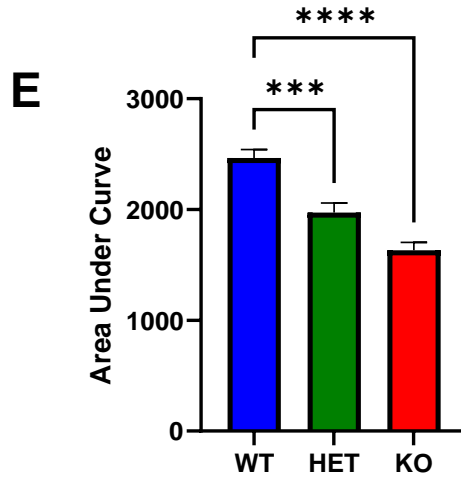
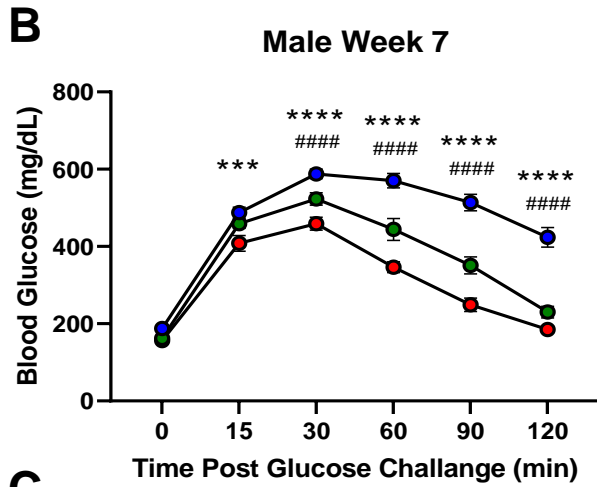
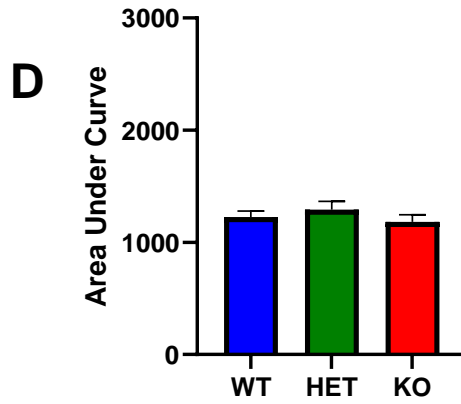
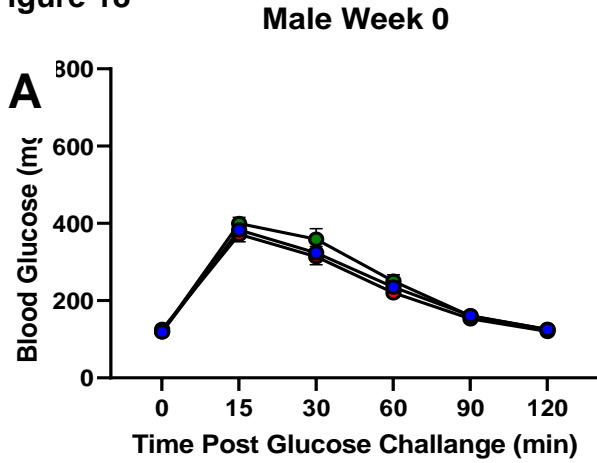


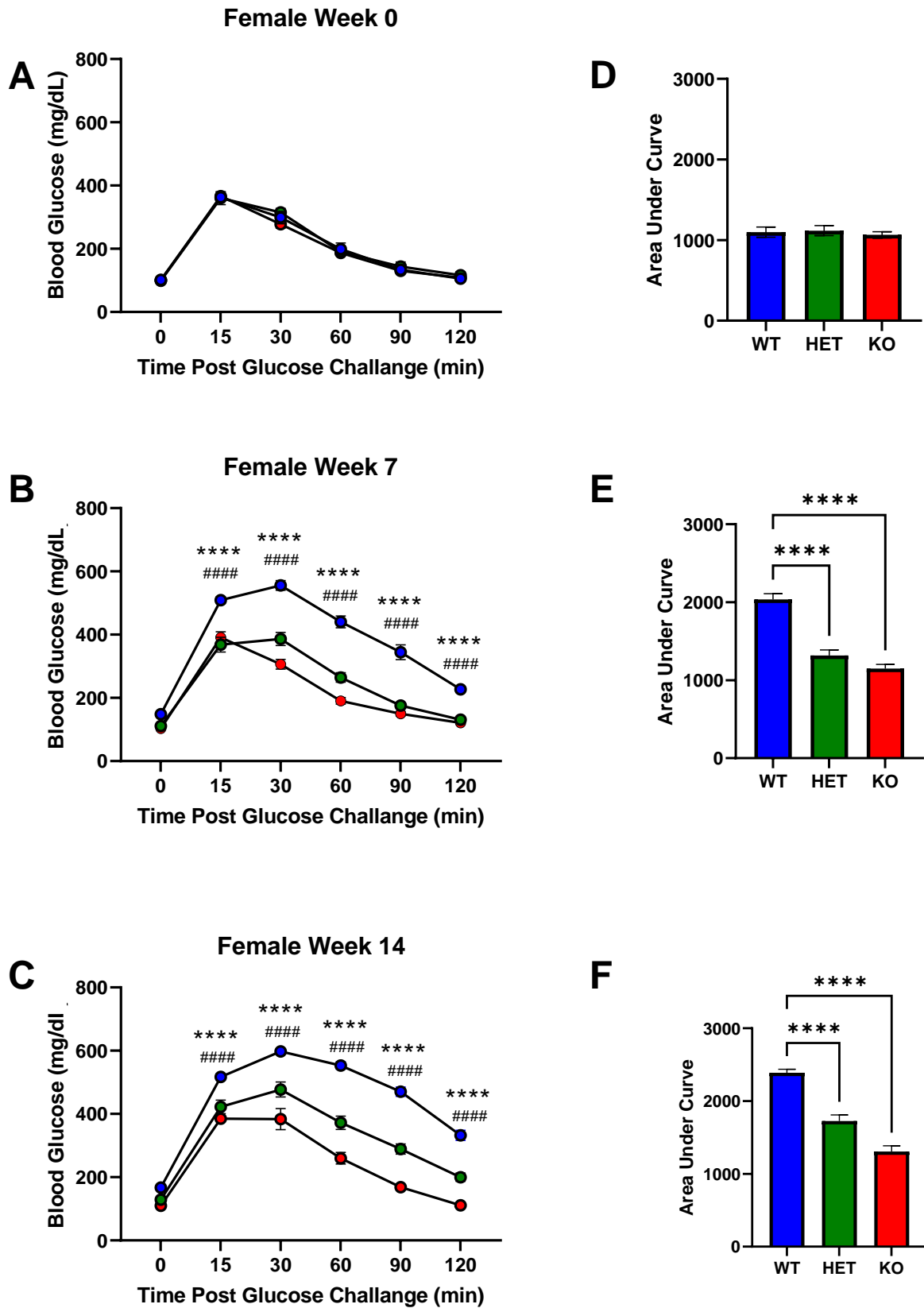
Figure 18 (above): *Gpr75* deficiency attenuates HFD-induced impairment of glucose clearance after glucose challenge in males (Hossain et al., 2023).

(A-C) Glucose tolerance test (GTT) as percent change from baseline for WT, HET, and KO males at weeks 0, 7 and 14 of HFD feeding. **(D-F)** Area under curve analysis. Results are mean±SE (n=8); ns, not significant; **p<0.01, *** P<0.001 and ****p<0.0001 by two-way ANOVA with Tukey's multiple comparison test (Hossain et al., 2023).

Figure 19 (below): *Gpr75* deficiency attenuates HFD-induced impairment of glucose clearance after glucose challenge in females (Hossain et al., 2023).

(A-C) Glucose tolerance test (GTT) as percent change from baseline for WT, HET, and KO females at weeks 0, 7 and 14 of HFD feeding. **(D-F)** Area under curve analysis. Results are mean±SE (n=8); ns, not significant; **p<0.01, *** P<0.001 and ****p<0.0001 by two-way ANOVA with Tukey's multiple comparison test (Hossain et al., 2023).

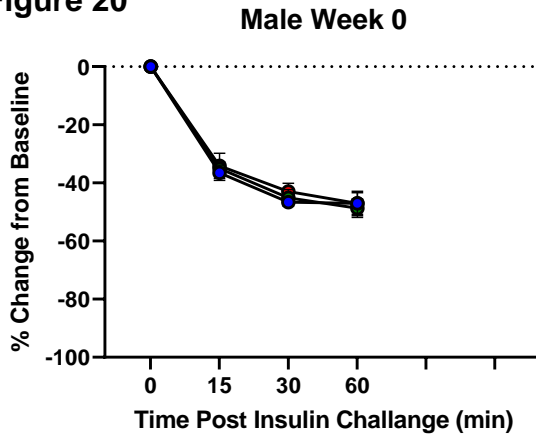
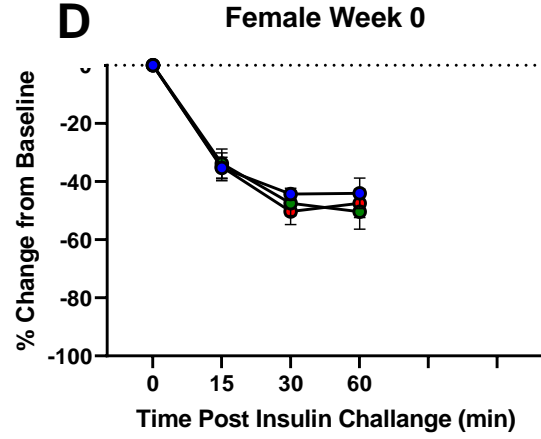
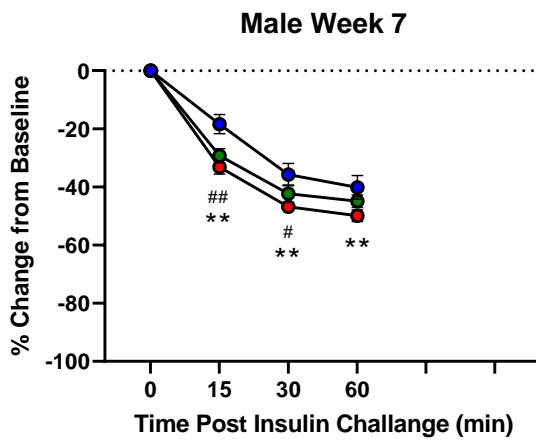
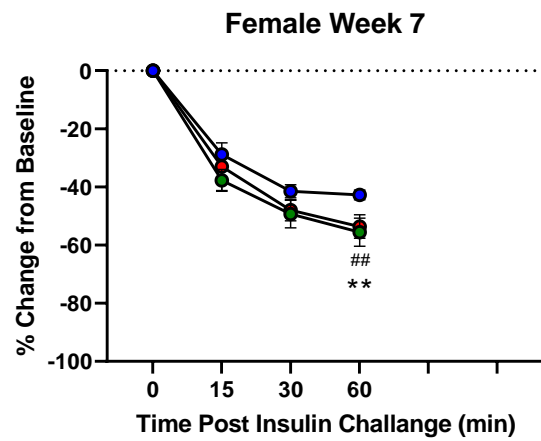
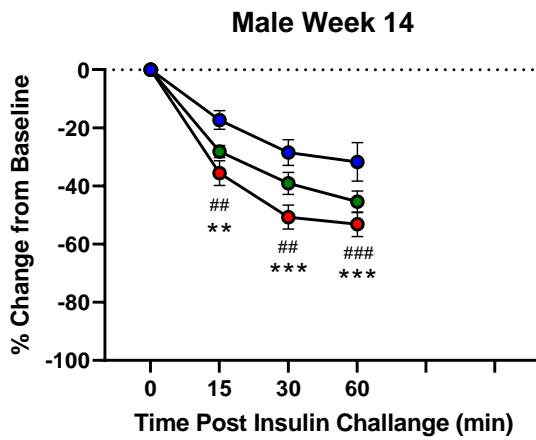
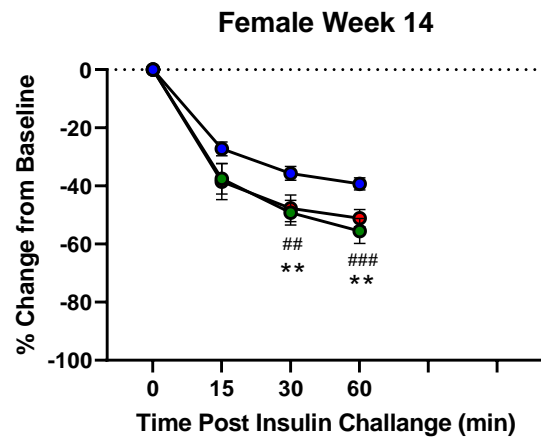
Figure 19



To further assess the HFD-induced impairment in glucose clearance seen in WT mice, an intraperitoneal insulin tolerance test was performed. **Figure 20A-C** shows measured blood glucose values for male WT, HET, and KO mice over a 120-minute interval post insulin challenge at weeks 0, 7, and 14 of HFD feeding. Again, area under the curve (AUC) analysis shows that male WT mice had a significant increase in AUC from week 0 to 14, while KO animals did not, 423.5 ± 14.04 vs 831.3 ± 58.12 and 431 ± 15 vs 412 ± 27 for WT and KO respectively (**not shown**). This indicates that HFD-feeding causes impairment in glucose clearance in WT mice even in the presence of insulin (i.e., insulin resistance). HET and KO mice showed significantly attenuated insulin resistance in an allele-dependent manner compared to WT mice. A similar pattern was seen in female mice with WT mice showing significant increases in AUC from week 0 to 14, 414.20 ± 23.22 vs 594.9 ± 17.63 and 369 ± 20 vs 372 ± 19 for WT and KO respectively (**Figure 20D-F**) (Hossain et al., 2023).

Figure 20 (below): *Gpr75* deficiency attenuates HFD-induced impairment of glucose clearance after insulin challenge (Hossain et al., 2023).

Insulin tolerance test (ITT) as percent change from baseline for WT, HET, and KO males (**A-C**) and females (**D-F**) at weeks 0, 7 and 14 of HFD feeding. (**D**) Area under curve analysis. Results are mean \pm SE (n=8); ns, not significant; **p<0.01, ***P<0.001 and ****p<0.0001 by two-way ANOVA with Tukey's multiple comparison test (Hossain et al., 2023).

A**Figure 20****D****B****E****C****F**

After 14 weeks of control diet feeding plasma insulin was not different between all three genotypes 2189 ± 106.08 , 2819 ± 361.91 , and 2136 ± 420 ng/mL for WT, HET, and KO respectively. However, in response to HFD feeding, levels of insulin rose by 6-fold in WT mice to 13288.06 ± 1582.211 ng/mL (**Figure 21A**). HET and KO mice displayed an attenuated increase in an allele-dependent manner. HFD-fed KO mice had plasma insulin levels rise by only 2-fold to 5195 ± 696.01 ng/mL (**Figure 21A**). Measurement of HOMA-IR, commonly used as an indices of insulin sensitivity, further indicated that *Gpr75* deficiency protects against the development of insulin resistance. Hence, HFD-fed WT mice displayed 3.5-fold higher HOMA-IR value than HFD-fed HET and KO mice (**Figure 21B**) (Hossain et al., 2023).

Figure 21

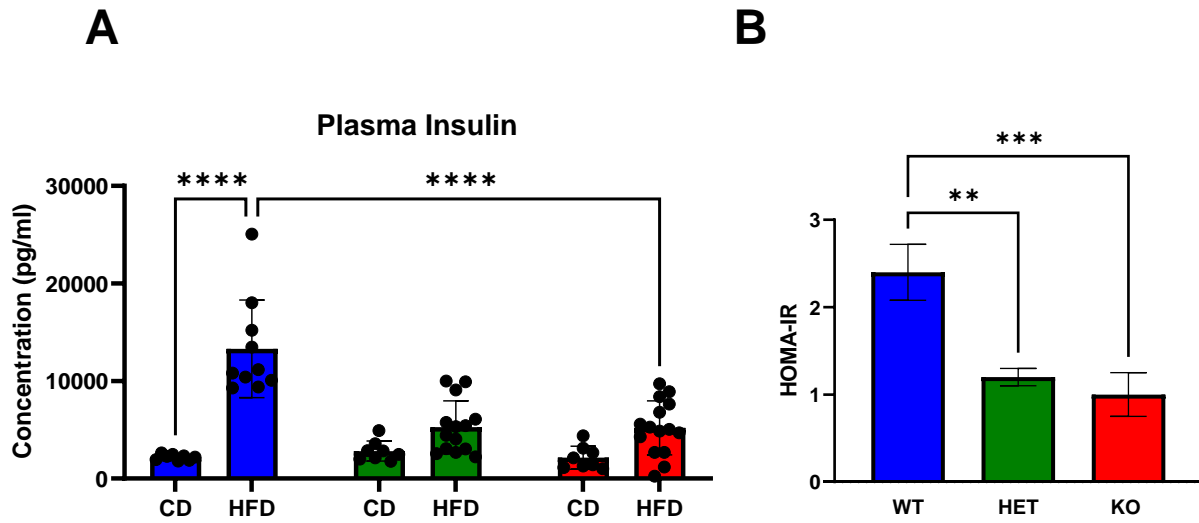


Figure 21: *Gpr75* deficiency prevents HFD-induced insulin resistance (Hossain et al., 2023).

(A) Plasma insulin after 14 weeks of chow diet (CD) or HFD feeding in WT, HET, and KO mice. **(B)** Homeostatic model assessment of insulin resistance (HOMA-IR) after 14 weeks of HFD-feeding. Results are mean \pm SE (n=10-20); ns, not significant; **p<0.01, *** P<0.001 and ****p<0.0001 by two-way ANOVA with Tukey's multiple comparison test (Hossain et al., 2023).

Aim 2: To determine if the protection from adiposity is linked to hypophagia or energy expenditure

Energy intake during CD feeding tended to be higher for KO males compared to WT, however it was not statistically significant (**Figure 22A**). When comparing energy intake at week 14 vs 0 of CD feeding no genotype displayed any differences (**Figure 22B**), which indicates stable caloric intake throughout the CD feeding period. Female KO mice showed a similar trend with KO tending to consume more than WT mice, through it was again not statistically significant (**Figure 23A-B**). Energy intake was not significantly different between WT, HET, and KO at week 0 or at any other week of the HFD feeding period, regardless of sex (week 0 energy intake 96.09 ± 4.13 , 96.68 ± 6.89 , 90.51 ± 3.04 kcal for WT, HET, and KO males: 93.06 ± 3.52 , 87.89 ± 2.98 , 88.89 ± 4.33 kcal for WT, HET, and KO females) (**Figure 24A-B and 25A-B**). All genotypes had higher energy intake at week 14 compared to week 0 of HFD feeding, regardless of sex (101.36 ± 2.91 , 97.27 ± 4.1 , and 107.96 ± 1.34 kcal for WT, HET, and KO males: 105.57 ± 2.19 , 103.72 ± 2.83 , and 103.78 ± 3.125 kcal for WT, HET, and KO females) (**Figure 24A-B and 25A-B**) (Hossain et al., 2023).

Figure 22

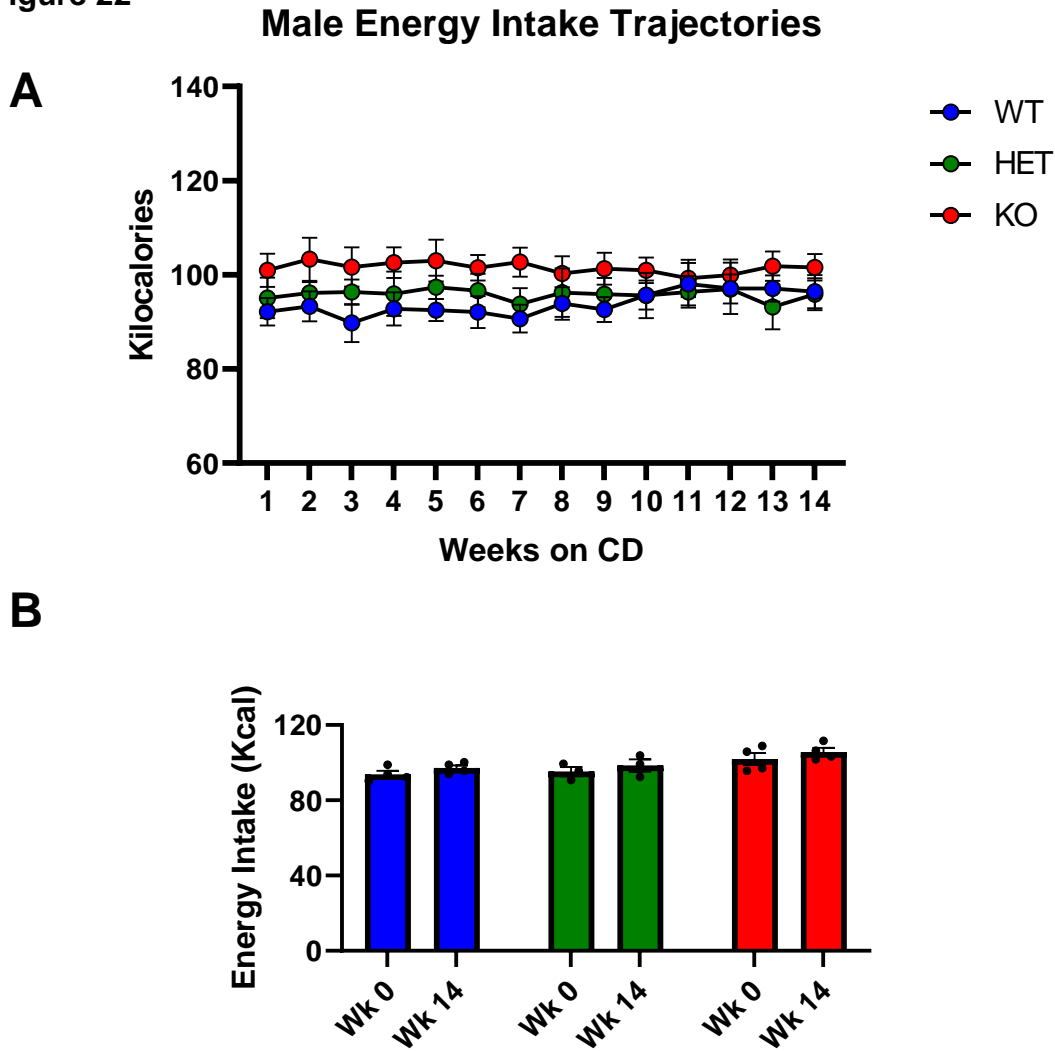


Figure 22: Male mice with *Gpr75* deficiency display no differences in energy intake compared to WT mice throughout 14 weeks of control diet (CD) feeding (Hossain et al., 2023).

(A) Energy intake calculated from food consumption for male WT, HET, and KO mice (n=3-4) **(B)** Comparison of energy intake at week 0 (baseline) and week 14 (end) of HFD-feeding. Results are mean±SE, ns, not significant, by two-way ANOVA with Tukey's multiple comparison test (Hossain et al., 2023).

Figure 23

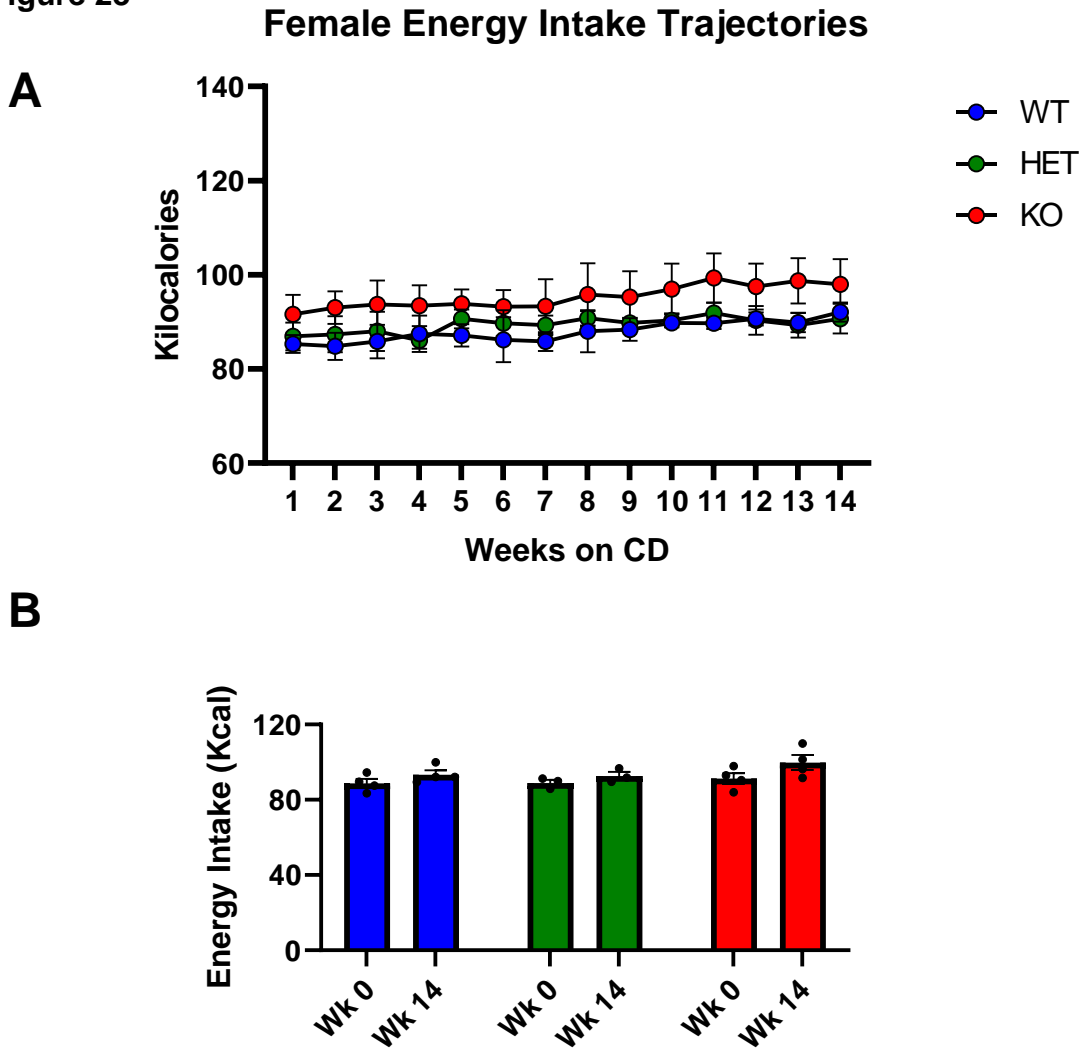


Figure 23: Female mice with *Gpr75* deficiency display no differences in energy intake compared to WT mice throughout 14 weeks of control diet (CD) feeding (Hossain et al., 2023).

(A) Energy intake calculated from food consumption for male WT, HET, and KO mice (n=3-4) **(B)** Comparison of energy intake at week 0 (baseline) and week 14 (end) of HFD-feeding. Results are mean \pm SE, ns, not significant, by two-way ANOVA with Tukey's multiple comparison test (Hossain et al., 2023).

Figure 24

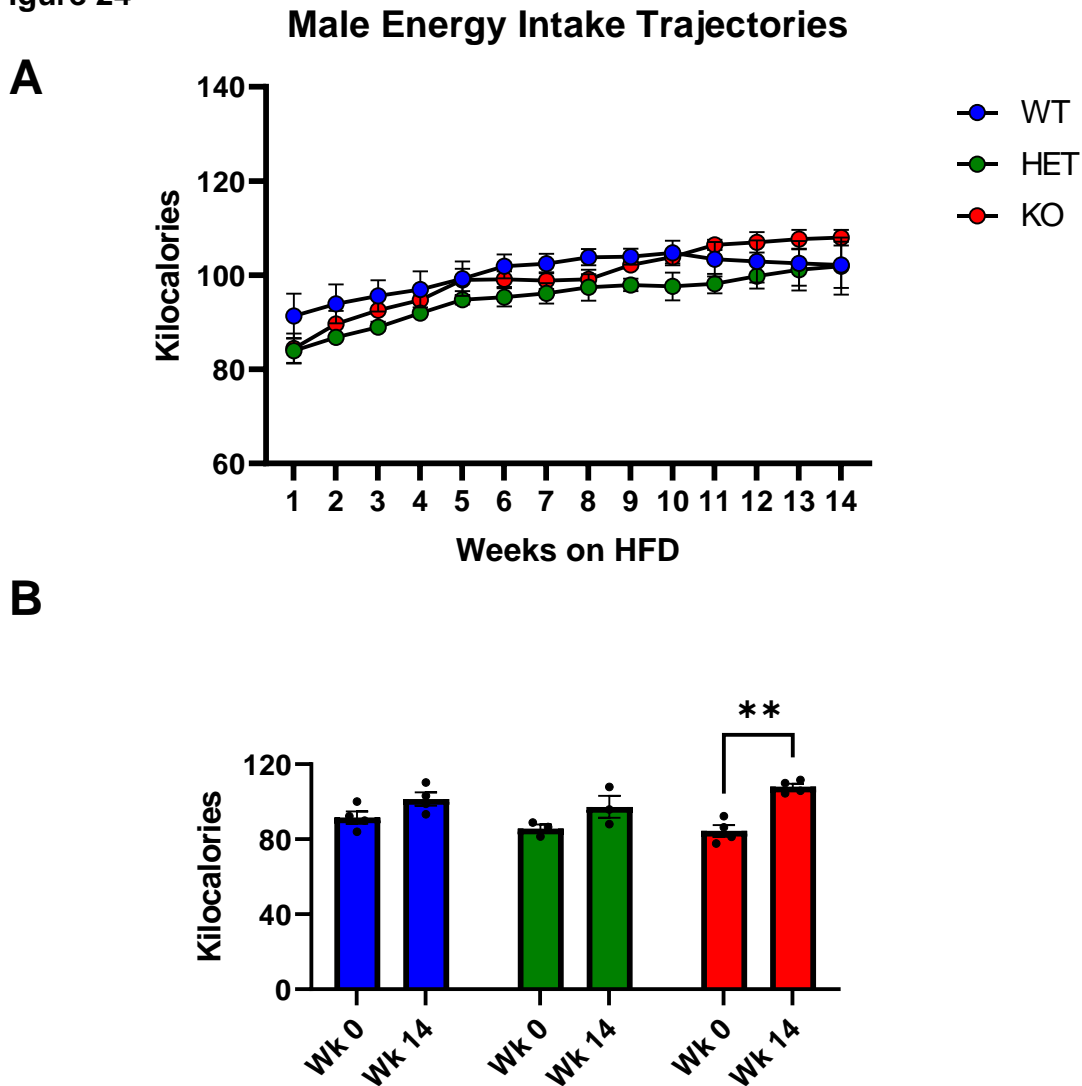


Figure 24: Male *Gpr75* deficient mice show no differences in energy intake compared to WT mice during HFD-feeding (Hossain et al., 2023).

(A) Energy intake calculated from food consumption for male WT, HET, and KO mice (n=3-4) **(B)** Comparison of energy intake at week 0 (baseline) and week 14 (end) of HFD-feeding. Results are mean±SE, ns, not significant; **p<0.01, by two-way ANOVA with Tukey's multiple comparison test (Hossain et al., 2023).

Figure 25

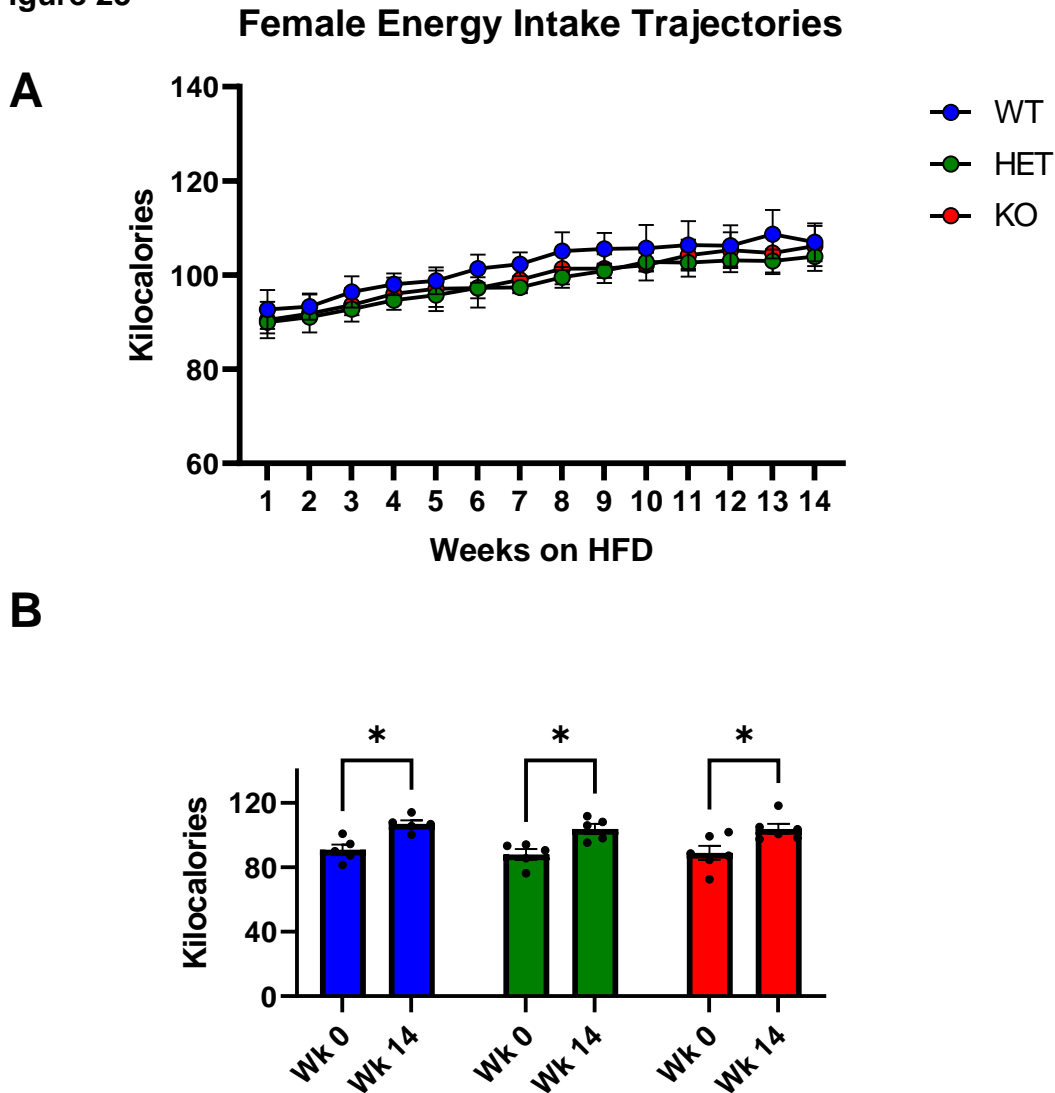


Figure 25: Female *Gpr75* deficient mice show no differences in energy intake compared to WT mice during HFD-feeding (Hossain et al., 2023).

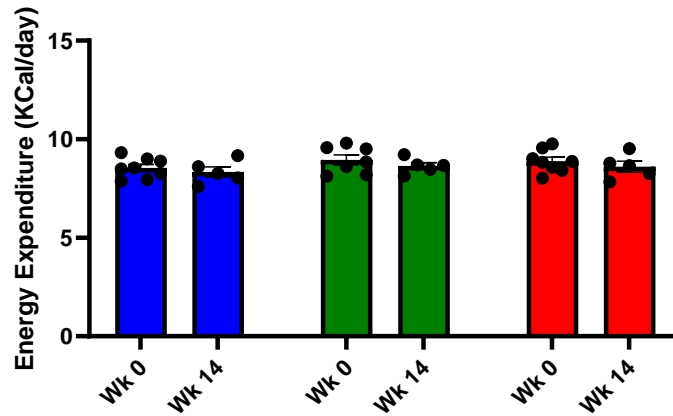
(A) Energy intake calculated from food consumption for male WT, HET, and KO mice (n=3-4) **(B)** Comparison of energy intake at week 0 (baseline) and week 14 (end) of HFD-feeding. Results are mean±SE, ns, not significant; *p<0.05, by two-way ANOVA with Tukey's multiple comparison test (Hossain et al., 2023).

Figure 26A-B shows that WT, HET, and KO mice had similar energy expenditure at baseline and after 14 weeks of CD feeding. Surprisingly, energy expenditure (EE) reduced by 25% in male and female WT animals after HFD feeding (8.74 ± 0.38 vs 6.50 ± 0.81 , week 0 vs week 14 for males: 8.83 ± 0.47 vs 6.33 ± 0.79 , week 0 vs week 14 for females (**Figure 27A-B**) and remained relatively unchanged in KO mice in response to HFD-feeding regardless of sex (9.02 ± 0.53 vs 8.22 ± 8.55 , week 0 vs week 14 for males: 9.00 ± 0.58 vs 8.61 ± 0.071 week 0 vs week 14 for females) (**Figure 27A-B**). Whereas EE reduced in male HET mice, it remained unchanged in female HET (**Figure 27A-B**) (Hossain et al., 2023).

Figure 26

A

Male



B

Female

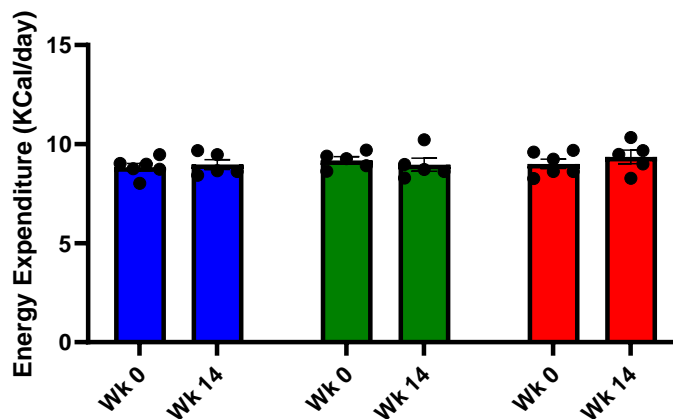
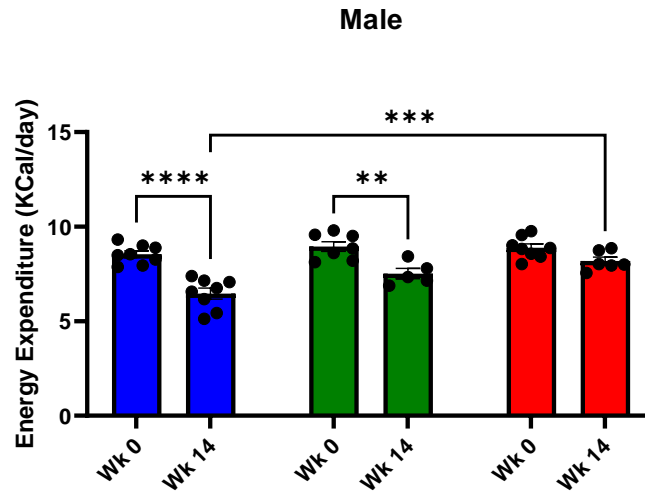


Figure 26: Male and female mice with *Gpr75* deficiency show no differences in energy expenditure compared to WT mice throughout 14 weeks of CD feeding (Hossain et al., 2023).

Energy expenditure calculated from VO₂ at week 0 (baseline) and week 14 (end) of CD-feeding for **(A)** males and **(B)** females (n=5-8). Results are mean±SE, ns, not significant by two-way ANOVA with Tukey's multiple comparison test (Hossain et al., 2023).

Figure 27

A



B

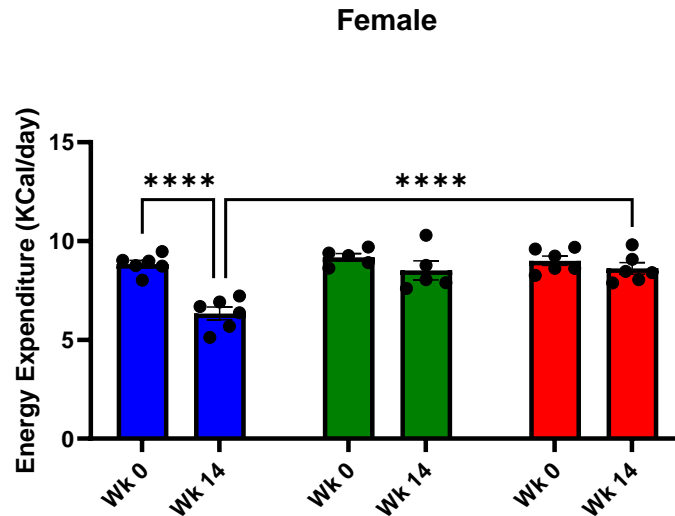


Figure 27: Male and female *Gpr75* deficient mice display attenuated HFD-driven decreases in energy expenditure (Hossain et al., 2023).

Energy expenditure calculated from VO₂ at week 0 (baseline) and week 14 (end) of HFD-feeding for (A) males and (B) females (n=5-8). Results are mean±SE, ns, not significant; **p<0.01, *** P<0.001 and ****p<0.0001 by two-way ANOVA with Tukey's multiple comparison test (Hossain et al., 2023).

Since energy expenditure can change in response to changes in body weight, we analyzed energy expenditure by ANCOVA using total body mass (TBM) or lean body mass (LBM) as covariates. This reiterated that at baseline KO and WT mice had no differences in energy expenditure (**Figure 28A-B males, and 30A-B, females**). As seen in **figure 29A-B** for males and **31A-B** for females, KO mice had higher energy expenditure compared to WT; however, the effect of TBM and LBM was not significant TBM $p=0.1229$ and LBM $p=0.4067$ for males, TBM $p=0.3356$ and LBM $p=0.5829$. This understates that differences in EE in response to HFD feeding are due to the genotype. Regarding the decreased EE in WT, while it might be assumed that the newly acquired fat mass (vide infra) should increase energy expenditure, the increase in inflammatory myokines may negatively affect the bioenergetics of white adipose tissue. Hence, it is plausible that WT animals can gain fat mass, have stable, albeit dysfunctional, fat-free mass, and a drop in energy expenditure (Hossain et al., 2023).

Figure 28

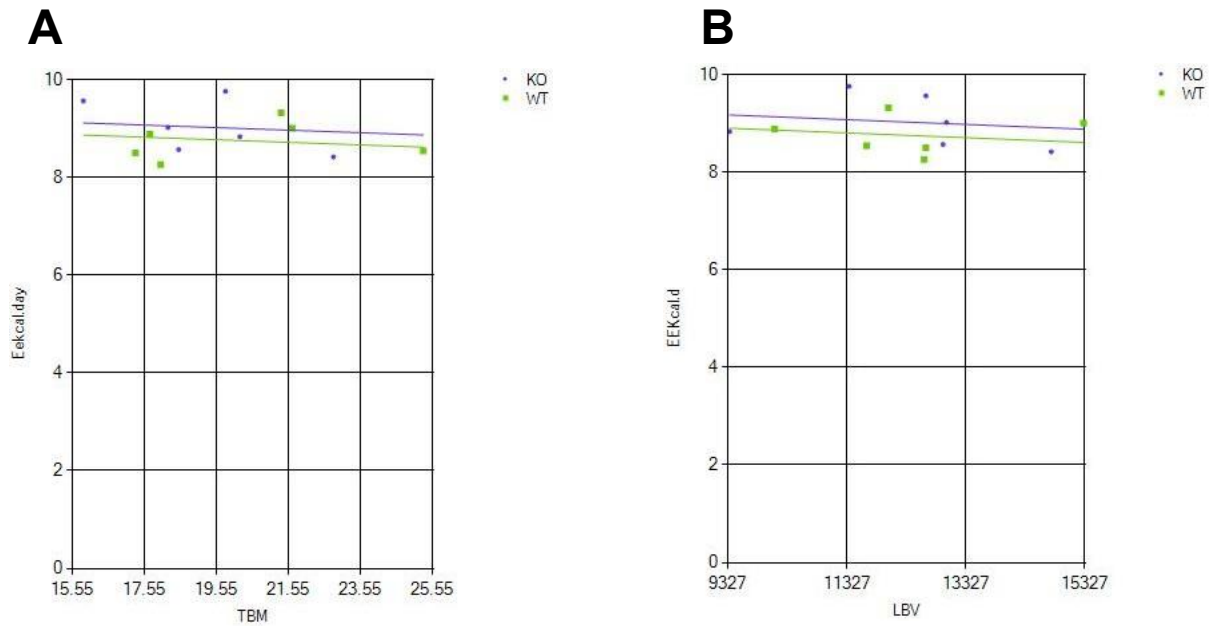


Figure 28: Baseline total energy expenditure (TEE) analyzed by ANCOVA with total body mass (TBM) or lean body mass (LBM) as covariates for males (Hossain et al., 2023).

Male *Gpr75* deficient and WT mice have no differences in energy expenditure at baseline with **(A)** total body mass (TBM) or **(B)** fat-free/lean body mass (LBM) as the covariates (n=5) (Hossain et al., 2023).

Figure 29

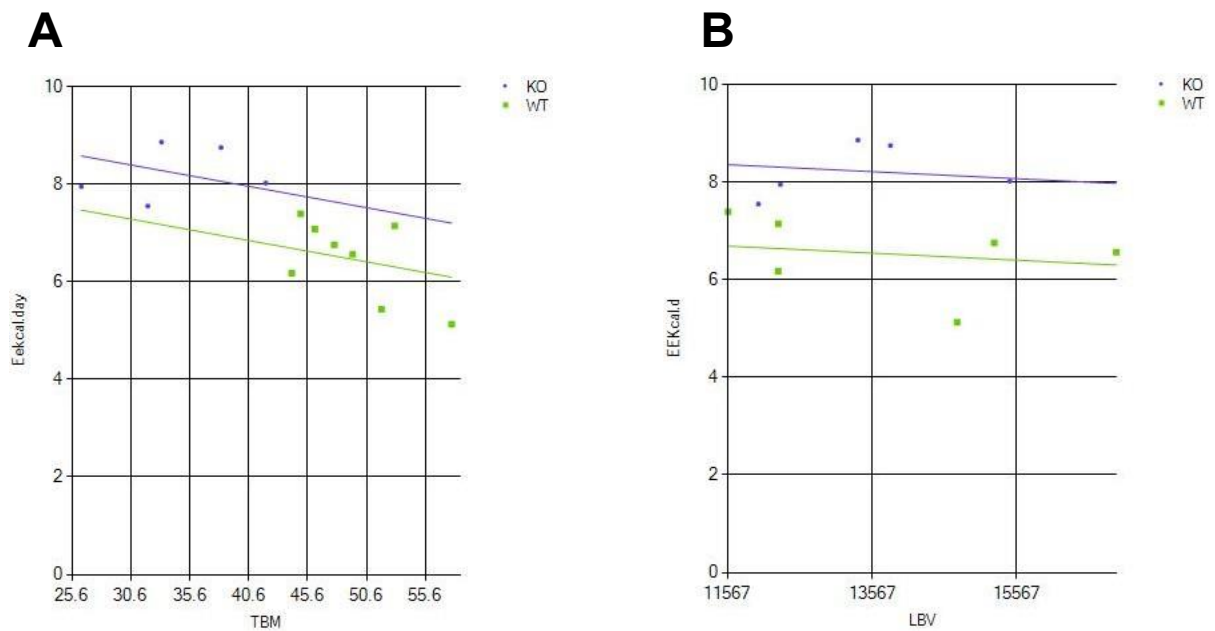


Figure 29: Male total energy expenditure (TEE) analyzed by ANCOVA with total body mass (TBM) or lean body mass (LBM) as covariates after HFD-feeding (Hossain et al., 2023).

Male *Gpr75* deficient mice have higher energy expenditure than WT mice after HFD feeding. However, covariates **(A)** total body mass ($p=0.1997$) or **(B)** lean body mass ($p=0.5359$) are not significant, which indicates that differences in energy expenditure are due to genotype ($n=5$) (Hossain et al., 2023).

Figure 30

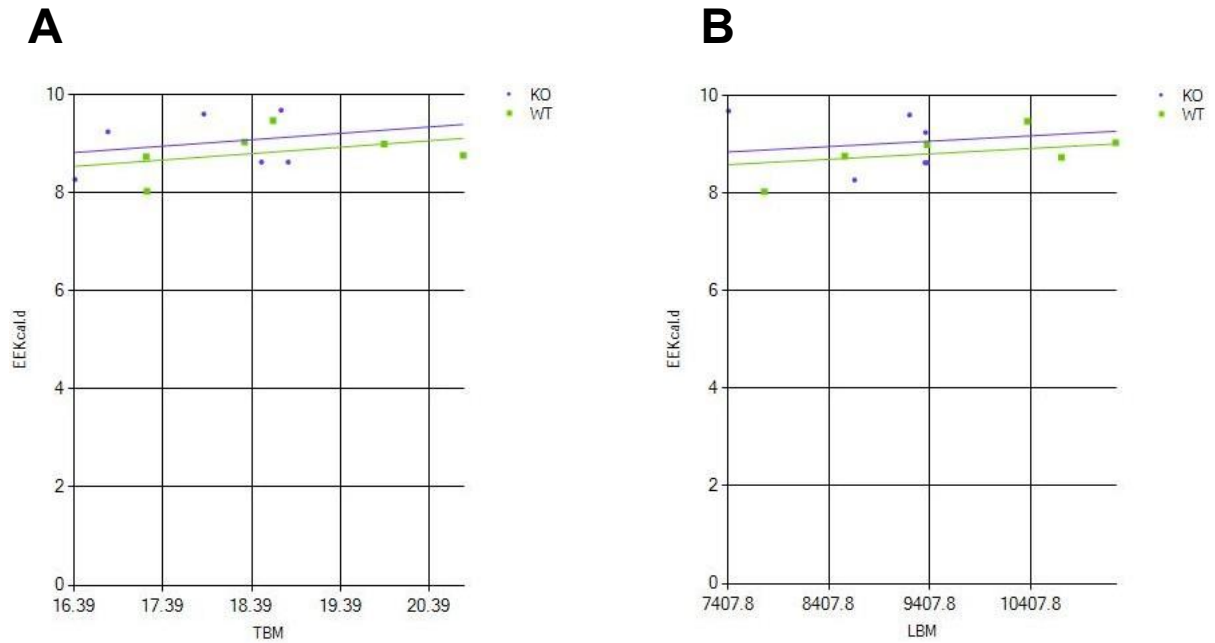


Figure 30: Baseline total energy expenditure (TEE) analyzed by ANCOVA with total body mass (TBM) or lean body mass (LBM) as covariates for females (Hossain et al., 2023).

Female *Gpr75* deficient and WT mice have no differences in energy expenditure at baseline with **(A)** total body mass (TBM) or **(B)** fat-free/lean body mass (LBM) as the covariates (n=5) (Hossain et al., 2023).

Figure 31

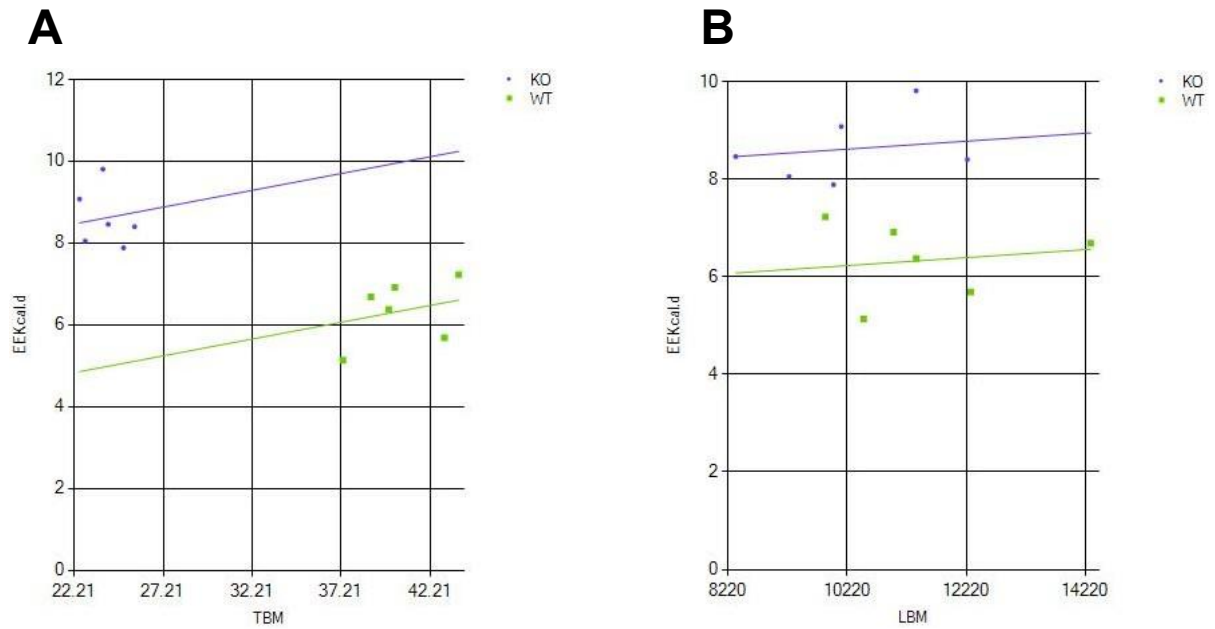


Figure 31: Female total energy expenditure (TEE) analyzed by ANCOVA with total body mass (TBM) or lean body mass (LBM) as covariates after HFD-feeding (Hossain et al., 2023).

Female *Gpr75* deficient mice have higher energy expenditure than WT mice after HFD feeding. However, covariates **(A)** total body mass ($p=0.1997$) or **(B)** lean body mass ($p=0.5359$) are not significant, which indicates that differences in energy expenditure are due to genotype ($n=5$) (Hossain et al., 2023).

Aim 3: To explore the potential cellular mechanisms underlying changes in weight and glucose handling

The gene expression of *Pgc1 α* , a transcriptional cofactor and master regulator of mitochondrial biogenesis which plays a critical role in the regulation of adipogenesis and in transforming WAT to brown fat-like adipocytes, was significantly increased, 1.5-fold, in both BAT and SAT of KO males (**Figure 32A-B**) compared to WT at after 14 weeks of HFD-feeding. Female KO animals displayed 1.5- and 2.5-fold increases in *Pgc1 α* expression in BAT and SAT respectively (**Figure 33A-B**). Interestingly this trend did not hold for VAT in males or females (**Figure 32C and 33C**). This correlated with significant, 2.5- and 2-fold, increases in *Ucp1* (uncoupling protein 1), a thermogenic gene marker, expression in BAT and SAT of KO (**Figure 34A-B**) compared to WT males. Females displayed 3-, 6-, 3-fold increases in *Ucp1* in BAT, SAT, and VAT (**Figure 35A-C**) compared to WT. **Figures 36 and 37** show that expression of *Ucp1* at baseline was significantly higher in KO BAT and SAT for both males and females compared to WT. In VAT *Ucp1* expression tended to be higher in KO compared to WT but it was not statistically significant (**Figure 36C and 37C**) (Hossain et al., 2023).

Figure 32

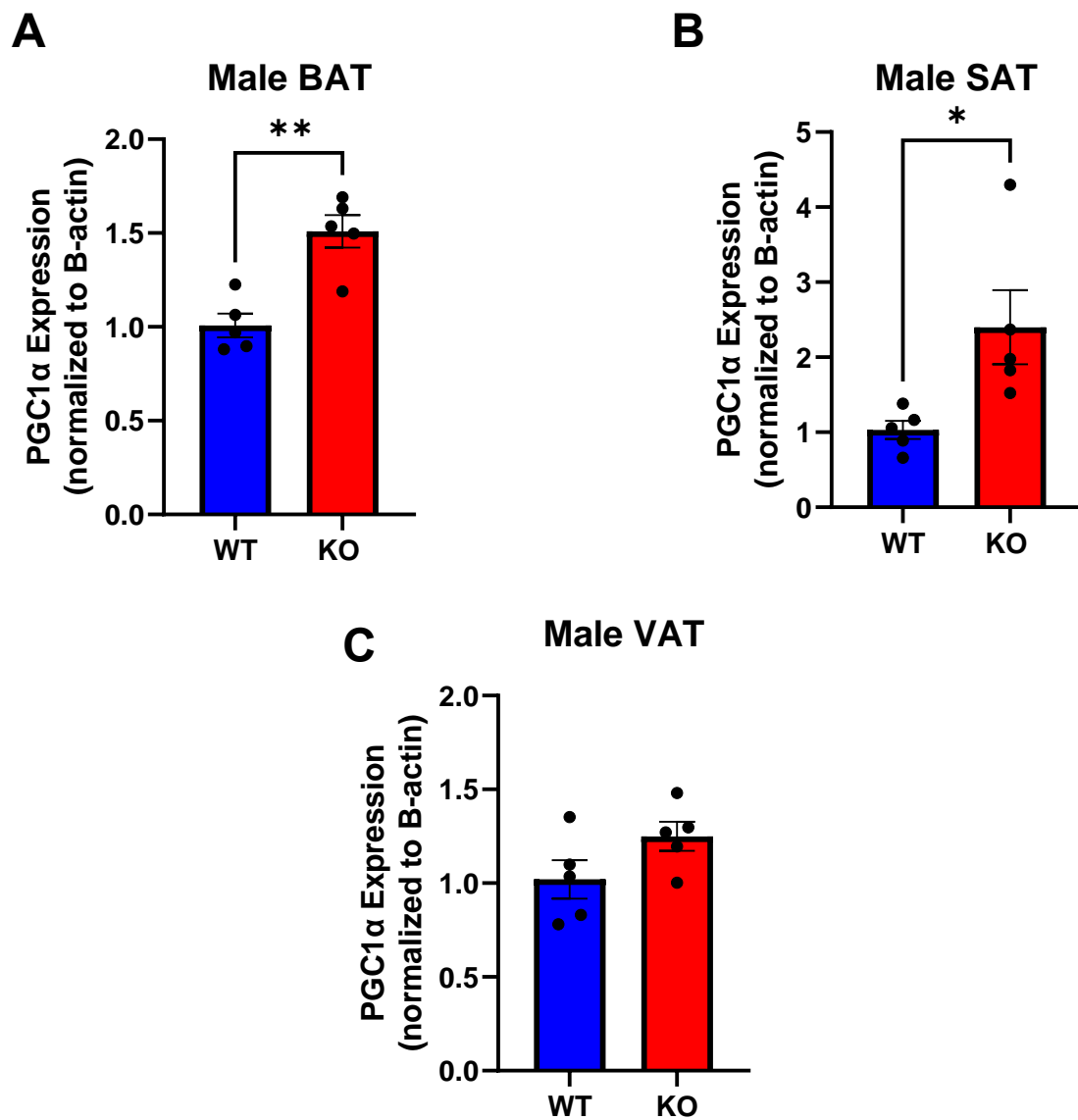


Figure 32: *Gpr75* deficient male mice display higher expression of *Pgc1 α* in BAT and SAT after 14 weeks of HFD feeding (Hossain et al., 2023).

(A) BAT, (B) SAT, (C) VAT mRNA expression of *Pgc1 α* in WT and KO mice after HFD feeding. Results are mean \pm SE (n=5); ns, not significant; * P<0.05, **P<0.01 by unpaired t-test (Hossain et al., 2023).

Figure 33

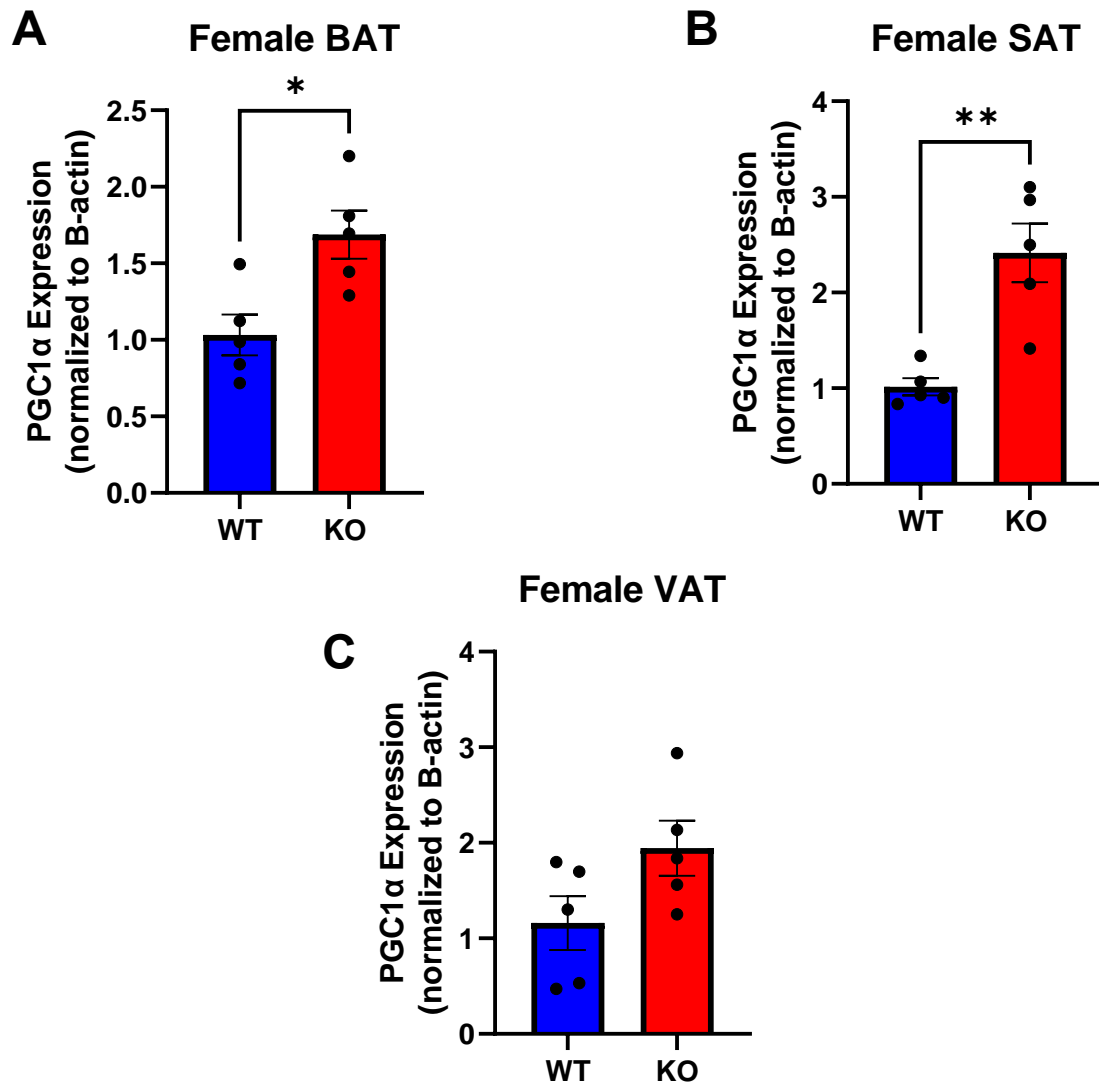


Figure 33: *Gpr75* deficient female mice display higher expression of *Pgc1α* in BAT and SAT after 14 weeks of HFD feeding (Hossain et al., 2023).

(A) BAT, (B) SAT, (C) VAT mRNA expression of *Pgc1α* in WT and KO mice after HFD feeding. Results are mean±SE (n=5); ns, not significant; * P<0.05, **P<0.01 by unpaired t-test (Hossain et al., 2023).

Figure 34

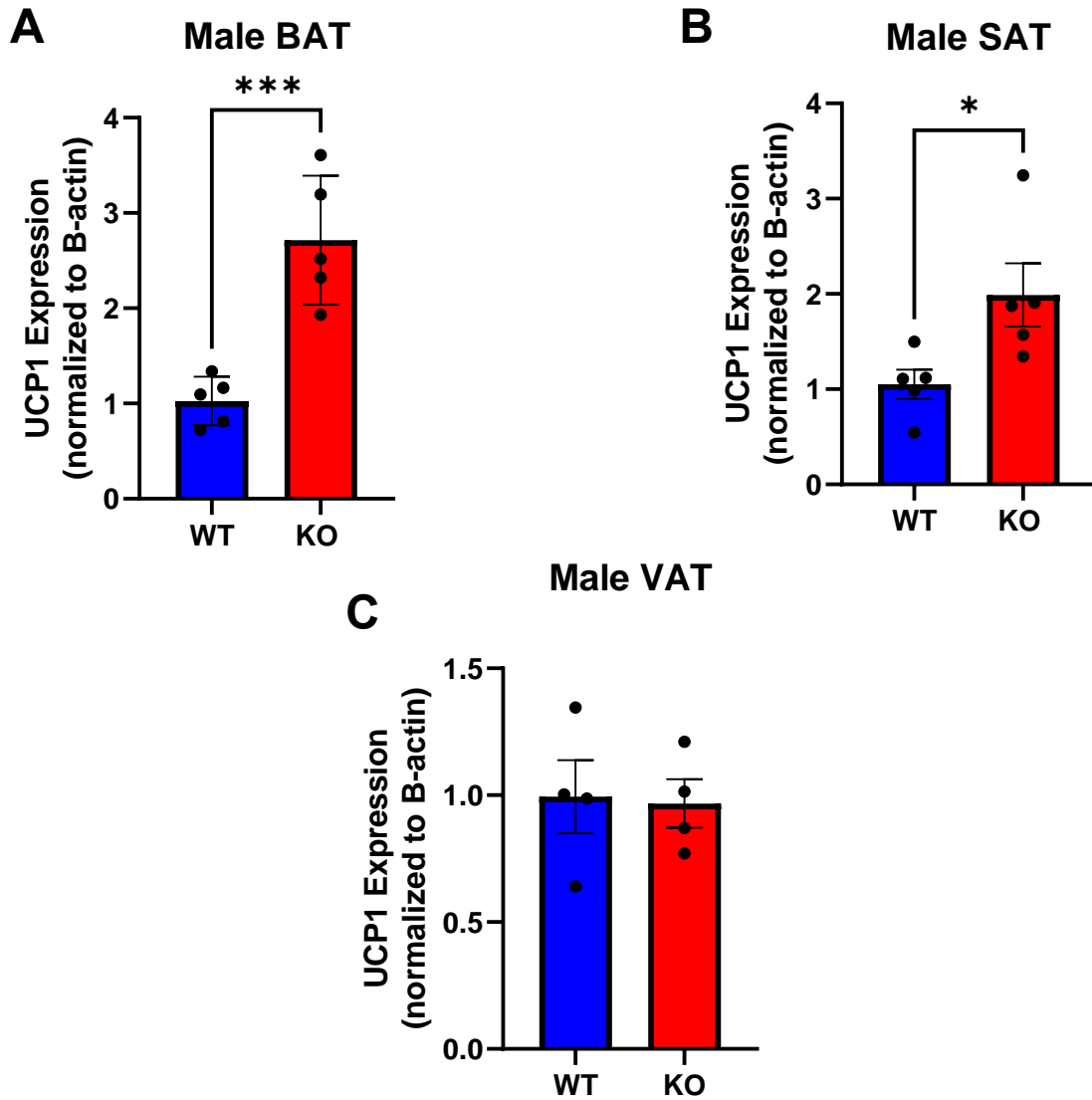


Figure 34: *Gpr75* deficient male mice display higher expression of *Ucp1* in BAT and SAT after 14 weeks of HFD feeding (Hossain et al., 2023).

(A) BAT, (B) SAT, (C) VAT mRNA expression of *Ucp1* in WT and KO mice after HFD feeding. Results are mean \pm SE (n=5); ns, not significant; * P<0.05, **P<0.01, ***P<0.001 by unpaired t-test (Hossain et al., 2023).

Figure 35

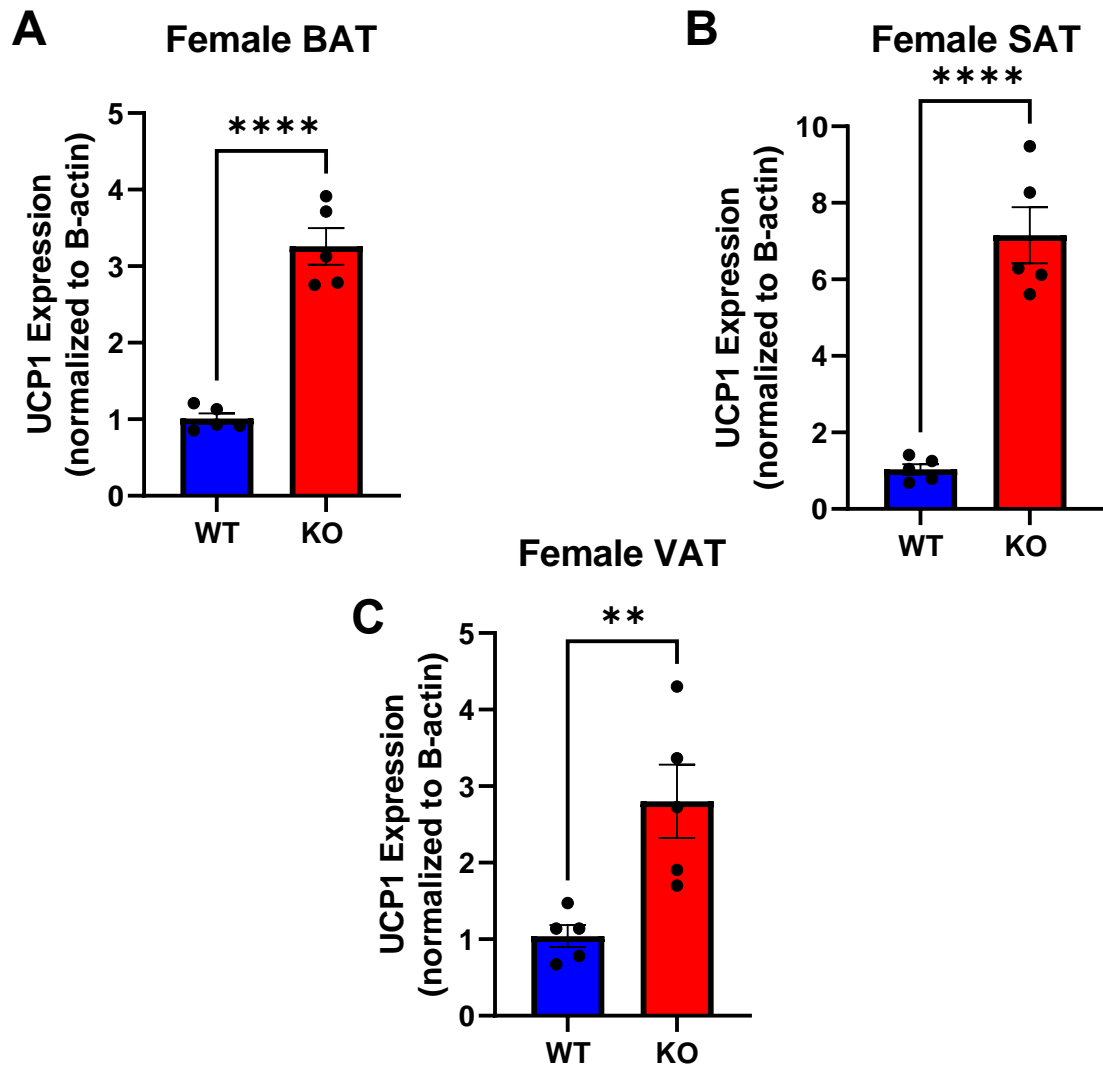


Figure 35: *Gpr75* deficient female mice display higher expression of *Ucp1* in BAT and SAT after 14 weeks of HFD feeding (Hossain et al., 2023).

(A) BAT, (B) SAT, (C) VAT mRNA expression of *Ucp1* in WT and KO mice after HFD feeding. Results are mean \pm SE (n=5); ns, not significant; **P<0.01, ****P<0.0001 by unpaired t-test (Hossain et al., 2023).

Figure 36

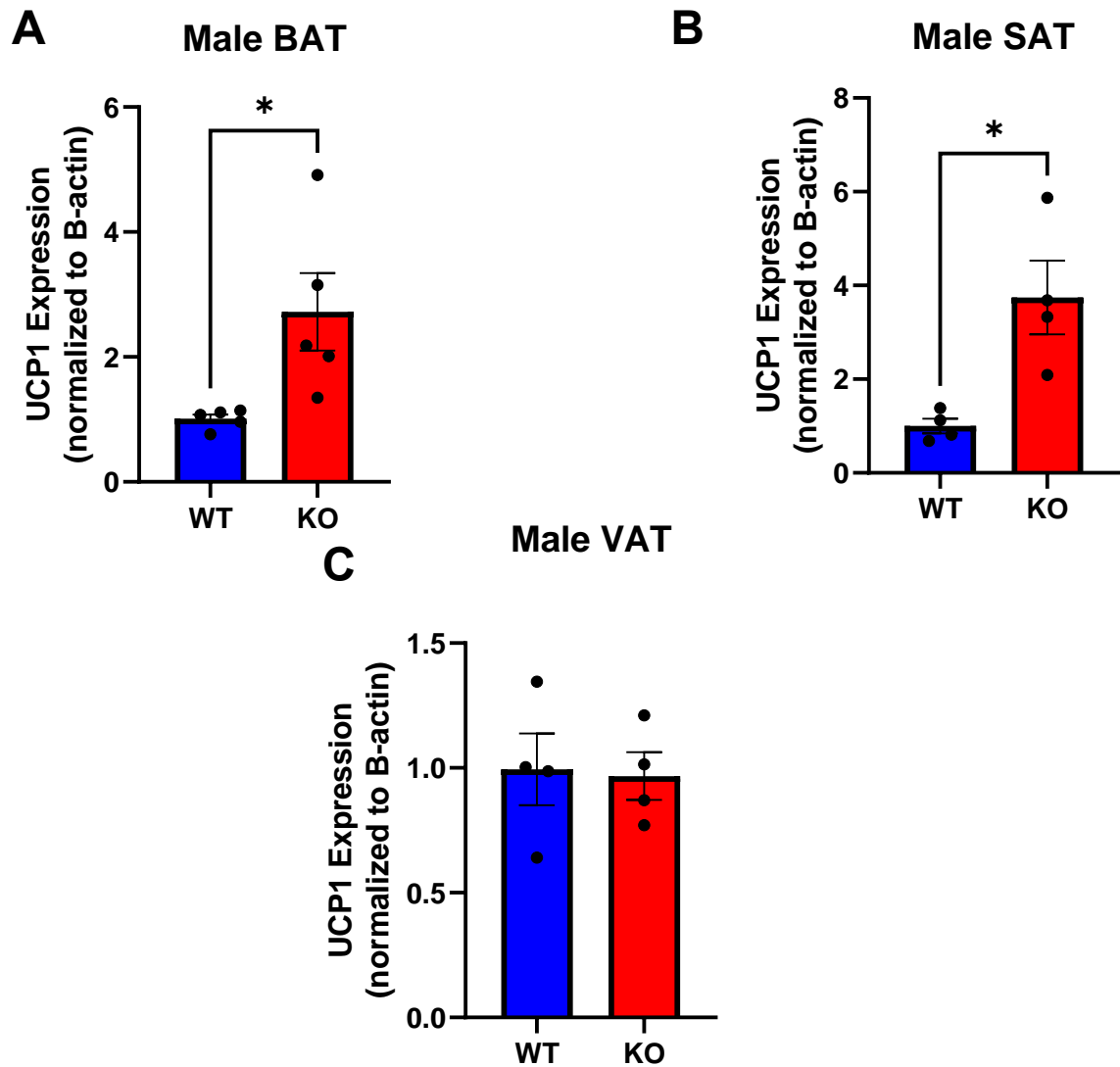


Figure 36: *Gpr75* deficient male mice display higher expression of *Ucp1* in BAT and SAT at baseline (Hossain et al., 2023).

(A) BAT, (B) SAT, (C) VAT mRNA expression of *Ucp1* in WT and KO mice after HFD feeding. Results are mean \pm SE (n=5); ns, not significant; * P<0.05, by unpaired t-test (Hossain et al., 2023).

Figure 37

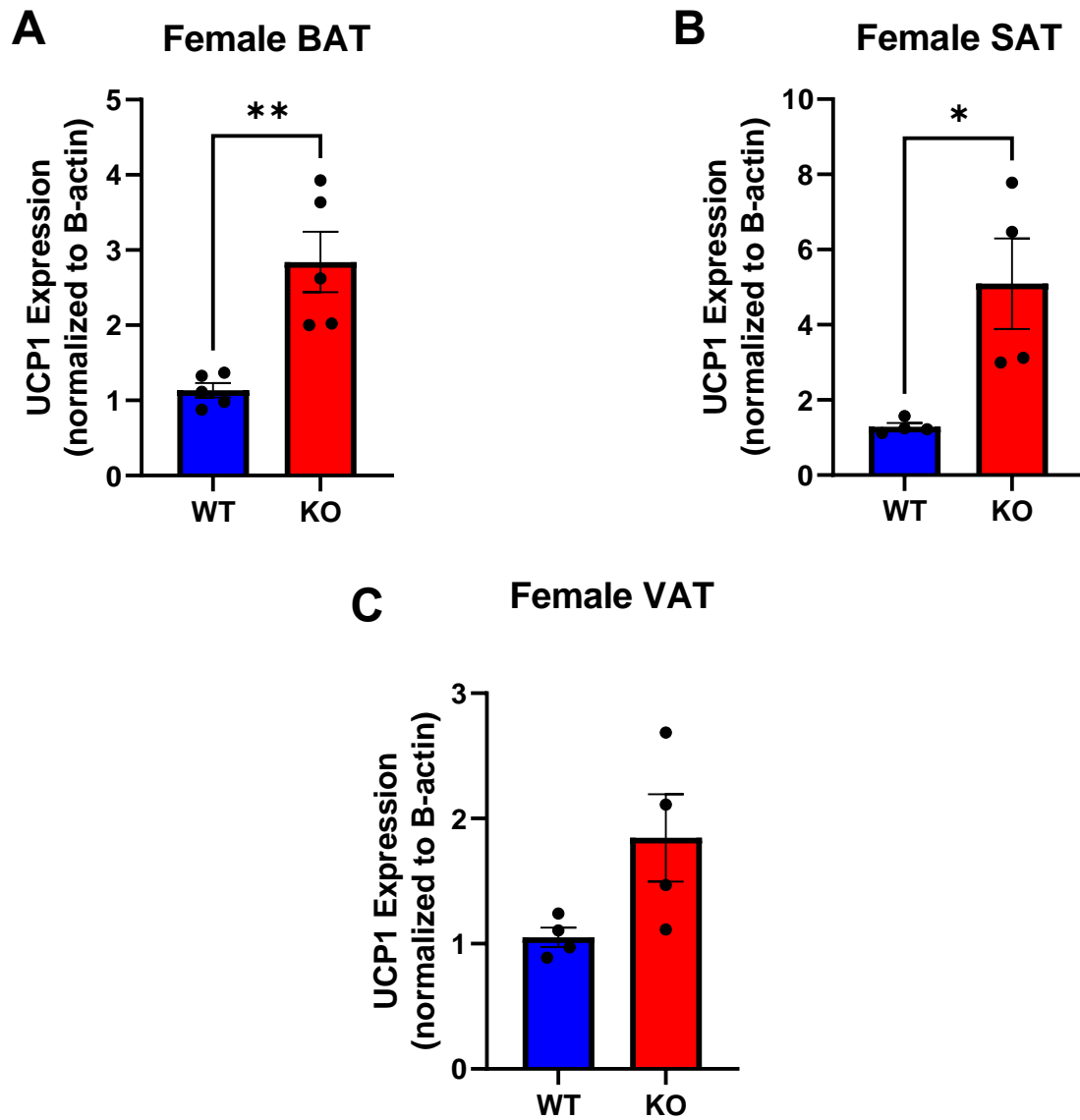


Figure 37: *Gpr75* deficient female mice display higher expression of *Ucp1* in BAT and SAT at baseline (Hossain et al., 2023).

(A) BAT, (B) SAT, (C) VAT mRNA expression of *Ucp1* in WT and KO mice after HFD feeding. Results are mean \pm SE (n=5); ns, not significant, *P<0.05, **P<0.01 by unpaired t-test (Hossain et al., 2023).

Western blot of UCP1 in BAT showed that KO had 1.37-fold higher protein expression compared to WT after HFD feeding. This indicates that the increase in *Ucp1* mRNA levels was associated with increased protein levels in KO compared to WT mice after HFD feeding (**Figure 38A-B**). Moreover, assessment of BAT mitochondrial function displays significantly higher maximal respiration in KO compared to WT in response to ADP stimulation (**Figure 39**), supporting, at least in part, the notion of increased thermogenic processes in KO mice compared to WT mice under conditions of HFD feeding. The skeletal muscle isoform of *Ucp1* is *Ucp3*. Our data indicates that there is a 1.5-fold increase in *Ucp3* gene expression in KO males compared to WT (**Figure 40A**). This is important as human beings do not possess large brown fat depots as in rodents and adaptive thermogenesis tends to occur in skeletal muscle. We also observed a 2-fold increase in mitofusin-1 (**Figure 40B**), in skeletal muscle, indicating improvements in mitochondrial function (Hossain et al., 2023).

Figure 38

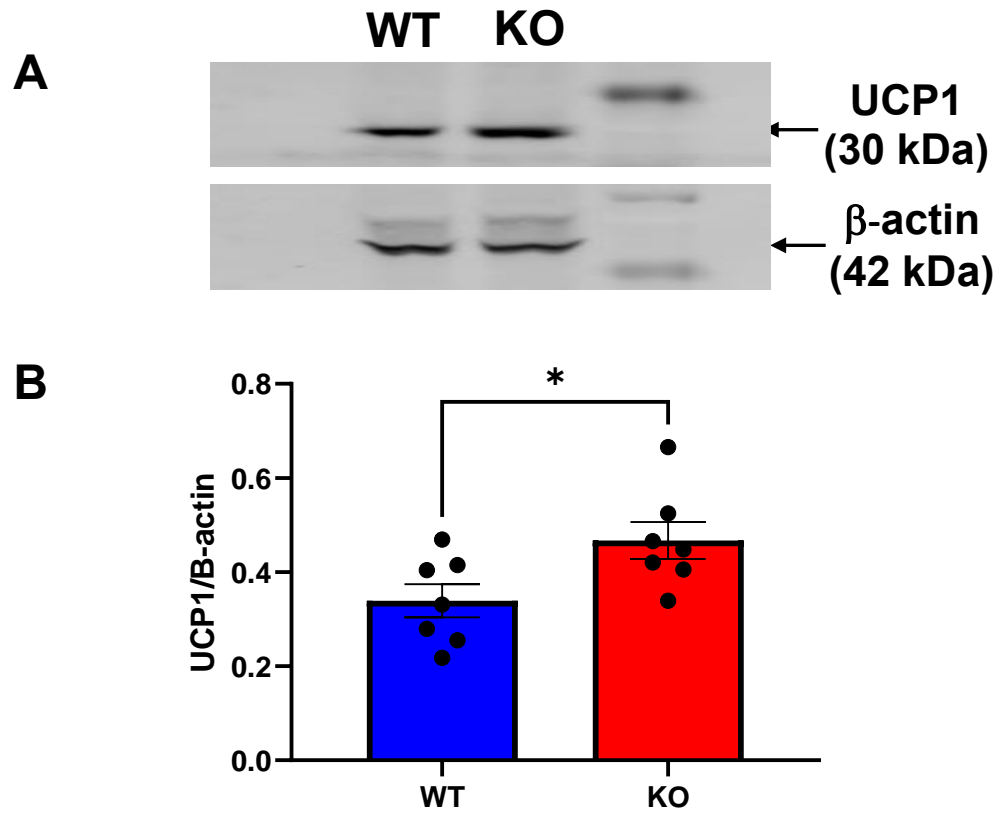


Figure 38: *Gpr75* deficient mice display higher UCP1 protein levels compared to WT after HFD feeding (Hossain et al., 2023).

(A) Western blot and (B) densitometry analysis of UCP1 in BAT from WT and KO mice after 14 weeks of HFD feeding. Results are mean \pm SE, n=6/group; *p<0.05 compared to WT by unpaired t-test (Hossain et al., 2023).

Figure 39

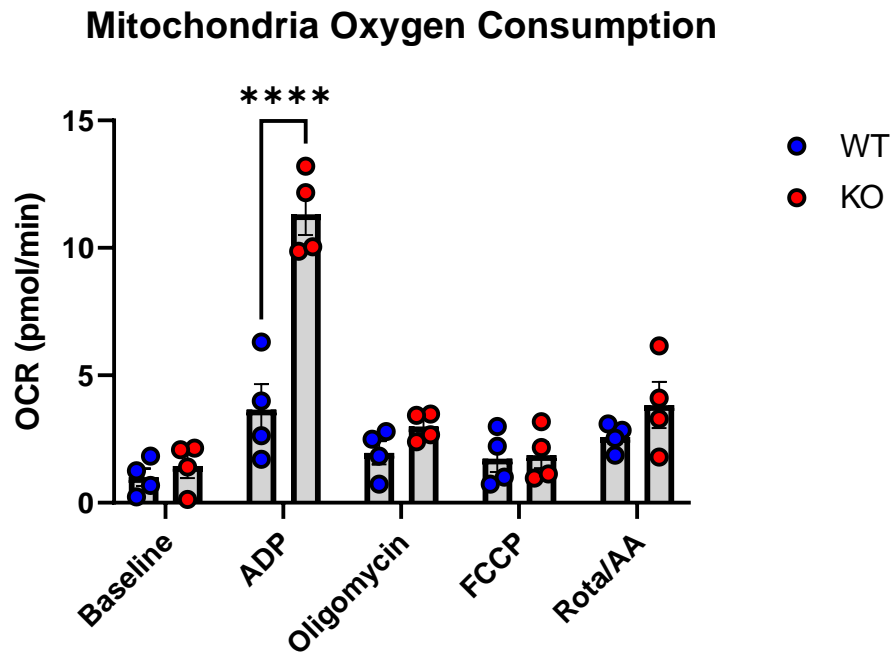


Figure 39: Mitochondria respiration in BAT from HFD-fed WT and KO mice (Hossain et al., 2023).

ADP-stimulated oxygen respiration in isolated mitochondria from BAT of WT and KO mice after 14 weeks of HFD feeding. Results are mean \pm SE, n=4/group, ****p<0.0001 by two-way ANOVA with Tukey's multiple comparison test (Hossain et al., 2023).

Figure 40

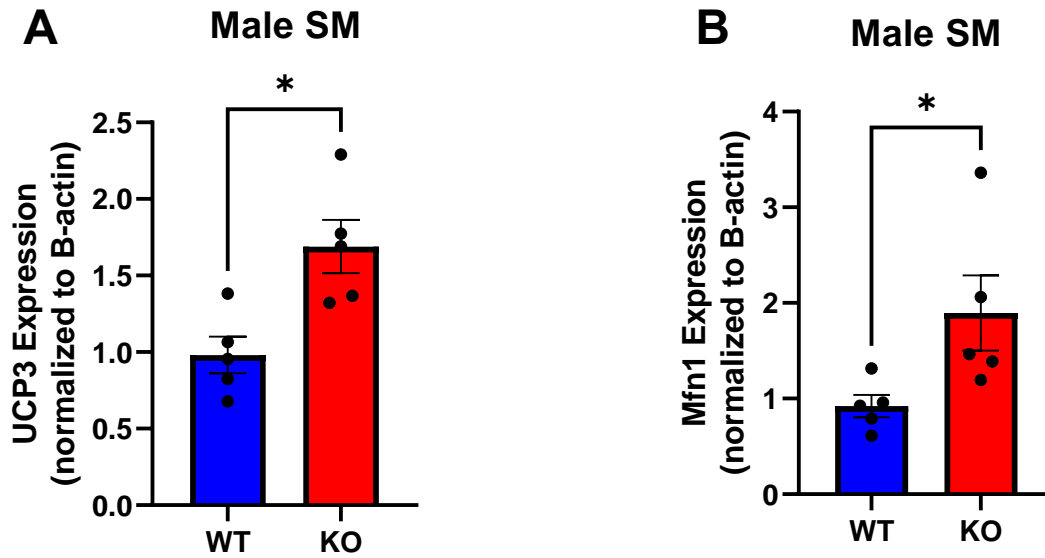


Figure 40: *Gpr75* deficient male mice display higher expression of *Ucp3* and *mfn1* in skeletal muscle after HFD feeding (Hossain et al., 2023).

(A) *Ucp3* and (B) *mfn1* mRNA expression in WT and KO mice after HFD feeding. Results are mean \pm SE (n=5); ns, not significant, *P<0.05, by unpaired t-test (Hossain et al., 2023).

As inflammation is a major consequence of obesity and implicated in the pathogenesis of insulin resistance, tumor necrosis factor-alpha (*Tnfα*) gene expression was measured in all three fat beds (VAT, SAT, and BAT). There were no significant differences in *Tnfα* expression between WT and KO mice at baseline for males (**Figure 41A-C**) or females (**Figure 42A-C**). After 14 weeks of HFD feeding there were significant increases in *Tnfα* gene expression in BAT, SAT, and VAT of WT mice compared to KO mice regardless of sex (**Figure 43, males and 44, females**). This correlated with a 1.5-fold increase in *Tnfα* gene expression in skeletal muscle (**Figure 45**). Since skeletal muscle is the site of almost 90% of insulin mediated glucose uptake, we measured the levels of phosphorylated insulin receptor (tyrosine 972). Our data shows that phosphorylation of the insulin receptor at tyrosine 972 was 5.61-fold higher in skeletal muscle of KO mice compared to WT mice after HFD feeding (**Figure 46A-B**). Furthermore, phosphorylated AKT (serine 473), which is a primary target of activated insulin receptor, was 2.82-fold higher in KO vs WT mice after HFD feeding (**Figure 47A-B**), suggesting that *Gpr75* deletion preserves insulin signaling and actions in the presence of HFD (Hossain et al., 2023).

Figure 41

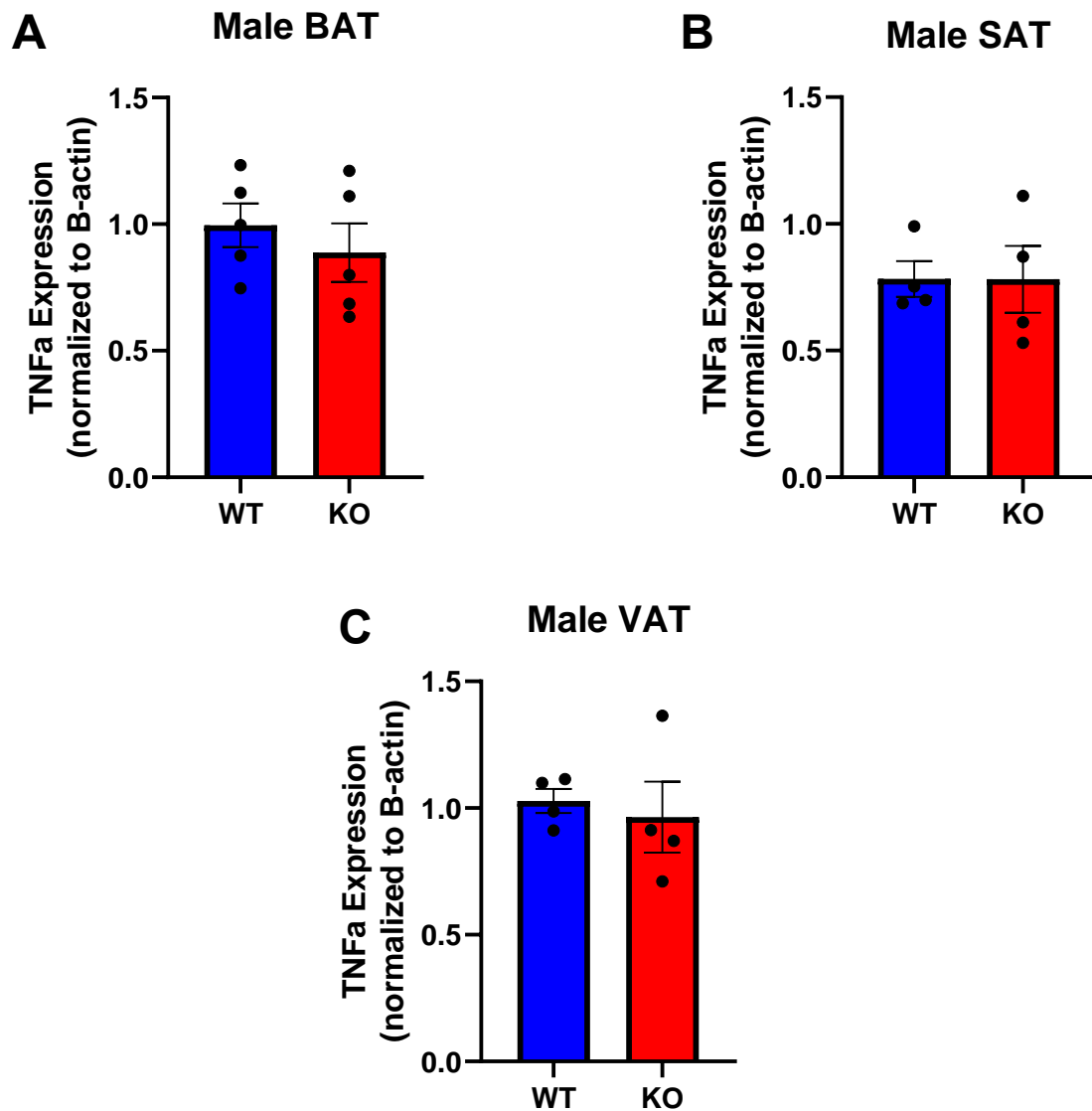


Figure 41: Male WT and *Gpr75* deficient mice show similar levels of tumor necrosis factor alpha (*Tnf α*) at baseline (Hossain et al., 2023).

(A) BAT, (B) SAT, (C) VAT mRNA expression of *Tnf α* in WT and KO mice at baseline. Results are mean \pm SE (n=4-6); ns, not significant; by unpaired t-test (Hossain et al., 2023).

Figure 42

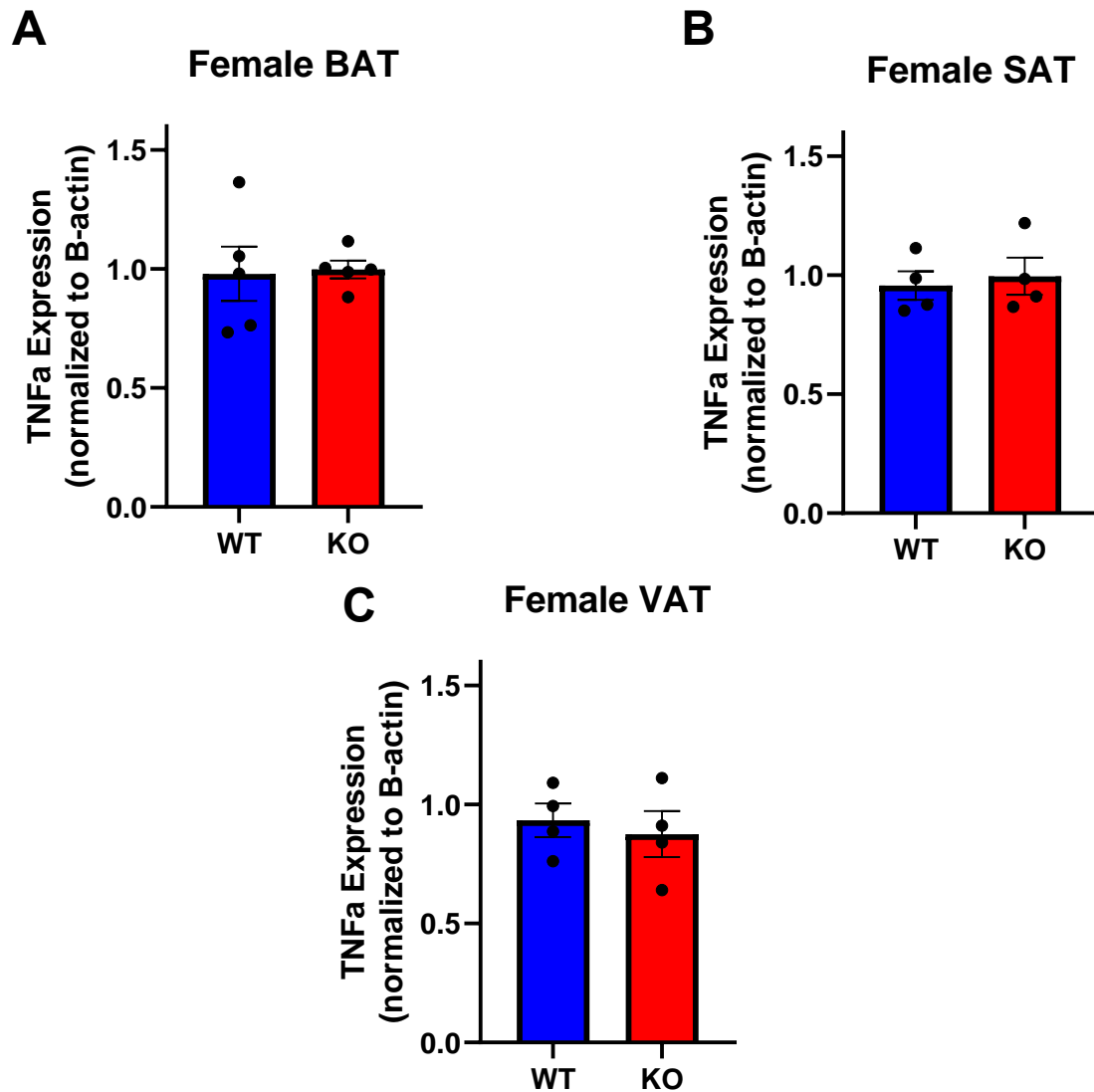


Figure 42: Female WT and *Gpr75* deficient mice show similar levels of tumor necrosis factor alpha (*Tnfα*) at baseline (Hossain et al., 2023).

(A) BAT, (B) SAT, (C) VAT mRNA expression of *Tnfα* in WT and KO mice at baseline. Results are mean±SE (n=4-5); ns, not significant; by unpaired t-test (Hossain et al., 2023).

Figure 43

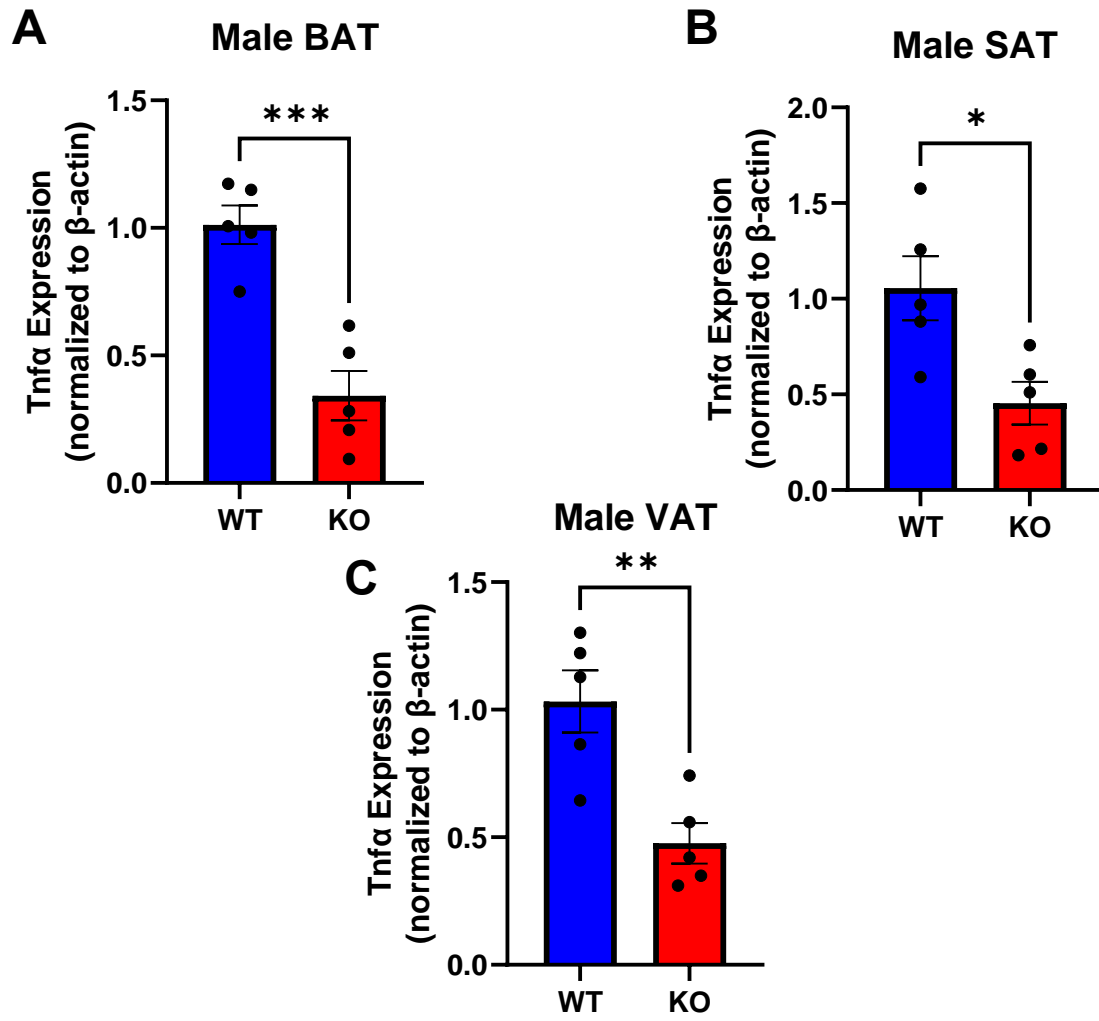


Figure 43: Male *Gpr75* deficient mice show protection from HFD-induced increases in tumor necrosis factor-alpha (*Tnfα*) (Hossain et al., 2023).

(A) BAT, (B) SAT, (C) VAT mRNA expression of *Tnfα* in WT and KO mice after HFD feeding. Results are mean \pm SE (n=5-6); ns, not significant; *** P<0.001 by unpaired t-test (Hossain et al., 2023).

Figure 44

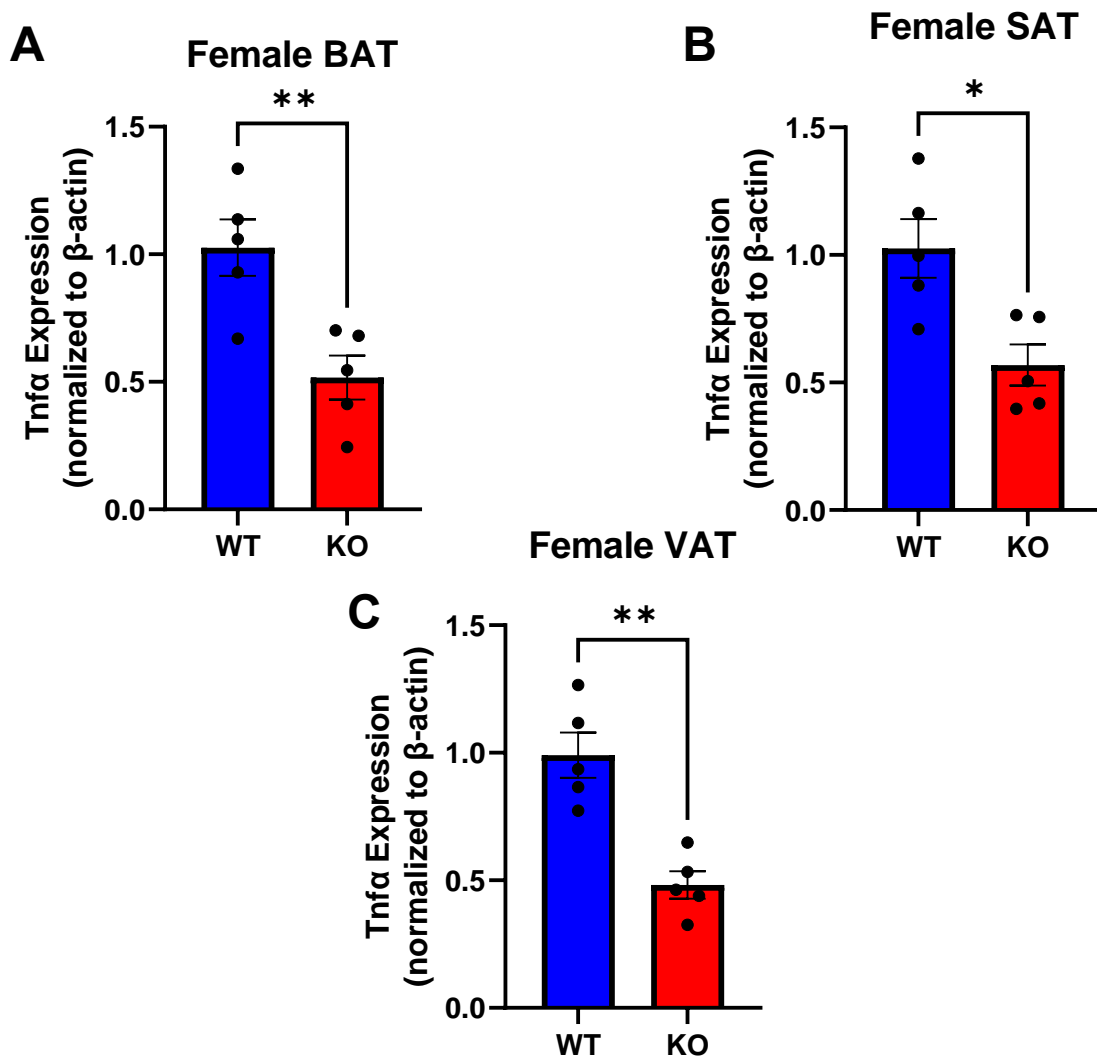


Figure 44: Female *Gpr75* deficient mice show protection from HFD-induced increases in tumor necrosis factor-alpha (*Tnfα*) (Hossain et al., 2023).

(A) BAT, (B) SAT, (C) VAT mRNA expression of *Tnfα* in WT and KO mice after HFD feeding. Results are mean \pm SE (n=5-6); ns, not significant; ** P<0.01 by unpaired t-test (Hossain et al., 2023).

Figure 45

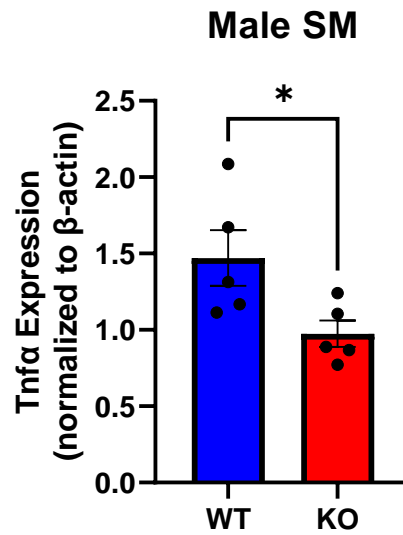


Figure 45: *Gpr75* deficient mice show protection from HFD-induced increases in tumor necrosis factor-alpha (*Tnfα*) in skeletal muscle (Hossain et al., 2023).

Skeletal muscle mRNA expression of *Tnfα* in WT and KO mice after HFD feeding. Results are mean±SE (n=5-6); * P<0.05 by unpaired t-test (Hossain et al., 2023).

Figure 46

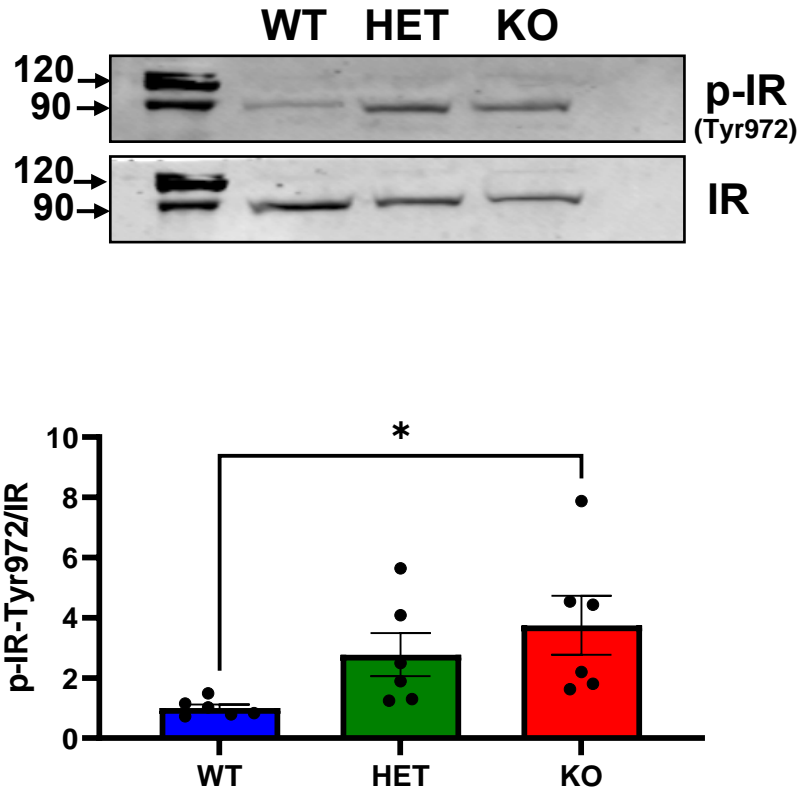


Figure 46: *Gpr75* deficiency prevents HFD-induced impairment of insulin receptor phosphorylation (Hossain et al., 2023).

(A) Representative skeletal muscle western blot of WT, HET, and KO mice after 14 weeks of HFD feeding. **(B)** Densitometry analysis of bands. Results are mean \pm SE (n=3); ns, not significant; *p<0.05, by two-way ANOVA with Tukey's multiple comparison test (Hossain et al., 2023).

Figure 47

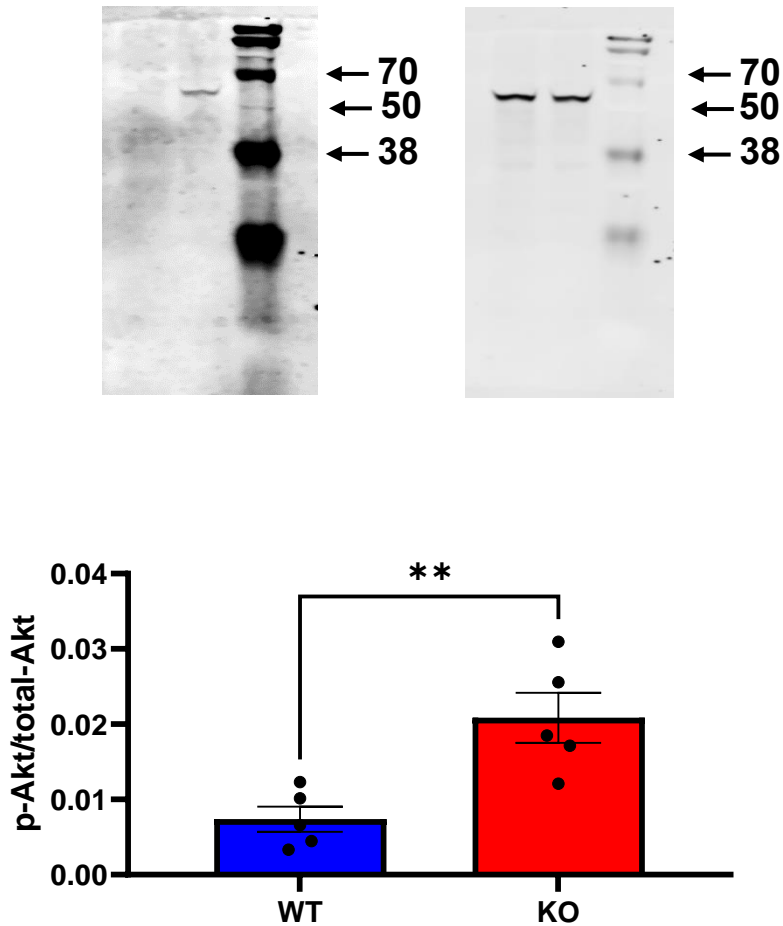


Figure 47: *Gpr75* deficiency prevents HFD-induced impairment of protein kinase B (Akt) phosphorylation (Hossain et al., 2023).

(A) Representative skeletal muscle western blot of WT and KO mice after 14 weeks of HFD feeding. (B) Densitometry analysis of bands. Results are mean \pm SE (n=3); ns, not significant; **p<0.01, *** P<0.001 and ****p<0.0001 by two-way ANOVA with Tukey's multiple comparison test (Hossain et al., 2023).

DISCUSSION

The role of GPR75 in diet-induced obesity (DIO) has become increasingly evident (Akbari *et al.*, 2021). While a 2022 report found that *Gpr75* deficiency attenuates HFD-driven weight gain as a result of hypophagia (Powell *et al.*, 2022), we did not observe any significant differences in caloric intake throughout our study. Importantly, numerous publications have shown that genetic background tends to influence phenotypes displayed by mutant mice (Doetschman, 2009). Therefore, it is plausible that differences in caloric intake between our study and the study by Powell *et al.* are the result of our *Gpr75* null mice having a C57BL/6NTacXSW background, compared to C57BL/6JX129SV by Powell *et al.* This undoubtedly merits further investigation, nonetheless, based on our data we hypothesized that *Gpr75* deficiency attenuates HFD-driven weight gain by impacting metabolic energy expenditure (Hossain *et al.*, 2023).

Our data indicates that at baseline *Gpr75* deficient mice were morphologically similar to WT mice and had no differences in body weight or body composition (i.e., fat volume). During 14 weeks of chow diet feeding (13% kilocalories from fat) *Gpr75* deficient and WT mice tend to display similar trajectories of weight gain; however, during 14 weeks of HFD feeding (60% kilocalories from fat) *Gpr75* deficiency significantly attenuates weight gain compared to WT mice in an allele dependent manner, regardless of sex. Our data indicates that when total body energy expenditure was calculated from CO₂ production and O₂ consumption using the Lusk equation ($1.232 \cdot RQ + 3.815 \cdot VO_2$) there were no differences in energy expenditure between WT and *Gpr75* deficient mice at baseline, regardless of sex.

However, HFD feeding significantly reduced energy expenditure compared to baseline in WT mice (-25%), regardless of sex. Surprisingly, *Gpr75* KO mice showed no significant differences in energy expenditure after HFD feeding, regardless of sex. These trends held true even after ANCOVA regression analysis with total body mass or lean body volume as covariates, which underscores that changes in energy expenditure seen in our study were the result of *Gpr75* expression rather than differences in body mass in WT compared to *Gpr75* deficient mice. Interestingly, WT and *Gpr75* deficient mice displayed similar volumes of fat-free mass (i.e., muscle mass) at baseline and after HFD feeding. This implies that HFD-driven changes in body weight between WT and *Gpr75* deficient mice were solely due to changes in fat mass accumulation. Importantly, fat tends to be metabolically inert, and the accumulation of fat typically has little effect on energy expenditure. However, numerous publications indicate that fat accumulation affects energy expenditure indirectly by impacting skeletal muscle function (Nesto *et al.*, 2005). For example, chronic overfeeding of saturated fatty acids has been shown to cause skeletal muscle dystrophy – highlighted by mitochondrial dysfunction and a shift toward mitochondrial fission rather than fusion – leading to a reduction in energy expenditure in obese mice (Mollica *et al.*, 2011). In fact, we have reported lower expression of mitofusin-1, a mitochondrial fusion protein, in WT compared to *Gpr75* deficient mice after HFD feeding (Hossain *et al.*, 2023).

Reduced HFD-driven weight gain in *Gpr75* deficient mice correlates with reduced volume in adipose depots, particularly in VAT and SAT – both of which are white adipose tissues (WAT). It has been well documented that excess energy is

stored in WAT, while BAT utilizes stored energy and dissipates heat (Ukropec *et al.*, 2006). Importantly, WAT has been shown to acquire a BAT-like phenotype through the expression of BAT-specific genes – particularly *Ucp1*. UCP1 is a carrier protein localized on the inner membrane of mitochondria. Because it transports protons into the mitochondrial matrix without ATP generation UCP1 “uncouples” ATP synthesis (Ukropec *et al.*, 2006). Numerous publications have shown that UCP1 is involved in regulation of energy homeostasis and plays an invaluable role in protection against obesity. For example, mice with genetic deletion of *Ucp1* have been shown to be sensitive to the development of obesity, while mice with overexpression of *Ucp1* generally results in reduced diet-induced weight gain (Feldmann *et al.*, 2008). Our data robustly shows that male and female *Gpr75* KO mice display higher expression of *Ucp1* in BAT after HFD feeding. This may indicate an activation of BAT, which typically occurs as a result of cold mediated sympathetic outflow and the activation of beta-3 adrenergic receptors. Surprisingly, we also observed significantly higher *Ucp1* expression in SAT of *Gpr75* KO mice compared to WT after HFD feeding. Under normal conditions the expression of *Ucp1* in WAT depots is negligible; therefore, our data clearly indicates that SAT of *Gpr75* KO mice has obtained a brown-like phenotype. Importantly, we did not observe any significant differences in *Ucp1* expression in the VAT of WT and *Gpr75* KO animals, regardless of sex. This indicates that *Gpr75* deficiency only stimulates a white-to-brown shift (“browning”) of SAT. However, it is worth mentioning that a UCP1-independent mechanism has been shown to regulate thermogenesis in the VAT (Ikeda *et al.*, 2017). This requires further investigation on our part. Finally, it should be noted that humans tend to

possess less BAT when compared to rodents, thus UCP1 homologues are a very important potential therapeutic target. UCP3 is a UCP1 homolog highly expressed in human skeletal and cardiac muscles. In fact, studies show that transgenic mice with *Ucp3* in skeletal muscle are protected against HFD-driven obesity and show increased energy metabolism (Ukropec *et al.*, 2006). Our data indicates that *Ucp3* expression was indeed increased in the skeletal muscle of *Gpr75* deficient mice compared to WT mice (Hossain *et al.*, 2023).

The expression of UCP1 is regulated by the PPAR γ transcription factor; however, numerous publications indicate that PPAR γ is unable to stimulate transcription in the absence of peroxisome proliferator-activated receptor gamma coactivator 1-alpha (Pgc-1 α) (Besse-Patin *et al.*, 2019). Our data shows that *Pgc-1 α* expression increased significantly in BAT and SAT of both male and female *Gpr75* deficient mice compared to WT mice – indicating a correlation between *Ucp1* and *Pgc1a* expression in our transgenic mice. Measurement of oxygen consumption from isolated mitochondria from the BAT indicates a higher respiration rate in *Gpr75* KO compared to WT mice after HFD feeding, which clearly indicates increased activity of the electron transport chain (ETC). In fact, isolated mitochondria from WT mice display a respiration rate that may signal mitochondrial dysfunction. It has been well documented that fatty acids are vulnerable to lipid peroxidation. Importantly, lipid peroxides have lipotoxic effects on mitochondria – particularly on mtDNA – leading to mitochondrial dysfunction (Li *et al.*, 2022). We hypothesize that increased activity of the electron transport chain, due to *Gpr75* deficiency, stimulates glycolysis and beta-oxidation of fatty acids, thus reducing circulating glucose and fatty acids.

However, we did not measure any markers of glycolysis and beta-oxidation of fatty acids, nor did we measure circulating free fatty acid levels. Furthermore, we did not measure markers of mitochondrial dysfunction, such as the presence of mtDNA or lipid peroxides in the plasma. In all, the roles of *Gpr75* in metabolism and mitochondrial bioenergetics undoubtedly merits further investigation (Hossain et al., 2023).

In the obese state, macrophage and T-lymphocyte migration into adipose tissue stimulates an inflammatory cascade through the release of pro-inflammatory cytokines such as $Tn\alpha$. It is now known that $Tn\alpha$ inhibits *Ucp1* expression in brown adipocytes by interfering with *Pgc1a* (Polyak et al., 2016). Furthermore, inflammatory macrophage infiltration is reported to suppress white adipocyte browning. While we did not measure immune cell infiltration into adipose tissue beds, our data indicates that $Tn\alpha$ expression in VAT and SAT of WT animals showed a 6-fold increase after HFD-feeding. Remarkably, VAT, SAT, and BAT of *Gpr75* deficient animals did not display significant increases in pro-inflammatory cytokine expression after HFD-feeding (Hossain et al., 2023).

Numerous publications have indicated that pro-inflammatory cytokines $Tn\alpha$, IL-6 and IL-18 directly impair normal insulin signaling through activation of JNK or IKK β /NF- κ B signaling pathways. JNK activation and phosphorylation of the insulin receptor substrate-1 (IRS-1) at serine-302 or serine-307 inhibits PI3K/Akt pathway activation required for GLUT4 translocation in skeletal muscle. Importantly, FFAs have been shown to directly induce activation JNK and IKK β /NF- κ B signaling and promote insulin resistance in the absence of cytokines (Puri et al., 2019; Sobczak et

al., 2019). As mentioned before, we did not measure the circulating levels of free fatty acids; however, we did find that *Tnfa* expression in skeletal muscle was significantly higher in WT compared to *Gpr75* deficient mice after HFD feeding, which correlates to the results seen in adipose tissue beds. Under normal conditions, insulin stimulates glucose disposal in skeletal muscle and inhibits lipolysis in adipose tissues. Our data shows that insulin receptor phosphorylation at Tyrosine 972 – a major activation site – in skeletal muscle was maintained in *Gpr75* deficient mice but not in WT mice after 14 weeks of HFD feeding. This correlated to hyperglycemia in WT mice after HFD feeding, which was largely attenuated in *Gpr75* deficient mice (FBS levels after 14 weeks of HFD feeding were 232 ± 7 , 195 ± 7 and 172 ± 6 mg/dL for WT, HET, and KO males, respectively; 167 ± 4 , 129 ± 5 and 109 ± 2 mg/dL for WT, HET, and KO females, respectively). It is worth noting that the hyperglycemia displayed by WT males after HFD feeding is significantly higher than published values for pure C57BL/6 mice. We assume these differences are due to the fact that our mice are on a C57BL/6NTacXSW background. In fact, Mekada and Yoshiki report that C57BL/6 substrains display different responses to high fat diet intervention. In addition to hyperglycemia, WT mice displayed delayed clearance of glucose from the blood in response to exogenous administration of insulin, which was significantly attenuated in *Gpr75* deficient mice. This may indicate a protection from insulin resistance – which is further supported by hyperinsulinemia in WT compared to *Gpr75* deficient mice (13288.06 ± 1582.21 vs 5195 ± 696.01 ng/mL for WT and KO respectively) and measurement of HOMA-IR (3.5-fold higher HOMA-IR in WT vs KO) after HFD feeding. In summary we hypothesize that obesity induced

inflammation, and a potential increase in circulating free fatty acids, impairs insulin signaling in skeletal muscle, thus causing hyperglycemia and hyperinsulinemia – hallmarks of T2DM (Hossain *et al.*, 2023).

The mechanisms underlying *Gpr75* deficiency and protection against HFD-driven adiposity and insulin resistance may in fact involve the GPR75 putative ligands – 20-hydroxyeicosatetraenoic acid (20-HETE) and C-C motif chemokine ligand 5 (CCL5) – both of which have been shown to be potent inflammatory mediators. 20-HETE has been shown to uncouple the endothelial nitric oxide synthase (eNOS), thus reducing nitric oxide production while increasing superoxide (Cheng *et al.*, 2008). The resulting activation of nuclear factor (NF)- κ B mediated pro-inflammatory program increases secretion of Il-6, Il-8, and Tnf α in the vasculature (Cheng *et al.*, 2010; Toth *et al.*, 2013). Furthermore, 20-HETE has been shown to stimulate neutrophil chemoattraction. Importantly, new studies indicate that neutrophils themselves stimulate 20-HETE production, which is mediated by hypochlorous acid (HOCl) induced activation of CYP4A11/20-HETE synthase (Azcona *et al.*, 2022). It is plausible that the HFD-driven expansion of adipose tissue and infiltration of neutrophils increases 20-HETE levels in WT mice compared to KO mice and affects insulin signaling. In fact, previous work from our lab found that 20-HETE directly inhibits insulin-mediated insulin receptor phosphorylation *in vitro* and *in vivo* (Gilani *et al.*, 2018). Moreover, treatment with 20-HETE receptor (GPR75) blockers prevented the 20-HETE-mediated inhibition of insulin signaling, suggesting that GPR75 is required for the 20-HETE effect (Gilani *et al.*, 2021; Hossain *et al.*, 2023).

CCL5, also known as RANTES, is a chemoattractant, therefore it stimulates the migration of leukocytes. Like 20-HETE, CCL5 has been shown to directly activate (NF)- κ B signaling (Liu *et al.*, 2014). It has also been shown to activate the mitogen-activated protein kinase (MAPK) and signal transducer and activator of transcription factor 3 (STAT3) pathways (Liu *et al.*, 2014; Wang *et al.*, 2012). The natural receptors for CCL5 have been established as C-C chemokine motif receptor 1 (CCR1), CCR3, and CCR5; however numerous publications indicate that CCL5 also tends to bind to GPR75 (Dedoni *et al.*, 2018; Liu *et al.*, 2013; Pascale *et al.*, 2022). The role of CCL5 in disease states is well established. For example, CCL5 has been shown to mediate fibrogenic events during NAFLD development, and the inhibition of CCL5 activity largely alleviates liver fibrosis in mice (Ambade *et al.*, 2019). Importantly, CCL5 has been shown to be a direct chemoattract for macrophages. Since macrophage recruitment and resulting inflammation play key roles in the development of adiposity, adipocyte dysfunction, and resulting insulin resistance in obesity (Curat *et al.*, 2004, 2006; Weisberg *et al.*, 2003; Zeyda *et al.*, 2007), it may be reasonable to assume that the pairing of CCL5 to GPR75 contributes and promotes to HFD-driven metabolic risk. Importantly, studies from the Schwartzman and Garcia Labs at New York Medical College have shown that 20-HETE is a high-affinity GPR75 ligand, while CCL5 tends to be a low affinity ligand. Furthermore, the binding of CCL5 to GPR75 inhibits 20-HETE pairing to GPR75 (Pascale *et al.*, 2022). Therefore, the exact contributions of GPR75 and its ligands to the metabolic complications of obesity merits further investigation. However, it is worth mentioning that HFD tends to induce 20-HETE producing enzymes, and the

excess production of 20-HETE may overwhelm CCL5-GPR75 pairing and play the predominate role in HFD-driven inflammation (Hossain et al., 2023).

In conclusion, our experiments have provided robust evidence that GPR75 contributes to diet-induced adiposity and insulin resistance, as previously reported by others (Akbari *et al.*, 2021) We now provide a possible mechanism by which *Gpr75* deficiency offers this protection (i.e., maintenance of mitochondria function and total body energy expenditure). This is inferred from results showing that *Gpr75*-deficient mice are protected from HFD-driven adiposity, hyperglycemia, and insulin resistance. This is also deduced from the bioactions of the putative GPR75 ligands, namely 20-HETE and CCL5, which are known proinflammatory mediators having detrimental effects on mitochondrial function and insulin signaling. Importantly, future studies should be directed towards the development of conditional *Gpr75* knockout mice in cells that contribute to the obese phenotype, e.g., beta cells and adipocytes. In fact, our lab recently generated an adipocyte specific *Gpr75* KO model, and our preliminary data indicates that after 14 weeks of HFD feeding *Gpr75* deficient mice have attenuated weight gain compared to WT animals. Thus, indicating that the primary site of GPR75 activity with regards to obesity may be in the adipose itself (not shown) (Hossain et al., 2023).

Significance

Obesity is now an epidemic in the United States. As mentioned before, the CDC, from 2000 through 2018, estimates the prevalence of obesity increased from 30.5% to 42.4%. Combined with obesity associated metabolic complications, including but not limited to hypertension, diabetes mellitus, cardiovascular diseases, and cancers, the morbidity rate of obesity cannot be ignored. The orphan G-protein-coupled receptor, GPR75, has been identified as a novel obesity gene, and *Gpr75* deficiency in humans is now associated with leanness. We have shown that deficiency of *Gpr75* in mice attenuates high fat-diet driven weight gain, adiposity, adipocyte hypertrophy, and insulin resistance. We further provide evidence that this protection is possibly accounted for by reduction of inflammation, preservation of mitochondria function, and maintenance of energy expenditure. It is clear that targeting GPR75 may present a novel strategy to combat obesity-driven cardiometabolic diseases and understanding the mechanisms underlying GPR75's contribution to obesity is paramount to any drug development (Hossain et al., 2023).

Limitations and Future Directions

While we have provided robust data suggesting that *Gpr75* deficiency attenuates HFD-driven obesity and glucose intolerance by impacting energy expenditure and adipose tissue phenotype, we acknowledge that this experiment was not conducted in a thermoneutral environment for rodents. Room temperature tends to stimulate sympathetic outflow in rodents and may impact indices of browning. Furthermore, while our data shows statistically significant differences in energy expenditure between WT and *Gpr75* deficient mice after HFD-feeding, we acknowledge that these differences are minor. Since both WT and *Gpr75* deficient mice tend to consume similar calories, it begs the question of whether nutrient malabsorption plays a role rather than energy expenditure alone. Unfortunately, we did not collect feces for nutrient analysis. Further investigation of plasma analytes – with particular emphasis on lipids – may provide some insight regarding dietary absorption. Also, our data indicates that while male and female *Gpr75* deficient mice show similar responses to HFD-feeding, females tend to have a stronger phenotype. In the present study we could not address this issue. A future study involving ovariectomy of *Gpr75* deficient females may provide some insight into the estrogen-GPR75 interaction. Finally, we acknowledge that genetic deletion of *Gpr75* offers only a preventative therapy for obesity, which is not clinically relative. A future study testing the effectiveness of GPR75 blockers in reversing obesity and metabolic complications is critical.

Bibliography

- Akbari P, Gilani A, Sosina O, Kosmicki JA, Khrimian L, Fang YY, Persaud T, Garcia V, Sun D, Li A, Mbatchou J, Locke AE, Benner C, Verweij N, Lin N, Hossain S, Agostinucci K, Pascale JV, Dirice E, Dunn M; Regeneron Genetics Center; DiscovEHR Collaboration; Kraus WE, Shah SH, Chen YI, Rotter JI, Rader DJ, Melander O, Still CD, Mirshahi T, Carey DJ, Berumen-Campos J, Kuri-Morales P, Alegre-Díaz J, Torres JM, Emberson JR, Collins R, Balasubramanian S, Hawes A, Jones M, Zambrowicz B, Murphy AJ, Paulding C, Coppola G, Overton JD, Reid JG, Shuldiner AR, Cantor M, Kang HM, Abecasis GR, Karalis K, Economides AN, Marchini J, Yancopoulos GD, Sleeman MW, Altarejos J, Della Gatta G, Tapia-Conyer R, Schwartzman ML, Baras A, Ferreira MAR, Lotta LA. (2021). Sequencing of 640,000 exomes identifies *GPR75* variants associated with protection from obesity. *Science*. 373(6550)
- Ambade A, Lowe P, Kodys K, Catalano D, Gyongyosi B, Cho Y, Iracheta-Vellve A, Adejumo A, Saha B, Calenda C, Mehta J, Lefebvre E, Vig P, Szabo G. (2019). Pharmacological Inhibition of CCR2/5 Signaling Prevents and Reverses Alcohol-Induced Liver Damage, Steatosis, and Inflammation in Mice. *Hepatology*. 69(3):1105-1121.
- Aouadi, M., Tencerova, M., Vangala, P., Yawe, J. C., Nicoloso, S. M., Amano, S. U., Cohen, J. L., & Czech, M. P. (2013). Gene silencing in adipose tissue macrophages regulates whole-body metabolism in obese mice. *Proceedings of the National Academy of Sciences of the United States of America*. 110(20):8278–8283.
- Azcona JA, Tang S, Berry E, Zhang FF, Garvey R, Falck JR, Schwartzman ML, Yi T, Jeitner TM, Guo AM. (2022). Neutrophil-Derived Myeloperoxidase and Hypochlorous Acid Critically Contribute to 20-Hydroxyeicosatetraenoic Acid Increases that Drive Postischemic Angiogenesis. *J Pharmacology & Experimental Therapeutics*. 381(3):204-216.
- Barden, A., Zilkens, R. R., Croft, K., Mori, T., Burke, V., Beilin, L. J., & Puddey, I. B. (2007). A reduction in alcohol consumption is associated with reduced plasma F2-isoprostanes and urinary 20-HETE excretion in men. *Free Radical Biology & Medicine*. 42(11):1730–1735.
- Beckman, J. A., Paneni, F., Cosentino, F., & Creager, M. A. (2013). Diabetes and vascular disease: pathophysiology, clinical consequences, and medical therapy: part II. *European Heart Journal*. 34(31):2444–2456.
- Besse-Patin A, Jeromson S, Levesque-Damphousse P, Secco B, Laplante M, Estall JL. (2019). PGC1A regulates the IRS1:IRS2 ratio during fasting to influence hepatic metabolism downstream of insulin. *Proceedings of the National Academy of Sciences of the United States of America*. 116(10):4285-4290.

- Blundell, J. E., Dulloo, A. G., Salvador, J., & Frühbeck, G. (2014). Beyond BMI - Phenotyping the Obesities. *Obesity Facts*. 7(5):322.
- Boucher, J., Kleinridders, A., & Ronald Kahn, C. (2014). Insulin Receptor Signaling in Normal and Insulin-Resistant States. *Cold Spring Harbor Perspectives in Biology*. 6(1).
- Boveris, A., & Chance, B. (1973). The mitochondrial generation of hydrogen peroxide. General properties and effect of hyperbaric oxygen. *Biochemical Journal*. 134(3): 707.
- Chen S, Liu X, Peng C, Tan C, Sun H, Liu H, Zhang Y, Wu P, Cui C, Liu C, Yang D, Li Z, Lu J, Guan J, Ke X, Wang R, Bo X, Xu X, Han J, Liu J. (2021) The phytochemical hyperforin triggers thermogenesis in adipose tissue via a Dlat-AMPK signaling axis to curb obesity. *Cell Metabolism*. 2021. 33(3):565-580.e7. doi:10.1016/j.cmet.2021.02.007.
- Chen Y, Medhora MM, Falck JR, Pritchard KA, & Jacobs ER (2006). Mechanisms of activation of eNOS by 20-hydroxyeicosatetraenoic acid and VEGF in bovine pulmonary artery endothelial cells. *American Journal of Physiology. Lung Cellular and Molecular Physiology* 291, L369–L377.
- Cheng J, Wu CC, Gotlinger KH, Zhang F, Falck JR, Narsimhaswamy D, & Schwartzman ML (2010). 20-hydroxy-5,8,11,14-eicosatetraenoic acid mediates endothelial dysfunction via I κ B kinase-dependent endothelial nitric-oxide synthase uncoupling. *The Journal of Pharmacology and Experimental Therapeutics*, 332:57–65.
- Chouchani, E. T., Kazak, L., Jedrychowski, M. P., Lu, G. Z., Erickson, B. K., Szpyt, J., Pierce, K. A., Laznik-Bogoslavski, D., Vetrivelan, R., Clish, C. B., Robinson, A. J., Gygi, S. P., & Spiegelman, B. M. (2016). Mitochondrial ROS regulate thermogenic energy expenditure and sulfenylation of UCP1. *Nature*. 532(7597):112.
- Curat, C. A., Miranville, A., Sengenès, C., Diehl, M., Tonus, C., Busse, R., & Bouloumié, A. (2004). From blood monocytes to adipose tissue-resident macrophages: induction of diapedesis by human mature adipocytes. *Diabetes*. 53(5):1285–1292.
- Curat, C. A., Wegner, V., Sengenès, C., Miranville, A., Tonus, C., Busse, R., & Bouloumié, A. (2006). Macrophages in human visceral adipose tissue: increased accumulation in obesity and a source of resistin and visfatin. *Diabetologia*. 49(4): 744–747.
- Dedoni, S., Campbell, L. A., Harvey, B. K., Avdoshina, V., & Mocchetti, I. (2018). The Orphan G Protein-coupled Receptor 75 Signaling is Activated by the Chemokine CCL5. *Journal of Neurochemistry*. 146(5): 526.

- de Munck, S., Provost, M., Kurikawa, M., Omori, I., Mukohyama, J., Felix, J., Bloch, Y., Abdel-Wahab, O., Bazan, J. F., Yoshimi, A., & Savvides, S. N. (2021). Structural basis of cytokine-mediated activation of ALK family receptors. *Nature*. 600(7887): 143.
- Di Angelantonio E, Bhupathiraju ShN, Wormser D, Gao P, Kaptoge S, Berrington de Gonzalez A, Cairns BJ, Huxley R, Jackson ChL, Joshy G, Lewington S, Manson JE, Murphy N, Patel AV, Samet JM, Woodward M, Zheng W, Zhou M, Bansal N, Barricarte A, Carter B, Cerhan JR, Smith GD, Fang X, Franco OH, Green J, Halsey J, Hildebrand JS, Jung KJ, Korda RJ, McLerran DF, Moore SC, O'Keeffe LM, Paige E, Ramond A, Reeves GK, Rolland B, Sacerdote C, Sattar N, Sofianopoulou E, Stevens J, Thun M, Ueshima H, Yang L, Yun YD, Willeit P, Banks E, Beral V, Chen Zh, Gapstur SM, Gunter MJ, Hartge P, Jee SH, Lam TH, Peto R, Potter JD, Willett WC, Thompson SG, Danesh J, Hu FB. (2016). Body-mass index and all-cause mortality: individual-participant-data meta-analysis of 239 prospective studies in four continents. *Lancet*. 388(10046): 776.
- Doetschman, T. (2009). Influence of genetic background on genetically engineered mouse phenotypes. *Methods in Molecular Biology*. 530:423–433.
- Escalante B, Sessa WC, Falck JR, Yadagiri P, Schwartzman ML. Cytochrome P450-dependent arachidonic acid metabolites, 19- and 20-hydroxyeicosatetraenoic acids, enhance sodium-potassium ATPase activity in vascular smooth muscle. (1990). *J Cardiovasc Pharmacology*. 16(3):438-43.
- Fedorenko, A., Lishko, P. v., & Kirichok, Y. (2012). Mechanism of Fatty-Acid-Dependent UCP1 Uncoupling in Brown Fat Mitochondria. *Cell*. 151(2):400.
- Feldmann HM, Golozoubova V, Cannon B, Nedergaard J. (2009). UCP1 ablation induces obesity and abolishes diet-induced thermogenesis in mice exempt from thermal stress by living at thermoneutrality. *Cell Metabolism*. 9(2):203-9.
- Fonseca, V. (2003). Effect of thiazolidinediones on body weight in patients with diabetes mellitus. *American Journal of Medicine*. 115(8 SUPPL. 1):42–48.
- Frayn, K. N. (2001). Adipose tissue and the insulin resistance syndrome. *The Proceedings of the Nutrition Society*. 60(3):375–380.
- Froogh G, Garcia V, Laniado Schwartzman M. (2022). The CYP/20-HETE/GPR75 axis in hypertension. *Advancements in Pharmacology*. 94:1-25
- Ganda, O. P. (2000). Lipoatrophy, lipodystrophy, and insulin resistance. *Annals of Internal Medicine*. 133(4):304–306.

- Garcia, V., Gilani, A., Shkolnik, B., Pandey, V., Zhang, F. F., Dakarapu, R., Gandham, S. K., Reddy, N. R., Graves, J. P., Gruzdev, A., Zeldin, D. C., Capdevila, J. H., Falck, J. R., & Schwartzman, M. L. (2017). 20- HETE Signals Through G Protein-Coupled Receptor GPR75 (Gq) to Affect Vascular Function and Trigger Hypertension. *Circulation Research*. 120(11):1776.
- Gavrilova, O., Marcus-Samuels, B., Graham, D., Kim, J. K., Shulman, G. I., Castle, A. L., Vinson, C., Eckhaus, M., & Reitman, M. L. (2000). Surgical implantation of adipose tissue reverses diabetes in lipoatrophic mice. *Journal of Clinical Investigation*. 105(3):271.
- Gilani, A., Agostinucci, K., Hossain, S., Pascale, J. v., Garcia, V., Adebessin, A. M., Falck, J. R., & Schwartzman, M. L. (2021). 20-HETE Interferes with Insulin Signaling and Contributes to Obesity-Driven Insulin Resistance. *Prostaglandins & Other Lipid Mediators*. 152:106485.
- Gilani, A., Pandey, V., Garcia, V., Agostinucci, K., Singh, S. P., Schragenheim, J., Bellner, L., Falck, J. R., Paudyal, M. P., Capdevila, J. H., Abraham, N. G., & Laniado Schwartzman, M. (2018). Obesity, Diabetes and Energy Homeostasis: High-fat diet-induced obesity and insulin resistance in CYP4a14^{-/-} mice is mediated by 20-HETE. *American Journal of Physiology - Regulatory, Integrative and Comparative Physiology*. 315(5):R934.
- Goossens, G. H. (2017). The Metabolic Phenotype in Obesity: Fat Mass, Body Fat Distribution, and Adipose Tissue Function. *Obesity Facts*. 10(3):207.
- Haeusler, R. A., McGraw, T. E., & Accili, D. (2018). Biochemical and cellular properties of insulin receptor signalling. *Nature Reviews. Molecular Cell Biology*. 19(1):31.
- Hardy, O. T., Perugini, R. A., Nicoloro, S. M., Gallagher-Dorval, K., Puri, V., Straubhaar, J., & Czech, M. P. (2011). BMI-independent inflammation in omental adipose tissue associated with insulin resistance in morbid obesity. *Surgery for Obesity and Related Diseases : Official Journal of the American Society for Bariatric Surgery*. 7(1):60.
- Hoopes, S. L., Garcia, V., Edin, M. L., Schwartzman, M. L., & Zeldin, D. C. (2015). Vascular actions of 20-HETE. *Prostaglandins & Other Lipid Mediators*, 120:9–16.
- Hossain S, Gilani A, Pascale J, Villegas E, Diegisser D, Agostinucci K, Kulaprazhazhe MM, Dirice E, Garcia V, Schwartzman ML. (2023). Gpr75-deficient mice are protected from high-fat diet-induced obesity. *Obesity*. 31(4):1024-1037.
- Hotamisligil, G. S., Murray, D. L., Choy, L. N., & Spiegelman, B. M. (1994). Tumor necrosis factor alpha inhibits signaling from the insulin receptor. *Proceedings of the National Academy of Sciences of the United States of America*, 91(11):4854–4858.

- Ibrahim, M. M. (2010). Subcutaneous and visceral adipose tissue: structural and functional differences. *Obesity Reviews : An Official Journal of the International Association for the Study of Obesity*, 11(1):11–18.
- Ikeda K, Kang Q, Yoneshiro T, Camporez JP, Maki H, Homma M, Shinoda K, Chen Y, Lu X, Maretich P, Tajima K, Ajuwon KM, Soga T, Kajimura S. (2017). UCP1-independent signaling involving SERCA2b-mediated calcium cycling regulates beige fat thermogenesis and systemic glucose homeostasis. *Nature Medicine*. 23(12):1454-1465.
- Kawai, T., Autieri, M. v., & Scalia, R. (2021). Inflammation: From Cellular Mechanisms to Immune Cell Education: Adipose tissue inflammation and metabolic dysfunction in obesity. *American Journal of Physiology - Cell Physiology*, 320(3):C375.
- Keophiphath, M., Rouault, C., Divoux, A., Clément, K., & Lacasa, D. (2010). CCL5 promotes macrophage recruitment and survival in human adipose tissue. *Arteriosclerosis, Thrombosis, and Vascular Biology*, 30(1):39–45.
- Kim, J. K., Gavrilova, O., Chen, Y., Reitman, M. L., & Shulman, G. I. (2000). Mechanism of insulin resistance in A-ZIP/F-1 fatless mice. *The Journal of Biological Chemistry*, 275(12):8456–8460.
- Kim, D. H., Puri, N., Sodhi, K., Falck, J. R., Abraham, N. G., Shapiro, J., & Schwartzman, M. L. (2013). Cyclooxygenase-2 dependent metabolism of 20-HETE increases adiposity and adipocyte enlargement in mesenchymal stem cell-derived adipocytes. *Journal of Lipid Research*, 54(3):786.
- Kopelman, P. G. (2000). Obesity as a medical problem. *Nature*, 404(6778):635–643.
- Kroetz DL, Xu F. (2005). Regulation and inhibition of arachidonic acid omega-hydroxylases and 20-HETE formation. *Annual Reviews in Pharmacology & Toxicology*. 45:413-38.
- Lakhkar A, Dhagia V, Joshi SR, Gotlinger K, Patel D, Sun D, Wolin MS, Schwartzman ML, Gupte SA (2016). 20-HETE-Induced Mitochondrial Superoxide and Inflammatory Phenotype in Vascular Smooth Muscle is Prevented by Glucose-6-Phosphate Dehydrogenase Inhibition. *American Journal of Physiology. Heart and Circulatory Physiology* 310, H1107–H1117
- Li, H., Meng, Y., He, S., Tan, X., Zhang, Y., Zhang, X., Wang, L., & Zheng, W. (2022). Macrophages, Chronic Inflammation, and Insulin Resistance. *Cells*, 11(19):3001.
- Li J, Wu H, Liu Y, Yang L. High fat diet induced obesity model using four strains of mice: Kunming, C57BL/6, BALB/c and ICR. (2020). *Experimental Animals/Japanese Association for Laboratory Animal Science*. 69(3):326-335

- Li, X., Zhao, G., Ma, B., Li, R., Hong, J., Liu, S., & Wang, D. W. (2014). 20-Hydroxyeicosatetraenoic Acid Impairs Endothelial Insulin Signaling by Inducing Phosphorylation of the Insulin Receptor Substrate-1 at Ser616. *PLoS ONE*, 9(4): 95841.
- Liesa, M., & Shirihai, O. S. (2013). Mitochondrial Dynamics in the Regulation of Nutrient Utilization and Energy Expenditure. *Cell Metabolism*, 17(4):491.
- Liu, B., Hassan, Z., Amisten, S., King, A. J., Bowe, J. E., Huang, G. C., Jones, P. M., & Persaud, S. J. (2013). The novel chemokine receptor, G-protein-coupled receptor 75, is expressed by islets and is coupled to stimulation of insulin secretion and improved glucose homeostasis. *Diabetologia*, 56(11):2467–2476.
- Ma, M., Quan, Y., Li, Y., He, X., Xiao, J., Zhan, M., Zhao, W., Xin, Y., Ligong, L. U., & Liangping, L. U. O. (2018). Bidirectional modulation of insulin action by reactive oxygen species in 3T3-L1 adipocytes. *Molecular Medicine Reports*, 18(1):807.
- Malis, C., Rasmussen, E. L., Poulsen, P., Petersen, I., Christensen, K., Beck-Nielsen, H., Astrup, A., & Vaag, A. A. (2005). Total and regional fat distribution is strongly influenced by genetic factors in young and elderly twins. *Obesity Research*, 13(12): 2139–2145.
- Manna, P., Achari, A. E., & Jain, S. K. (2017). Vitamin D supplementation inhibits oxidative stress and upregulate SIRT1/AMPK/GLUT4 cascade in high glucose-treated 3T3L1 adipocytes and in adipose tissue of high fat diet-fed diabetic mice. *Archives of Biochemistry and Biophysics*, 615:22–34.
- Manning, B. D., & Toker, A. (2017). AKT/PKB Signaling: Navigating the Network. *Cell*, 169(3):381.
- Mayoral, L. P. C., Andrade, G. M., Mayoral, E. P. C., Huerta, T. H., Canseco, S. P., Rodal Canales, F. J., Cabrera-Fuentes, H. A., Cruz, M. M., Pérez Santiago, A. D., Alpuche, J. J., Zenteno, E., Ruíz, H. M., Cruz, R. M., Jeronimo, J. H., & Perez-Campos, E. (2020). Obesity subtypes, related biomarkers & heterogeneity. *The Indian Journal of Medical Research*, 151(1):11.
- McDonnell, M. E., Ganley-Leal, L. M., Mehta, A., Bigornia, S. J., Mott, M., Rehman, Q., Farb, M. G., Hess, D. T., Joseph, L., Gokce, N., & Apovian, C. M. (2012). B lymphocytes in human subcutaneous adipose crown-like structures. *Obesity*. 20(7): 1372.
- Mekada K, Yoshiki A. Substrains matter in phenotyping of C57BL/6 mice. (2021) *Experimental Animals/Japanese Association for Laboratory Animal Science*. 70(2):145-160.

- Mishra, P., & Chan, D. C. (2016). Metabolic regulation of mitochondrial dynamics. *The Journal of Cell Biology*, 212(4):379.
- Mollica MP, Lionetti L, Putti R, Cavaliere G, Gaita M, Barletta A. (2011). From chronic overfeeding to hepatic injury: role of endoplasmic reticulum stress and inflammation. *Nutr Metab Cardiovasc Dis*. 21(3):222-30.
- Muthalif MM, Uddin MR, Fatima S, Parmentier JH, Khandekar Z, & Malik KU (2001). Small GTP binding protein Ras contributes to norepinephrine-induced mitogenesis of vascular smooth muscle cells. *Prostaglandins & Other Lipid Mediators*, 65:33–43
- Nesto RW. Obesity: a major component of the metabolic syndrome. (2005). *Tex Heart Inst J*. 32(3):387-9.
- Pascale, J. V., Park, E. J., Adebessin, A. M., Falck, J. R., Schwartzman, M. L., & Garcia, V. (2021). Uncovering the signalling, structure and function of the 20-HETE-GPR75 pairing: Identifying the chemokine CCL5 as a negative regulator of GPR75. *British Journal of Pharmacology*, 178(18):3813–3828.
- Patel, P., & Abate, N. (2013). Body Fat Distribution and Insulin Resistance. *Nutrients*, 5(6):2019.
- Pelletier, R. M., Layeghkhavidaki, H., & Vitale, M. L. (2020). Glucose, insulin, insulin receptor subunits α and β in normal and spontaneously diabetic and obese ob/ob and db/db infertile mouse testis and hypophysis. *Reproductive Biology and Endocrinology* :18(1)
- Peterson, S. J., Vanella, L., Gotlinger, K., Jiang, H., Singh, S. P., Sodhi, K., Maher, E., O'Hanlon, K., Shapiro, J. I., & Abraham, N. G. (2016). Oxidized HDL is a potent inducer of adipogenesis and causes activation of the Ang-II and 20-HETE systems in human obese females. *Prostaglandins & Other Lipid Mediators*, 123:68–77.
- Pilis, K., Stec, K., Pilis, A., Mroczek, A., Michalski, C., & Pilis, W. (2019). Body composition and nutrition of female athletes. *Roczniki Panstwowego Zakladu Higieny*, 70(3):243–251.
- Polyák Á, Winkler Z, Kuti D, Ferenczi S, Kovács KJ. Brown adipose tissue in obesity: Fractalkine-receptor dependent immune cell recruitment affects metabolic-related gene expression. (2016). *Biochim Biophys Acta*. 1861(11):1614-1622.
- Posner, B. I. (2017). Insulin Signalling: The Inside Story. *Canadian Journal of Diabetes*, 41(1):108.

- Powell, D. R., Doree, D. D., Dacosta, C. M., Platt, K. A., Brommage, R., Buhning, L., Revelli, J. P., & Shadoan, M. K. (2022). Mice Lacking Gpr75 are Hypophagic and Thin. *Diabetes, Metabolic Syndrome and Obesity: Targets and Therapy*, 15(45)
- Puri, K., Lal, N., Shang, R., Ghosh, S., Flibotte, S., Dyer, R., Hussein, B., & Rodrigues, B. (2019). Diabetes Mellitus Severity and a Switch from Using Lipoprotein Lipase to Adipose-Derived Fatty Acid Results in a Cardiac Metabolic Signature That Embraces Cell Death. *Journal of the American Heart Association: Cardiovascular and Cerebrovascular Disease*, 8(21).
- Randriamboavonjy V, Busse R, & Fleming I (2003). 20-HETE-induced contraction of small coronary arteries depends on the activation of Rho-kinase. *Hypertension* 41:801–806
- Rausch, M. E., Weisberg, S., Vardhana, P., & Tortoriello, D. v. (2008). Obesity in C57BL/6J mice is characterized by adipose tissue hypoxia and cytotoxic T-cell infiltration. *International Journal of Obesity*, 32(3):451–463.
- Reale, R., Burke, L. M., Cox, G. R., & Slater, G. (2020). Body composition of elite Olympic combat sport athletes. *European Journal of Sport Science*, 20(2):147–156.
- Reasner, C. A. (2002). Where thiazolidinediones will fit. *Diabetes/Metabolism Research and Reviews*, 18(SUPPL. 2).
- Rondinone, C. M., & Smith, U. (1996). Okadaic acid exerts a full insulin-like effect on glucose transport and glucose transporter 4 translocation in human adipocytes. Evidence for a phosphatidylinositol 3-kinase-independent pathway. *Journal of Biological Chemistry*, 271(30):18148–18153.
- Rui, L., Aguirre, V., Kim, J. K., Shulman, G. I., Lee, A., Corbould, A., Dunaif, A., & White, M. F. (2001). Insulin/IGF-1 and TNF- α stimulate phosphorylation of IRS-1 at inhibitory Ser307 via distinct pathways. *Journal of Clinical Investigation*, 107(2):181.
- Samuel, V. T., & Shulman, G. I. (2012). Integrating Mechanisms for Insulin Resistance: Common Threads and Missing Links. *Cell*, 148(5):852.
- Shukla, A., Kumar, K., & Singh, A. (2014). Association between Obesity and Selected Morbidities: A Study of BRICS Countries. *PLoS ONE*, 9(4):94433.
- Snijder, M. B., Zimmet, P. Z., Visser, M., Dekker, J. M., Seidell, J. C., & Shaw, J. E. (2004). Independent and opposite associations of waist and hip circumferences with diabetes, hypertension and dyslipidemia: the AusDiab Study. *International Journal of Obesity and Related Metabolic Disorder: Journal of the International Association for the Study of Obesity*, 28(3):402–409.

- Sobczak, A. I. S., Blindauer, C. A., & Stewart, A. J. (2019). Changes in Plasma Free Fatty Acids Associated with Type-2 Diabetes. *Nutrients*, 11(9).
- Starkov, A. A., & Fiskum, G. (2003). Regulation of brain mitochondrial H₂O₂ production by membrane potential and NAD(P)H redox state. *Journal of Neurochemistry*, 86(5): 1101–1107.
- Stec D, Gannon KP, Beaird JS, & Drummond HA. (2007). 20-Hydroxyeicosatetraenoic acid (20-HETE) stimulates migration of vascular smooth muscle cells. *Cellular Physiology and Biochemistry* 19:121–128
- Stefanovic-Racic, M., Yang, X., Turner, M. S., Mantell, B. S., Stolz, D. B., Sumpster, T. L., Sipula, I. J., Dedousis, N., Scott, D. K., Morel, P. A., Thomson, A. W., & O'Doherty, R. M. (2012). Dendritic cells promote macrophage infiltration and comprise a substantial proportion of obesity-associated increases in CD11c + cells in adipose tissue and liver. *Diabetes*, 61(9):2330–2339.
- Stenholm, S., Harris, T. B., Rantanen, T., Visser, M., Kritchevsky, S. B., & Ferrucci, L. (2008). Sarcopenic obesity: definition, cause and consequences. *Current Opinion in Clinical Nutrition and Metabolic Care*, 11(6):693–700.
- Stinkens, R., Goossens, G. H., Jocken, J. W. E., & Blaak, E. E. (2015). Targeting fatty acid metabolism to improve glucose metabolism. *Obesity Reviews: An Official Journal of the International Association for the Study of Obesity*, 16(9):715–757.
- Sumamo Schellenberg, E., Dryden, D. M., Vandermeer, B., Ha, C., & Korownyk, C. (2013). Lifestyle interventions for patients with and at risk for type 2 diabetes: a systematic review and meta-analysis. *Annals of Internal Medicine*, 159(8):543–551.
- Tang, X., Sun, Y., Li, Y., Ma, S., Zhang, K., Chen, A., Lyu, Y., & Yu, R. (2022). Sodium butyrate protects against oxidative stress in high-fat-diet-induced obese rats by promoting GSK-3 β /Nrf2 signaling pathway and mitochondrial function. *Journal of Food Biochemistry*, 46(10).
- Tang, F., Tang, G., Xiang, J., Dai, Q., Rosner, M. R., & Lin, A. (2002). The Absence of NF- κ B-Mediated Inhibition of c-Jun N-Terminal Kinase Activation Contributes to Tumor Necrosis Factor Alpha-Induced Apoptosis. *Molecular and Cellular Biology*, 22(24):8571.
- Toi, P. L., Anothaisintawee, T., Chaikledkaew, U., Briones, J. R., Reutrakul, S., & Thakkinstian, A. (2020). Preventive Role of Diet Interventions and Dietary Factors in Type 2 Diabetes Mellitus: An Umbrella Review. *Nutrients*, 12(9):1–17.

- Toth P, Csiszar A, Tucsek Z, Sosnowska D, Gautam T, Koller A, Schwartzman ML, Sonntag WE, Ungvari Z. (2013). Role of 20-HETE, TRPC channels, and BKCa in dysregulation of pressure-induced Ca²⁺ signaling and myogenic constriction of cerebral arteries in aged hypertensive mice. *Am J Physiol Heart Circ Physiol*. 305(12):H1698-708
- Tsai, I. J., Croft, K. D., Mori, T. A., Falck, J. R., Beilin, L. J., Puddey, I. B., & Barden, A. E. (2009). 20-HETE and F2-isoprostanes in the metabolic syndrome: the effect of weight reduction. *Free Radical Biology & Medicine*, 46(2):263–270.
- Tunaru, S., Bonnavion, R., Brandenburger, I., Preussner, J., Thomas, D., Scholich, K., & Offermanns, S. (2018). 20-HETE promotes glucose-stimulated insulin secretion in an autocrine manner through FFAR1. *Nature Communications*, 9(1).
- Ukropec, J., Anunciado, R. P., Ravussin, Y., Hulver, M. W., & Kozak, L. P. (2006). UCP1-independent thermogenesis in white adipose tissue of cold-acclimated Ucp1-/- mice. *The Journal of Biological Chemistry*, 281(42):31894–31908.
- Wang Q, Li D, Cao G, Shi Q, Zhu J, Zhang M, Cheng H, Wen Q, Xu H, Zhu L, Zhang H, Perry RJ, Spadaro O, Yang Y, He S, Chen Y, Wang B, Li G, Liu Z, Yang C, Wu X, Zhou L, Zhou Q, Ju Z, Lu H, Xin Y, Yang X, Wang C, Liu Y, Shulman GI, Dixit VD, Lu L, Yang H, Flavell RA, Yin Z. (2021) IL-27 signalling promotes adipocyte thermogenesis and energy expenditure. *Nature*. 600(7888):314-318.
- Wang SW, Wu HH, Liu SC, Wang PC, Ou WC, Chou WY, Shen YS, Tang CH. CCL5 and CCR5 interaction promotes cell motility in human osteosarcoma. (2012) *PLoS One*. 7(4):e35101. doi: 10.1371/journal.pone.0035101.
- Watanabe, Y., Nagai, Y., Honda, H., Okamoto, N., Yanagibashi, T., Ogasawara, M., Yamamoto, S., Imamura, R., Takasaki, I., Hara, H., Sasahara, M., Arita, M., Hida, S., Taniguchi, S., Suda, T., & Takatsu, K. (2019). Bidirectional crosstalk between neutrophils and adipocytes promotes adipose tissue inflammation. *FASEB Journal : Official Publication of the Federation of American Societies for Experimental Biology*, 33(11):11821–11835.
- Weisberg, S. P., McCann, D., Desai, M., Rosenbaum, M., Leibel, R. L., & Ferrante, A. W. (2003). Obesity is associated with macrophage accumulation in adipose tissue. *The Journal of Clinical Investigation*, 112(12):1796–1808.
- Wernstedt Asterholm, I., Tao, C., Morley, T. S., Wang, Q. A., Delgado-Lopez, F., Wang, Z. v., & Scherer, P. E. (2014). Adipocyte Inflammation is Essential for Healthy Adipose Tissue Expansion and Remodeling. *Cell Metabolism*, 20(1):103.

- Wu, J., Boström, P., Sparks, L. M., Ye, L., Choi, J. H., Giang, A. H., Khandekar, M., Virtanen, K. A., Nuutila, P., Schaart, G., Huang, K., Tu, H., van Marken Lichtenbelt, W. D., Hoeks, J., Enerbäck, S., Schrauwen, P., & Spiegelman, B. M. (2012). Beige Adipocytes are a Distinct Type of Thermogenic Fat Cell in Mouse and Human. *Cell*, 150(2):366.
- Xu, H., Barnes, G. T., Yang, Q., Tan, G., Yang, D., Chou, C. J., Sole, J., Nichols, A., Ross, J. S., Tartaglia, L. A., & Chen, H. (2003). Chronic inflammation in fat plays a crucial role in the development of obesity-related insulin resistance. *Journal of Clinical Investigation*, 112(12):1821.
- Yasmin, S., & Jayaprakash, V. (2017). Thiazolidinediones and PPAR orchestra as antidiabetic agents: From past to present. *European Journal of Medicinal Chemistry*, 126:879–893.
- Yoneshiro, T., Aita, S., Matsushita, M., Kayahara, T., Kameya, T., Kawai, Y., Iwanaga, T., & Saito, M. (2013). Recruited brown adipose tissue as an antiobesity agent in humans. *The Journal of Clinical Investigation*, 123(8):3404.
- Yusuf, S., Hawken, S., Ôunpuu, S., Bautista, L., Franzosi, M. G., Commerford, P., Lang, C. C., Rumboldt, Z., Onen, C. L., Lisheng, L., Tanomsup, S., Wangai, P., Razak, F., Sharma, A. M., & Anand, S. S. (2005). Obesity and the risk of myocardial infarction in 27,000 participants from 52 countries: a case-control study. *Lancet*. 366(9497): 1640–1649.
- Zeng Z, Lan T, Wei Y, Wei X. (2022). CCL5/CCR5 axis in human diseases and related treatments. *Genes & Diseases*. 9(1):12-27
- Zeyda, M., Farmer, D., Todoric, J., Aszmann, O., Speiser, M., Györi, G., Zlabinger, G. J., & Stulnig, T. M. (2007). Human adipose tissue macrophages are of an anti-inflammatory phenotype but capable of excessive pro-inflammatory mediator production. *International Journal of Obesity*, 31(9):1420–1428.